AD-A174 718 THE MULTIPATH AND FADING PROFILE OF THE HIGH LATITUDE METEOR BURST COMMUNICATION CHANNEL(U) SIGNATRON INC LEXINGTON MA J A WEITZEN OCT 86 A447-15 RADC-TR-86-166 1/2

UNCLASSIFIED F19628-84-C-0117 F/G 17/2 1 NL

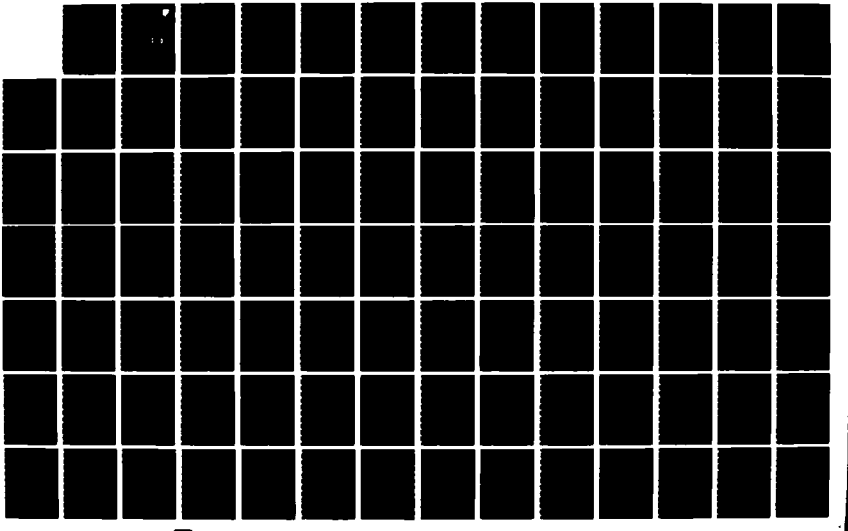

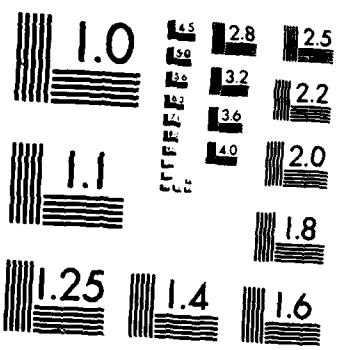

CROCOPY RESOLUTION TEST CHART
NATIONAL BUREAU OF STANDARDS 1963-A

(12)

RADC-TR-86-166
Interim Report
October 1986

THE MULTIPATH AND FADING PROFILE OF THE HIGH LATITUDE METEOR BURST COMMUNICATION CHANNEL

Signatron, Inc.

Jay A. Weitzen

APPROVED FOR PUBLIC RELEASE; DISTRIBUTION UNLIMITED

ROME AIR DEVELOPMENT CENTER
Air Force Systems Command
Griffiss Air Force Base, NY 13441-5700

This report has been reviewed by the RADC Public Affairs Office (PA) and is releasable to the National Technical Information Service (NTIS). At NTIS it will be releasable to the general public, including foreign nations.

RADC-TR-86-166 has been reviewed and is approved for publication.

APPROVED: Michael J Sowa

MICHAEL J. SOWA
Project Engineer

APPROVED: Allan C Schell

ALLAN C. SCHELL
Chief, Electromagnetic Sciences Division

FOR THE COMMANDER: John A. Ritz

JOHN A. RITZ
Plans and Programs Division

If your address has changed or if you wish to be removed from the RADC mailing list, or if the addressee is no longer employed by your organization, please notify RADC (EEPS) Hanscom AFB MA 01731-5000. This will assist us in maintaining a current mailing list.

Do not return copies of this report unless contractual obligations or notices on a specific document requires that it be returned.

UNCLASSIFIED
SECURITY CLASSIFICATION OF THIS PAGE

AD-A174 718

REPORT DOCUMENTATION PAGE

1a. REPORT SECURITY CLASSIFICATION UNCLASSIFIED	1b. RESTRICTIVE MARKINGS N/A
2a. SECURITY CLASSIFICATION AUTHORITY N/A	3. DISTRIBUTION/AVAILABILITY OF REPORT Approved for public release; distribution unlimited
2b. DECLASSIFICATION/DOWNGRADING SCHEDULE N/A	
4. PERFORMING ORGANIZATION REPORT NUMBER(S) A447-15	5. MONITORING ORGANIZATION REPORT NUMBER(S) RADC-TR-86-166
6a. NAME OF PERFORMING ORGANIZATION Signatron, Inc.	6b. OFFICE SYMBOL (If applicable)
6c. ADDRESS (City, State, and ZIP Code) 110 Hartwell Avenue Lexington MA 02173	7a. NAME OF MONITORING ORGANIZATION Rome Air Development Center (EEPS)
8a. NAME OF FUNDING/SPONSORING ORGANIZATION Rome Air Development Center	8b. OFFICE SYMBOL (If applicable) EEPS
8c. ADDRESS (City, State, and ZIP Code) Hanscom AFB MA 01731-5000	7b. ADDRESS (City, State, and ZIP Code) Hanscom AFB MA 01731-5000
	9. PROCUREMENT INSTRUMENT IDENTIFICATION NUMBER F19628-84-C-0117
	10. SOURCE OF FUNDING NUMBERS

PROGRAM ELEMENT NO.	PROJECT NO.	TASK NO.	WORK UNIT ACCESSION NO.
62702F	4600	16	66

11. TITLE (Include Security Classification)
THE MULTIPATH AND FADING PROFILE OF THE HIGH LATITUDE METEOR BURST COMMUNICATION CHANNEL

12. PERSONAL AUTHOR(S)
Jay A. Weitzen

13a. TYPE OF REPORT	13b. TIME COVERED	14. DATE OF REPORT (Year, Month, Day)	15. PAGE COUNT
Interim	FROM Jan 85 TO Aug 86	October 1986	116

16. SUPPLEMENTARY NOTATION
N/A

17 COSATI CODES		
FIELD	GROUP	SUB-GROUP
17	02	2.1
20	14	

18. SUBJECT TERMS (Continue on reverse if necessary and identify by block number)
Auroral scatter, meteor scatter communication, Meteor scatter high latitude effects, VHF propagation, multipath measurement, meteor scatter propagation

19. ABSTRACT (Continue on reverse if necessary and identify by block number)

High latitude propagation phenomenon such as scatter from the aurora and sporadic-E propagation can alter the communication characteristics of the high latitude meteor communication channel. This report describes the results of several experiments conducted for the purpose of characterizing the fading and multipath profile of the high latitude meteor communication channel. The effect of high latitude propagation phenomena on the capacity and reliability of meteor burst communications is discussed.

20. DISTRIBUTION/AVAILABILITY OF ABSTRACT	21. ABSTRACT SECURITY CLASSIFICATION
☐ UNCLASSIFIED/UNLIMITED ☐ SAME AS RPT ☒ OTIC USERS	UNCLASSIFIED

22a. NAME OF RESPONSIBLE INDIVIDUAL	22b. TELEPHONE (Include Area Code)	22c. OFFICE SYMBOL
Michael J. Sowa	(617) 861-1500	RADC (EEPS)

DD FORM 1473, 84 MAR 83 APR edition may be used until exhausted
All other editions are obsolete.

SECURITY CLASSIFICATION OF THIS PAGE
UNCLASSIFIED

TABLE OF CONTENTS

LIST OF FIGURES

LIST OF FIGURES (Continued)

LIST OF FIGURES (Continued)

LIST OF FIGURES (Concluded)

LIST OF TABLES

ABSTRACT

High latitude propagation phenomenon such as scatter from the aurora and sporadic-E propagation can alter the communication characteristics of the high latitude meteor communication channel. This report describes the results of several experiments conducted for the purpose of characterizing the fading and multipath profile of the high latitude meteor communication channel. The effect of high latitude propagation phenomena on the capacity and reliability of meteor burst communications is discussed.

EXECUTIVE SUMMARY

Meteor burst communications has several potential advantages over conventional HF communications at high latitudes. Because it does not depend upon ionospheric reflection, it is not subject to the diurnal, seasonal and solar induced changes in the maximum usable frequency (MUF) as is HF. Network control is therefore much simpler since single frequency operation can be used and no adaptive frequency management is required. Meteor burst, due to its small reflecting area, has a certain degree of inherent AJ and LPI to ground based interceptors and jammers. Meteor burst operates at higher frequencies than HF (40 to 100 MHz for meteor burst versus 2 to 30 for HF) making it much less vulnerable to ionospheric absorption events. For these reasons, meteor burst is being considered or is being applied to several high latitude communication missions.

There are several high latitude propagation effects which can alter the communication characteristics of the channel; some of which can be considered beneficial, while some could be detrimental. The objective of the program described in this report was to design a relatively inexpensive experiment to characterize the various propagation mechanisms in addition to meteors which are observed at high latitudes. The primary objective was to determine the Doppler and multipath spreads of the various propagation modes, and to determine their potential effect on conventional meteor communication. In particular, three propagation mechanisms which result in multipath and fading at VHF at high latitudes have been characterized: one is multipath due to multiple and/or warped meteor trails, another is sporadic-E scatter, and the third is scatter from the aurora.

i) The simultaneous occurrence of more than one meteor on a single link can, for a short period of time, produce multipath spreads as high as 1000 μs; however, for a typical link configuration, only on 1 to 2 percent of all meteor trails will there be significant multipath interference due to multiple trails. On occasion, individual trails can warp so that multiple reflection points are produced creating potential multipath up to a maximum of about 5 μs. This occurrence is fairly rare and even then the coherence bandwidth limit due to multipath is several hundred kb/s. Warping of individual trails due to high altitude wind shears with multipath spreads less than 1 μs is a primary source of fading observed on many meteor trails. This and several other studies have shown that the meteor channel is primarily signal strength limited as opposed to multipath limited channels, such as the troposcatter channel. Advanced adaptive techniques which adapt throughput to channel signal strength, such as the variable data rate modem, can operate on the meteor channel and can greatly increase throughput.

ii) Sporadic-E layer scatter at low VHF frequencies (30 to 60 MHz) occurs frequently at high latitudes resulting in a continuous strong signal which exhibits little multipath dispersion. Due to the unreliability and low predictability of the sporadic-E channel, as opposed to the intermittent yet more reliable meteor channel, this channel is best considered as a "bonus" channel rather than as the primary survivable, reliable backup channel. There are several ramifications of the frequent occurrence of sporadic-E at high latitudes. Protocols for meteor communication systems must be designed to operate in a high contention environment when a continuous channel to many links may exist simultaneously for long periods of time. Simple meteor burst networks operate on the principle that the duty cycle on any link is so low that collisions between transmissions are

rare. The sporadic-E channel due to its large reflection area, has much lower jam and intercept resistance than does the meteor channel, subjecting the meteor network to potential interference from unintentional or intentional signal sources operating on adjacent frequencies. The primary multipath source on the sporadic-E channel is ironically the occurrence of meteors off to the side of the great circle path producing intermittent multipath spreads up to 1000 μs on longer links. The Doppler spread of sporadic-E channels is on the order of 10 to 30 Hz or less. Figures ES-1 and ES-2 show the multipath and Doppler profile of a typical sporadic-E channel. We observe the occurrence of meteors in Figure ES-1 in frames 21, 33, 38, 44 and 49.

iii) Scatter from the aurora is a localized phenomenon occurring when the aurora and the meteor link are oriented such that conditions for specular scatter from elongated irregularities in the ionosphere are satisfied. When present, auroral scatter can represent an additional background interference source, or on occasion, depending on the link power, antenna patterns and density of the auroral ionization, it can create a high multipath (multipath spreads up to 1000 μs or more), fast fading (200 Hz Doppler spread), high signal strength, continuous channel. Auroral scatter is much more localized than is sporadic-E since the requirements for field aligned auroral scatter, outlined in the companion report by Málaga [1986], are much more restrictive than for simple layered sporadic-E.

Figure ES-3 shows a series of multipath snapshots of the Anchorage-Bethel, Alaska meteor channel acquired every six seconds on September 19, 1985. In Figure ES-3 the large peaks in frames 47, 53, and 54 represent large meteor echoes and the remainder is due to auroral scatter. The five-minute average rms multipath spread in Figure ES-3 is 801 μs. Figure ES-4 shows the Doppler spread. In Figure ES-4, the component centered at zero

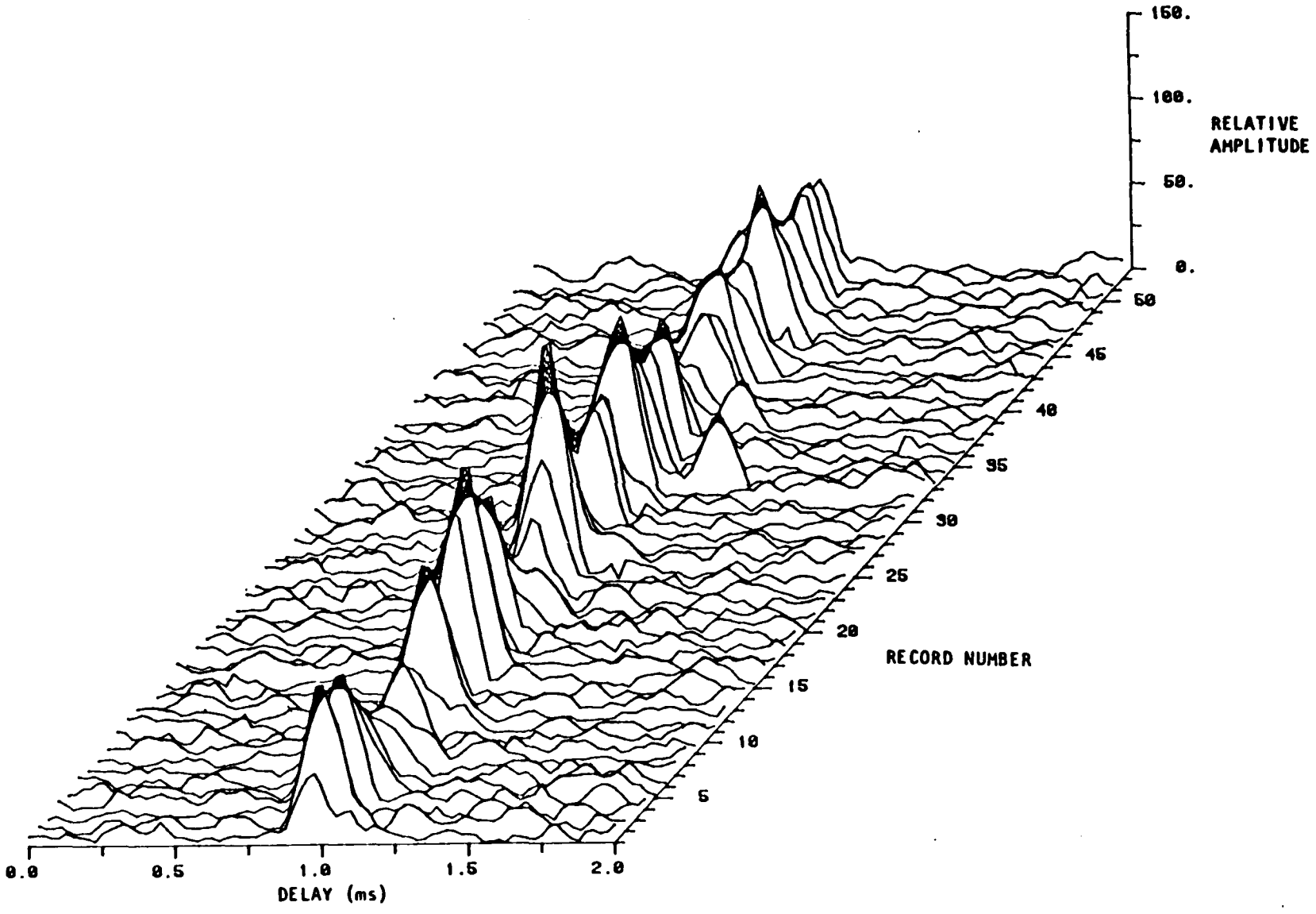

Figure ES-1 Series of multipath snapshots showing Sporadic-E event on 1 July 1985 at 0300 UT. Snapshots were acquired every 6 seconds. Multipath due to meteors is clearly visible in snapshots 21, 33, 38, 44 and 49.

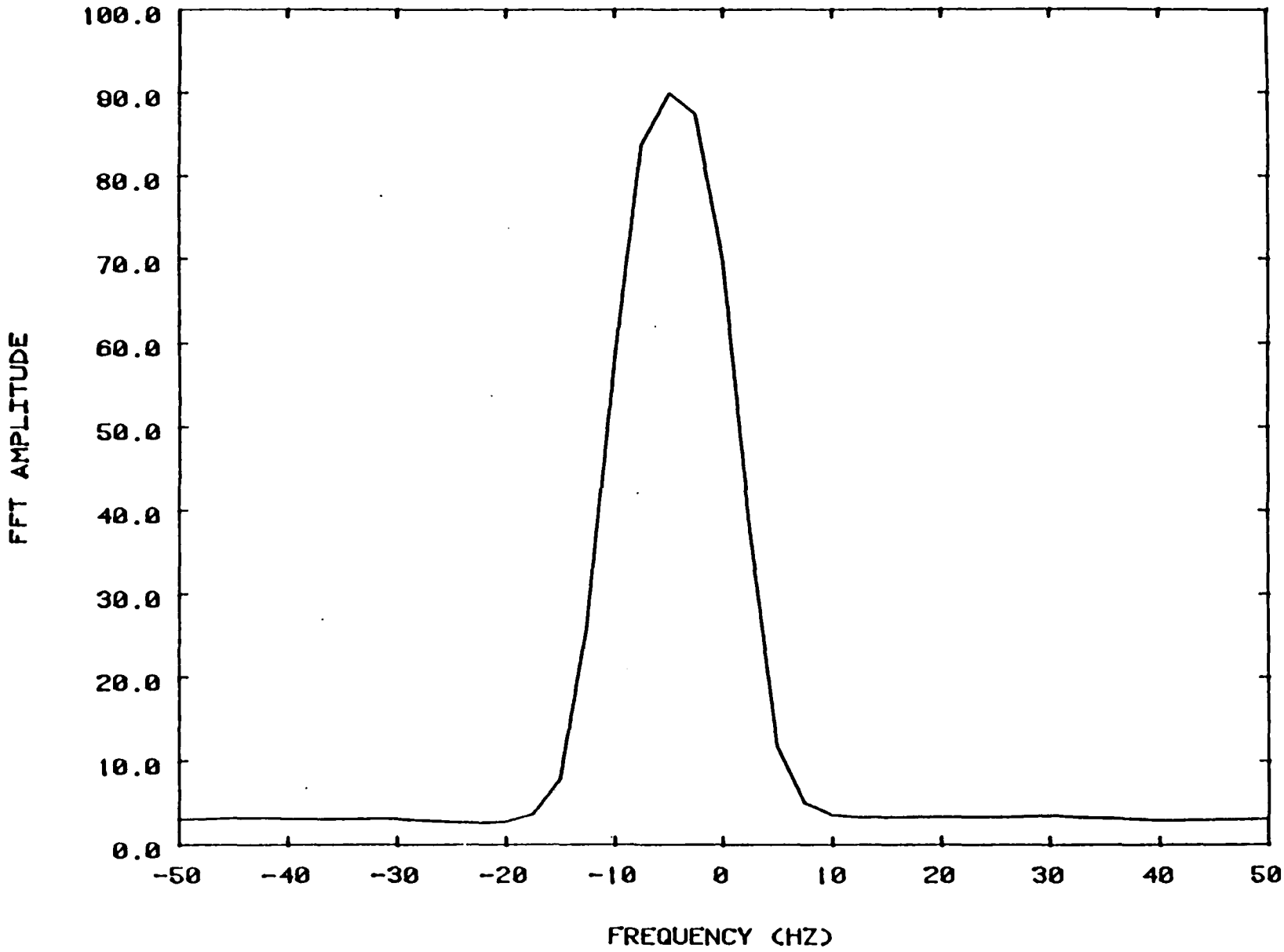

Figure ES-2 Composite FFT formed by averaging 10 FFT records acquired every 25 seconds for four minutes preceding the snapshots in Figure ES-1. The 2σ Doppler spread is 11.79 Hz.

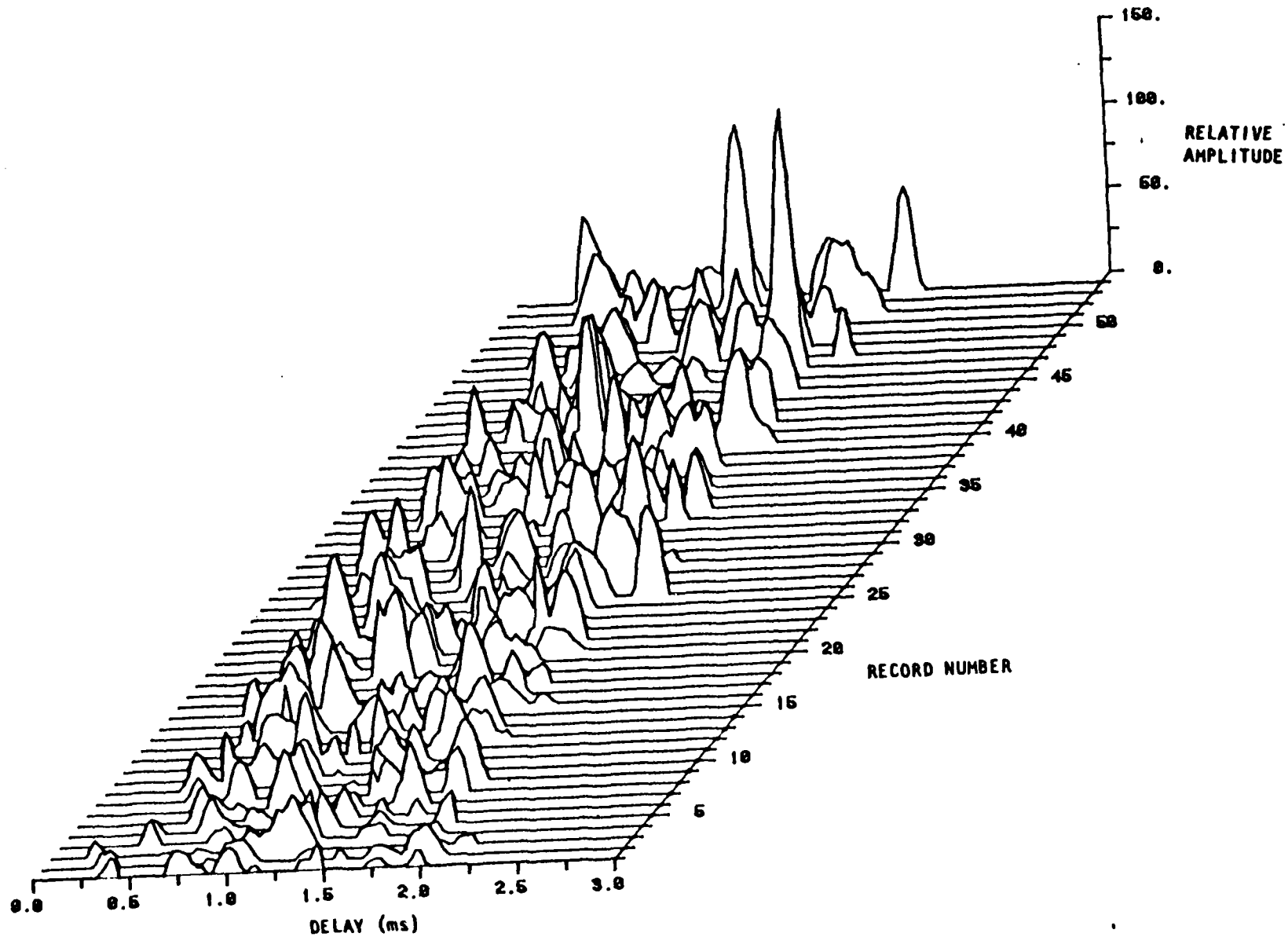

Figure ES-3 Series of multipath snapshots on 19 September 1985 with antenna's on great circle path showing combination of meteors and auroral scatter. Large meteors are evident in snapshots 46, 53 and 54.

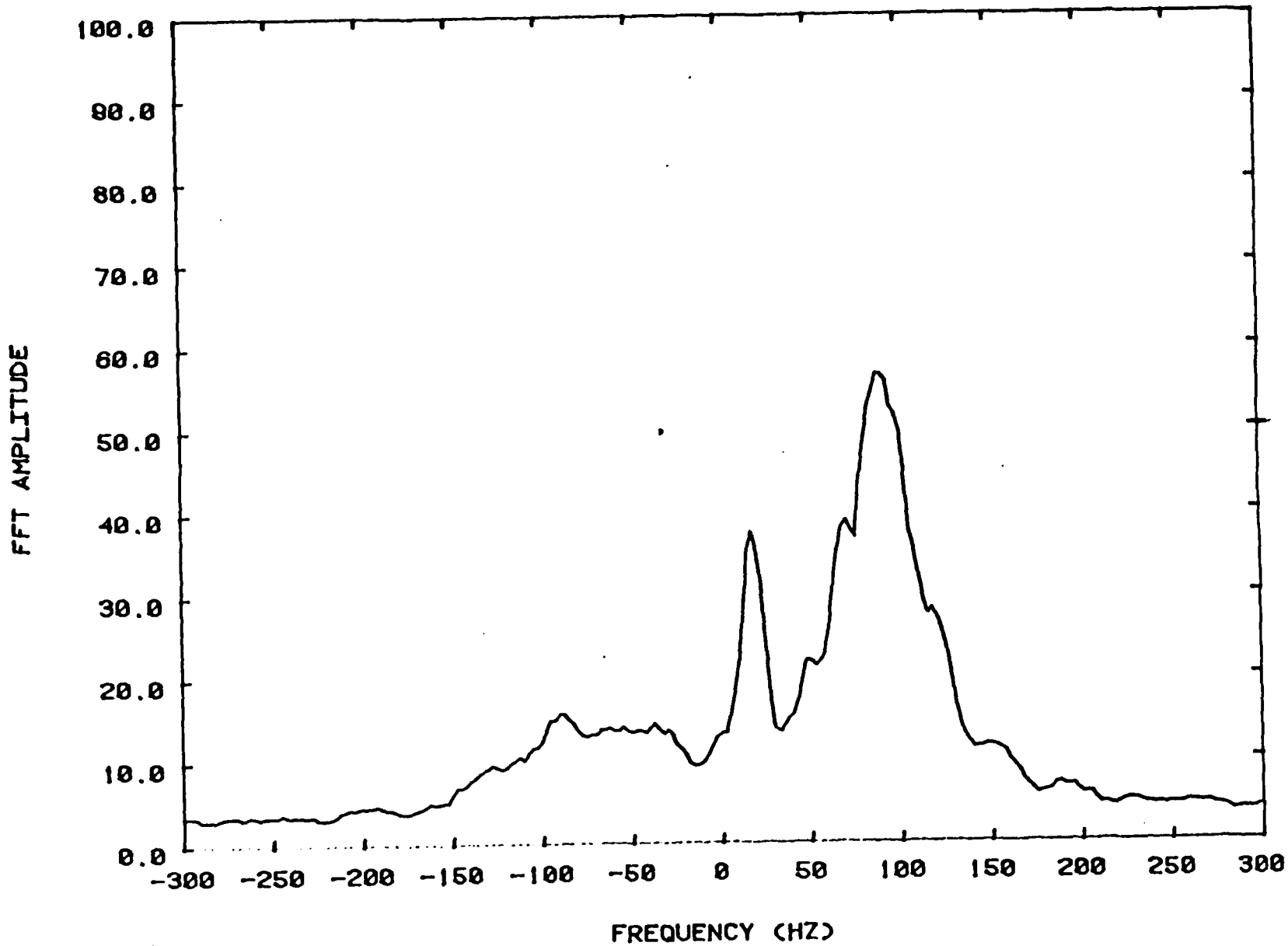

Figure ES-4 Composite Doppler profile for period shown in Figure ES-3. Component centered on zero shift corresponds to meteor propagation and the shifted component is due to the auroral scatter.

frequency is due to scatter for meteors and the component centered at about 80 Hz is due to scatter from the aurora. These figures show how auroral scatter can transform the benign meteor scatter channel into a fast fading high multipath channel.

The degree, if any, to which auroral scatter will disrupt a given meteor communication link depends upon the antenna patterns, transmitter power, and the location, orientation and ionization density of the aurora relative to the link. In the experiment, we have demonstrated that the potential exists for disruption. Communication using coherent modulation at conventional meteor burst data rates (4 to 8 kbps) in the fast fading, high multipath environment shown in Figures ES-3 and ES-4 would be virtually impossible.

At a minimum, protocols for a network operating in auroral regions must be designed to allow operation of a network even if there are continuous, yet potentially unusable channels contending for the network. To actually communicate over the disturbed auroral channel two techniques can be used. Advanced equalization techniques using implicit diversity (such as those applied to the multipath-limited troposcatter channel) can be used to exploit the characteristics of the multipath spread. A simpler technique is to reduce the data rate to less than the multipath spread and use coding with non-coherent modulation to maintain communication.

Taking into account the undesirable occasional disruption due to auroral scatter, meteor burst still has many advantages over HF which can be even more effected by these same phenomena. Auroral scatter degradation at meteor burst frequencies, may be absorption blackout conditions at HF.

The work described in this and the companion theoretical development by Málaga represent an important first step in scientifically evaluating the reliability of meteor burst communica-

tion at high latitudes. The research results must now be applied to practical communication systems. A new meteor burst comunication network will become operational in 1986 to provide austere backup communication between remote radar sites in Alaska and the regional control center in Anchorage. A natural and important follow-on to the experiment described in this report should be to collect data from the Alaskan Air Command on the performance of the various links in the network to assess which links are dominated by sporadic-E channels, and which links, if any, are limited by auroral scatter effects. Data should be compared to the predictions of Málaga to calibrate and validate the model.

Links showing auroral scatter performance degradation should be instrumented to determine the multipath and Doppler spread. Using the validated model and data from the experiment, techniques to mitigate the degradation could be developed including adaptive antenna steering, reduced data rate operation, increased operating frequency, and adaptive message routing.

ACKNOWLEDGMENTS

The authors and participants in the experiment are grateful to Mr. John Williford and his successor Mr. Fred Jack of the Federal Aviation Administration in Bethel, Alaska, for their assistance in the experiment. They and their staff provided a site for the receiver equipment and performed routine maintenance on the equipment. Their help and support, above and beyond their normal duties, was key to the success of the program.

We would like to thank Meteor Data Corporation in Anchorage who provided the transmission services for their cooperation in the experiment and tireless maintenance of the high power transmitter required for the experiment.

A number of engineers and scientists both at SIGNATRON and the U.S. Air Force RADC/EEPS contributed to the success of the program. Software to control the data acquisition equipment and perform on-site data processing was written by Mr. Mike Sowa of the USAF-RADC/EEPS. The installation of the equipment in Bethel, under very trying conditions, was performed by Second Lt. Robert Scofideo of the Air Force and Mr. Michael Bosowski of SIGNATRON. Dr. Alfonso Málaga of SIGNATRON developed the theory of VHF scatter presented in a previous report and advised and reviewed the design of the experiment and the proposal for the data analysis and reduction. Dr. Steen Parl of SIGNATRON was overall program manager and participated in the design review and his contributions were valuable.

Finally the idea of establishing a dedicated link in Alaska to measure multipath and Doppler as part of the High Latitude Meteor Burst Measurement program was attributable to branch chief Mr. John Rasmussen, currently with Air Force Geophysics Laboratory. His successors, Dr. Paul Kossy and Mr. John Hecksher carried the ideas through to completion.

SECTION 1
INTRODUCTION

Meteor burst communication uses the ionized trails of meteors for long distance digital communication. At high latitudes meteor burst has several potential advantages over HF for long haul digital communication applications. Because meteor burst operates at higher frequencies, 40 to 100 MHz versus 2 to 30 MHz for HF, it is much less sensitive to polar cap absorption events which can create HF blackout conditions. Meteor burst can operate at a constant frequency unlike HF which requires frequency management due to the diurnal and seasonal changes in the maximum usable frequency (MUF). Meteor burst is, however, not totally immune to high latitude effects and in order to accurately assess the reliability of meteor burst as an alternative to HF at high latitudes, a thorough understanding of the characteristics of the high latitude meteor channel is required.

Previous high latitude meteor burst efforts [Maynard, 1972; Ostergaard, 1985; Cannon, 1985] have focused on determining the statistics of meteor arrivals, durations, waiting time distributions and the effect of polar cap absorption events on these statistics. The fading and multipath profile of the high latitude channel has been assumed to be similar to the mid-latitude channel. Recent experiments indicate that this assumption is not totally valid because it neglects the effects of frequently occurring high latitude propagation phenomena such as scatter from the aurora and sporadic-E layer propagation. This report discusses the results of several experiments in which the fading and multipath profiles of the high latitude meteor channel were characterized. The results are combined with the knowledge of the mid-latitude channel to develop a latitude dependent multipath and Doppler profile for the meteor channel.

Development of a multipath model for the high latitude meteor channel begins in Section 2 with a review of the characterization of the middle latitude meteor channel. Multipath on the middle latitude meteor channel occurs primarily due to the occasional occurrence of more than one meteor or due to multiple reflections from a single trail which has warped due to high altitude wind shears. Results from several middle latitude multipath characterization experiments are presented.

Section 3 of this report discusses several propagation mechanisms occurring primarily at high latitudes which can degrade or enhance meteor communication. These mechanisms incude scatter from the aurora, and sporadic-E related phenomena. The theory of these propagation mechanisms is presented in Málaga [1986]. Two experiments to characterize multipath phenomena of VHF channels at high latitudes are described.

The first experiment, described in Section 4, used the large bandwidth (330 KHz) allocation on the 1260 km USAF high latitude meteor burst test bed from Sondrestram AB, Greenland to Thule AB, Greenland. High resolution multipath measurements were performed on sporadic-E and meteor channels in the 45 MHz band.

The second experiment described in Section 5, used a dedicated link (640 km) from Anchorage, Alaska, to Bethel, Alaska, operating at 42.4 MHz to perform lower resolution multipath measurements on sporadic-E, auroral, and meteor channels. The Alaska link represented the primary research tool in the multipath measurement program.

Finally, Section 6 discusses the ramifications of the findings on the reliability of meteor burst communication at high latitudes.

SECTION 2

THE MULTIPATH STRUCTURE OF THE METEOR CHANNEL

2.1 DIFFUSE MULTIPATH FROM A SINGLE METEOR TRAIL

Meteor channels form when the ionized trails of meteors entering the atmosphere satisfy the following geometric requirements shown in Figure 2-1.

1. The point of tangency of a line defining the center of a cylindrical meteor trail to an ellipsoid of revolution with foci at the receiver and transmitter lies within the volume common to both the receive and transmit antenna patterns.

2. The region of the cylinder defining the meteor trail which contains ionization fills at least one-half of the Principal Fresnel Zone. The Principal Fresnel Zone is the region of the trail such that the distance from transmitter to receiver through a point on the trail differs by less than one-half wavelength from the distance to the point of tangency. All scatterers within this region contribute constructively to the received signal while scatterers within higher order Fresnel zones, which are much smaller, contribute alternately constructively and destructively to the received signal. The length of the Fresnel Zone is dependent on link distance and frequency. Typical meteor trails are 15 to 50 km in length and the Principal Fresnel Zone is about 1 to 4 km at 50 MHz.

At the time of formation, meteor trails can be modeled as lines or narrow cylinders of electrons. Immediately after formation, the trails begin to expand due to diffusion. In most trails the electron density is low enough so that each electron is assumed to scatter independently of all other electrons and the received power is computed by integrating the contribution from all scatterers over the entire trail. This type of trail is referred to as an underdense trail. Closed form solutions for the power scattered by underdense trails and its decay as the trail expands have been derived by Eshlemman [1955].

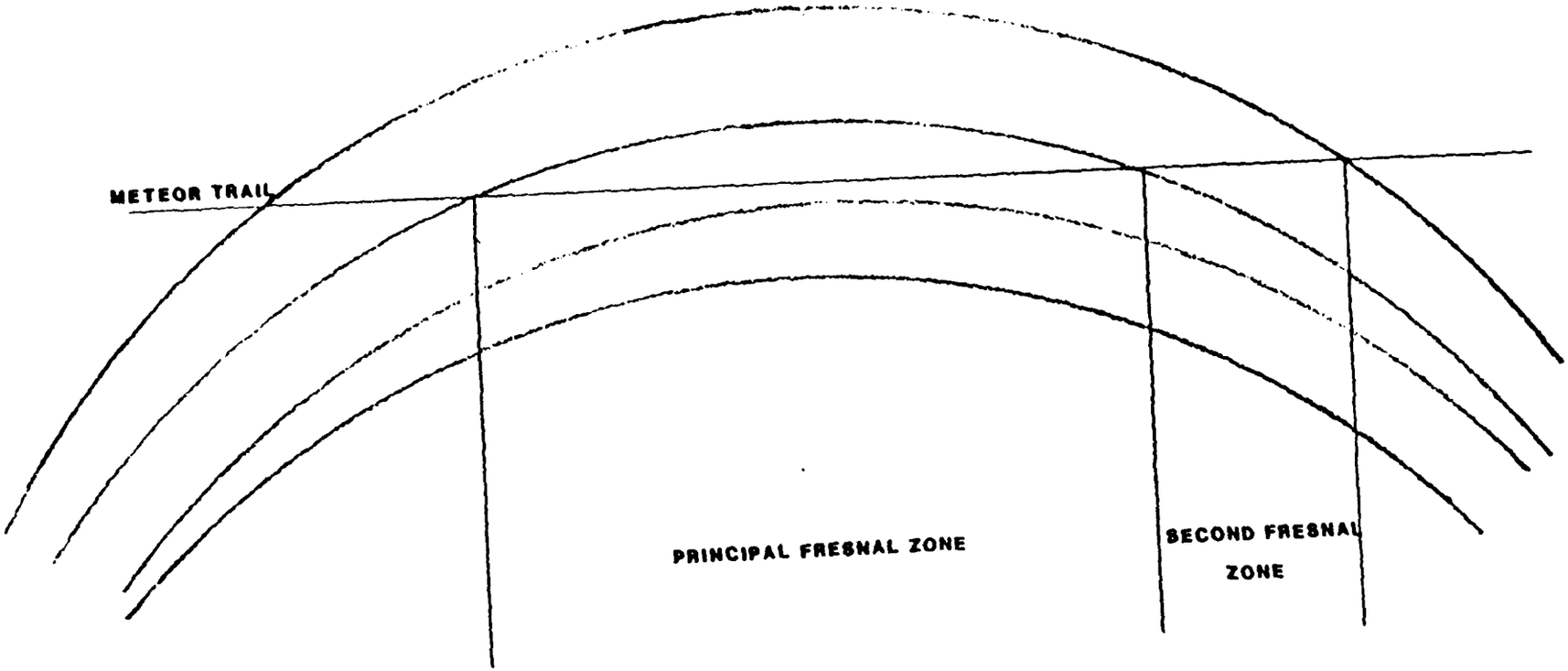

Figure 2-1 Initially Linear Meteor Trail Showing Primary and Secondary Fresnel Zones.

Underdense trails form rapidly and then decay exponentially with time constants on the order of 200 to 400 ms at 50 MHz [Sugar, 1964]. From a multipath viewpoint, the underdense meteor channel is very benign, limited only by the several Fresnel zone diameter of the trail as it expands. Each Fresnel zone into which the trail radially expands adds multipath corresponding to one-half wavelength path delay or about 10 ns at 50 Mhz. It is the integration of the Gaussian radial electron density of the trail as it diffuses radially into higher order Fresnel zones that causes the exponential decay of the total scattered power.

The coherence bandwidth, defined as the inverse of the delay spread, is a measure of the maximum data rate that can be transmitted without intersymbol interference. If symbols are transmitted at a rate greater than the coherence bandwidth, total overlap of adjacent symbols will occur. For practical systems which do not employ equalization, the maximum symbol rate to avoid intersymbol interference should be about one-tenth the coherence bandwidth. The coherence bandwidth of underdense meteor channels is on the order of several megahertz allowing symbol rates without intersymbol interference as high as 1 million symbols/sec. Unfortunately, the several megahertz coherence bandwidth of the underdense trails is difficult to exploit since in most meteor communication applications, the channel is signal power limited (due to the 150 to 160 dB path loss) rather than multipath limited. Many trails can support data rates in the hundreds of kilobits per second for a short time if fully adaptive communication systems are used [Weitzen, 1983, Weitzen, et al., 1984].

As the trail density and received signal power increases, the model for the trails begins to change as the assumption that all electrons scatter independently begins to break down. The model for the received power becomes complicated as the electrons begin to interact and only rough closed form approximations to

the received power exist [Hines and Forsythe, 1957]. These trails are referred to as overdense. As the trails become denser, the lifetime above a given signal threshold tends to increase so that high altitude wind shears have time to effect the trail geometry. These winds can act on an initially linear meteor trail shown in Figure 2-1 until it becomes warped and distorted as shown in Figure 2-2. Fresnel zones are superimposed on both Figures 2-1 and 2-2 for reference. Note in Figure 2-2 that portions of the trail which were initially in the Principal Fresnel zone contributing constructively to the received signal are now in higher order Fresnel zones contributing destructively. The result of the time changing trail distortion is fading, although the delay spread of the trail is still very small because the majority of the trail lies within several Fresnel zones.

2.2 DISCRETE MULTIPATH FROM A DISTORTED METEOR TRAIL

On occasion, a trail can distort so that several regions in the trail meet the requirements for specular reflections outlined earlier. This phenomenon, which occurs much more frequently for backscatter geometries than forward scatter, was first described by Manning [1959]. Sugar, et al. [1960] extended the backscatter work of Manning to forward scatter and estimated some worst case multipath spreads. As an example, consider a 1200 km link with a 20 km meteor trail oriented normal to the great circle path with one end of the trail at the mid-point of the path. Assume that a second reflection point occurs at the far end of the trail. Using simple geometry, the worst case delay between the two components would be 3.7 μs. Most spreads are far less than the worst case. These spreads coincide with the experimental measurements of Weitzen [1983] and Carpenter and Ochs [1962].

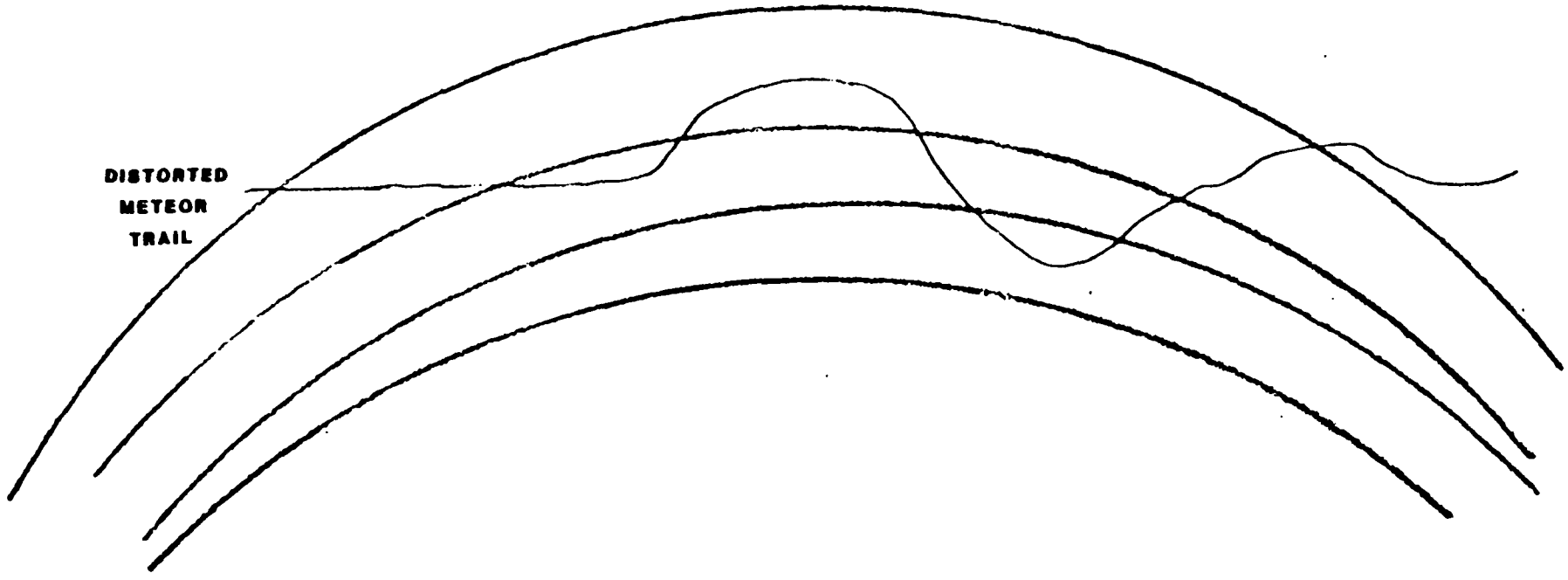

Figure 2-2 Warping of an Initially Linear Meteor Trail Due to High Altitude Wind Shears. Fresnel Zones are Superimposed to Show How Fading With Very Low Multipath Spread Can Occur.

2.3 DISCRETE MULTIPATH FROM MULTIPLE METEOR TRAILS

An event that could cause more severe multipath interference is the simultaneous occurrence of two or more meteors within the common volume of the receiver-transmitter antenna pattern. Relative delays beween components of 1 ms are possible.

We now attempt to predict how often this event might occur. Let T_L be the lifetime of a trail defined as the interval during which the power scattered by the trail exceeds an arbitrary signal threshold. A multiple trail event occurs when, during the lifetime of a given trail, T_L, one or more additional trails occur which exceed the received signal threshold.

Meteor trails arrive randomly so that the probability of exactly k trails arriving within a time T, $P_k(t)$, can be described by a Poisson process as

$$p_k(T) = \frac{e^{-L_c T}}{k!} (L_c T)^k \qquad (2.1)$$

where L_c is the average arrival rate (trails/sec)of meteor trails whose scattered signal strength exceeds the minimum signal strength required for reliable communications. To aid the analysis, we will assume that all meteor trails decay according to the underdense model. This assumption is often used because it allows the memoryless property of the exponential decay to be used to develop closed form solutions. Using this assumption, the distribution of trail lifetimes, T_L, was theorized by Sugar [1964] to be exponentially distributed as

$$P(T_L > T) = e^{-\frac{T_L}{\tau}} \qquad (2.2)$$

where

T_L is the lifetime of the trail

τ is the average trail lifetime $\frac{\lambda^2 \sec^2 \phi}{16\pi^2 \bar{D}}$

λ is the wavelength of the carrier

$\bar{D}$ is the average diffusion constant = 8 m^2/sec

ϕ is the angle of the incident wave relative to the normal to the trail.

The probability that during the lifetime T_L of a trail, one or more trails occur which exceed the communication threshold is given by

$$P(\text{one or more trails} \mid \text{trail with lifetime } T_L) = \sum_{k=1}^{\infty} \frac{(L_c T_L)^k}{k!} e^{-L_c T_L} = 1 - e^{-L_c T_L} . \quad (2.3)$$

It can be seen from Equation (2.3) that for trails with short duration, the probability of multiple trail occurrence is very small. The probability of multipath interference, P_m, is determined by integrating the density conditioned on lifetime Equation (2.3) over the exponential density of lifetimes Equation (2.2) as

$$P_m = \int_0^{\infty} \frac{e^{-\frac{T}{\tau}}}{\tau} (1 - e^{-L_c T}) dT = 1 - \frac{1}{\tau L_c + 1} \quad (2.4)$$

As an example, assume that the arrival rate L_c of meteor trails which exceed the communication threshold is 2.5 trails per minute (0.0416 trails/sec). Let the average lifetime τ of the trails be 400 ms. From Equation (2.4), there is a 1.6 percent probability that there will be some degradation in the error probability due to multipath interference.

2.4 REVIEW OF PREVIOUS MULTIPATH EXPERIMENTS

Several experimental efforts have been undertaken to characterize the multipath profile of the meteor channel at mid-latitudes. Carpenter and Ochs [1962], conducted the most extensive experimental program using an 800 kW (standard meteor communication systems generally have transmitters with less than 1 kW output) peak pulsed power forward scatter radar with a 3 μs pulse duration operating at a frequency of 41 MHz. With the high pulsed power signal, a weak component due to ionospheric scatter was observed in addition to meteor propagation. The primary multipath mechanism observed by Carpenter and Ochs was the simultaneous occurrence of more than one meteor within the common volume. With the 800 kW transmitter, the average time between the arrival of meteors was on the order of several hundred milliseconds. They observed that on about 6 percent of the meteor channels, a second discrete component less than 6 dB down from the main component was present. Multipath spreads varied from the resolution of the equipment up to the maximum 1 ms resolution.

In order to predict the effect of two-trail multipath on actual communication systems, they interpolated the results of the 800 kW experiment to a 1 kW communication link and compared the predictions to the performance of an actual system [Sugar, et al., 1960]. Depending on the value of several constants, they predicted that multipath would occur from 1 percent to 3 percent of the time. The predictions compare well to their experimental measurements and to Equation 2.4.

On many occasions, they observed enhanced propagation due to sporadic-E or enhanced E-layer propagation. The majority of these events were characterized by one discrete component; however, during one of these events, two discrete layers with 20 μs relative delay were observed. In addition to multipath due to discrete layers, the combination of sporadic-E located near the mid-point of the great circle path and large meteors several hundred kilometers to the side of the mid-point path caused multipath with spreads up to the 900 μs resolution of the experiment.

On one occasion during a solar disturbance, scattering from what is believed to be the aurora was observed. Continuous spreads of at least 500 μs were observed for two hours.

Weitzen, et al. [1984] performed an experiment using television signals at 50 MHz (Channel 2) as a wideband probing waveform, (6 MHz bandwidth) extending the work of Grossi and Javed [1971]. One microsecond resolution was obtained and little multipath was observed, confirming the findings of Carpenter and Ochs.

SECTION 3
EXPERIMENTS TO CHARACTERIZE THE HIGH-LATITUDE VHF CHANNEL

The characteristics of the VHF meteor channel at high latitudes appear, from preliminary results obtained using the USAF High Latitude Meteor Test Bed [Ostergaard, et al., 1985], to be similar to the characteristics at middle latitudes. However other propagation mechanisms, such as scatter from the aurora and sporadic-E propagation, occur much more frequently at high latitudes than at middle latitudes, creating the potential for extended periods when meteors are not the dominant propagation mode on a VHF link.

We have taken a two-step approach to characterizing the effects of these mechanisms on meteor communication links. Prior to an experimental program Málaga [1986] developed the theory of VHF scatter from the aurora so we would know what to expect from the experiment. Next, a two phase experimental program was developed which is described in the next sections.

3.1 EXPERIMENTAL GOALS AND REQUIREMENTS

The objective of the experimental program was to develop and implement a relatively inexpensive technique to characterize multipath and Doppler spreads on a number of different types of channels. To characterize the channel completely, multipath spread, Doppler spread, and signal strength statistics are required. In the experiment we decided signal strength statistics, though desirable, would be secondary to the primary multipath and Doppler spread statistics. This decision was based on the added costs required to accurately calibrate and maintain calibration on the receiver, the potential inability to maintain constant transmitter power on the Alaska multipath link, and the fact that detailed signal strength statistics for meteor scatter propaga-

tion and sporadic-E propagation are currently being collected on the high latitude testbed. A further concern during the experiment design was the requirement that the equipment be totally automated to a point where the only service required would be, at most, bi-weekly maintenance to change data tapes.

A real-time RAKE receiver or a very high power wide-band pulsed radar are two techniques which are best suited to multipath probing. Both techniques are, however, expensive and difficult to implement: the real-time RAKE, due to the complicated hardware required to perform correlations in real-time, and the pulsed radar due to the very high power (Carpenter and Ochs used 800 kW) transmitter required. Acquiring data and processing it at a later time is a third technique which has the advantage of being much less expensive than the real-time RAKE receiver. The disadvantages of this technique are large data storage requirements, potentially high data analysis costs, and inability to provide on-site monitoring of multipath and Doppler spreads.

The compromise solution selected for the experiment was to use the signal processing capability of the Data Precision D-6000 signal analyzer to preprocess the data on-site. Data would be collected during a portion of each hour and processed during the remaining time providing near real-time monitoring of channel conditions. Only preprocessed data would be retained for analysis at a later time. The D-6000 analyzers were available due to their extensive use in the high latitude program as were the cassette tape drives and the HP-85 controller. While other equipment might have been more optimal for the application, the cost savings incurred using the existing equipment and the experience of RADC/EEPS personnel in the design of experiments based on this equipment weighed heavily in the decision.

A preliminary experiment was designed to test the correlation, data processing, and control algorithms on the existing

USAF High Latitude Meteor Test Bed in Greenland. A secondary objective was to use the 330 KHz bandwidth available on the link to investigate the fine-structure of sporadic-E multipath and/or multiple meteor trail occurrences. The results of this experiment are described in Section 4. Figure 3-1 shows the 1260 Greenland link from Sondrestrom to Thule.

With the lessons of the preliminary experiment, a large scale experiment was undertaken to characterize the multipath and Doppler spreads of auroral scatter, sporadic-E and meteor channels. Cost constraints required scaling down the experiment to use leased transmission time from a meteor burst common carrier company in Anchorage instead of a dedicated link for transmission services. The results, nevertheless, were successful and are described in Section 5. Figure 3-2 shows the Primary Link from Anchorage to Bethel, Alaska.

Figure 3-1 Location of High Latitude Meteor Burst Test Bed in Greenland.

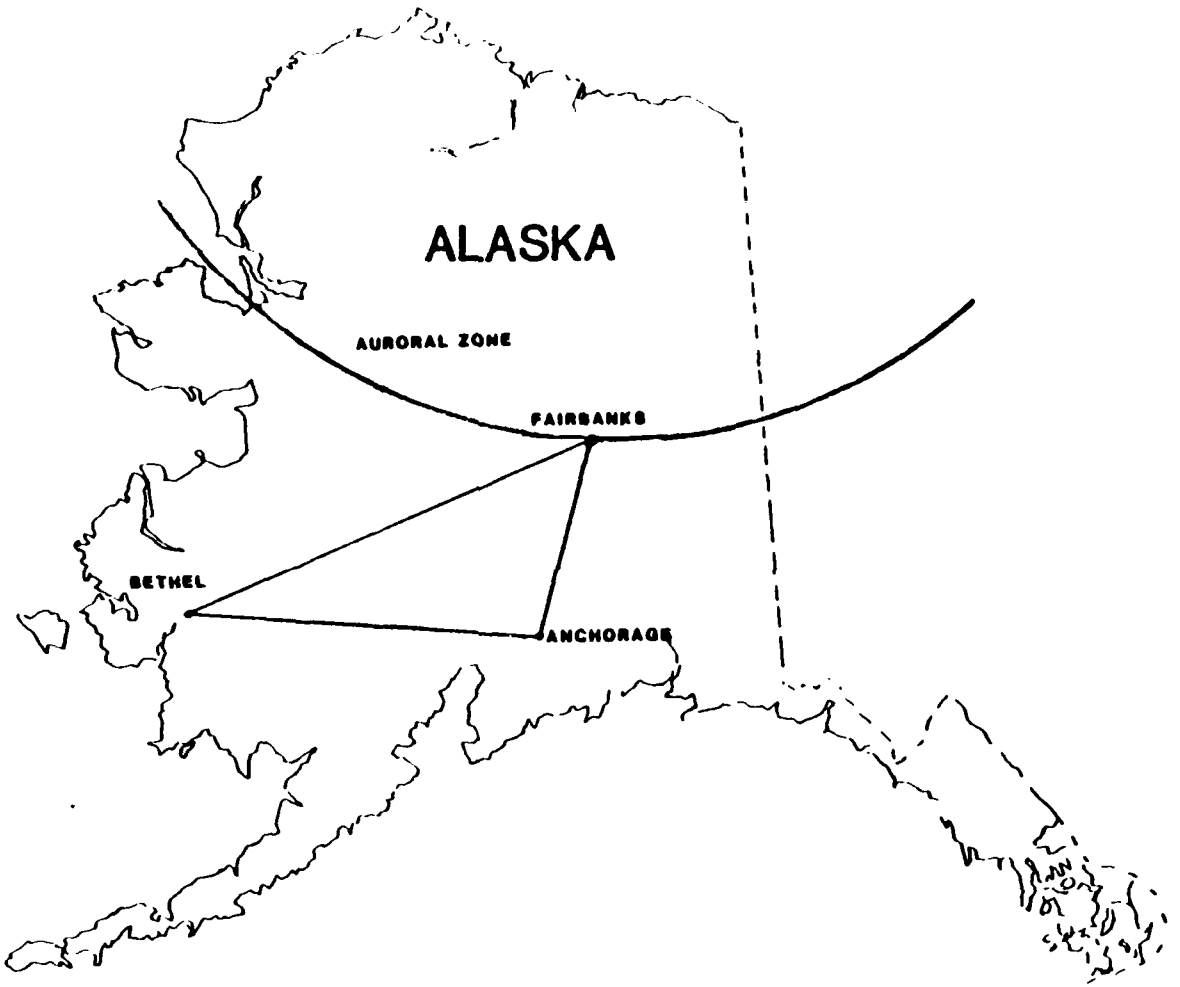

Figure 3-2 Location of Auroral Scatter Multipath Measurement Link in Alaska.

SECTION 4
PRELIMINARY MULTIPATH EXPERIMENT IN GREENLAND

A preliminary experiment to develop and test channel probing algorithms and waveforms and to characterize the sporadic-E channel with a 330 KHz waveform was performed in Greenland using the U.S. Air Force High Latitude Meteor Burst test bed with transmitter at Sondrestrom Air Base and receiver at Thule Air Base. This link is one of the few locations where wide transmission bandwidths are still available in the low VHF band (crowding in the low VHF band would prevent an experiment such as the Carpenter and Ochs experiment from being repeated in the continental United States in the foreseeable future). The link is well above the auroral oval and auroral scatter is not generally observed on the link; however, high latitude sporadic-E propagation is frequently observed.

4.1 *EQUIPMENT FOR GREENLAND EXPERIMENT*

Transmit equipment located at Sondrestrom Air Base, Greenland, shown in Figure 4-1a, consisted of an 800 Watt synthesized transmitter with 330 kHz bandwidth allocations at 45 MHz, 65 MHz and 104 MHz. The frequency allocation at 45 MHz was selected to maximize the observation of sporadic-E and meteors. Five element Yagi antennas, 1.5 wavelengths above the ground were used at both the transmit and receive locations. The peak gain of the antennas was about 10.5 dBi.

A maximal length cyclic pseudorandom (PR) sequence was transmitted as the probing waveform (instead of a pulsed waveform as in the Carpenter and Ochs experiment), to provide processing gain to offset the lower transmitter power. The tradeoff in using the PR sequence is that more complicated receiver processing is required. The length of the PR sequence was chosen so as

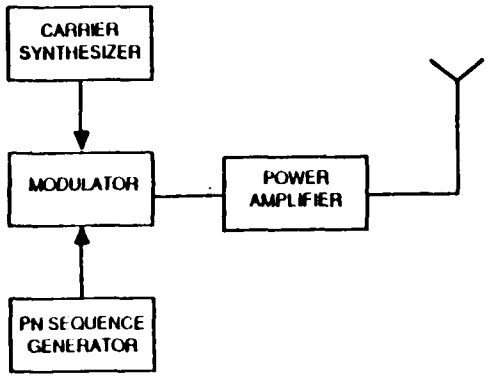

Figure 4-1a Configuration of Transmit Equipment for Preliminary Multipath Experiment in Greenland.

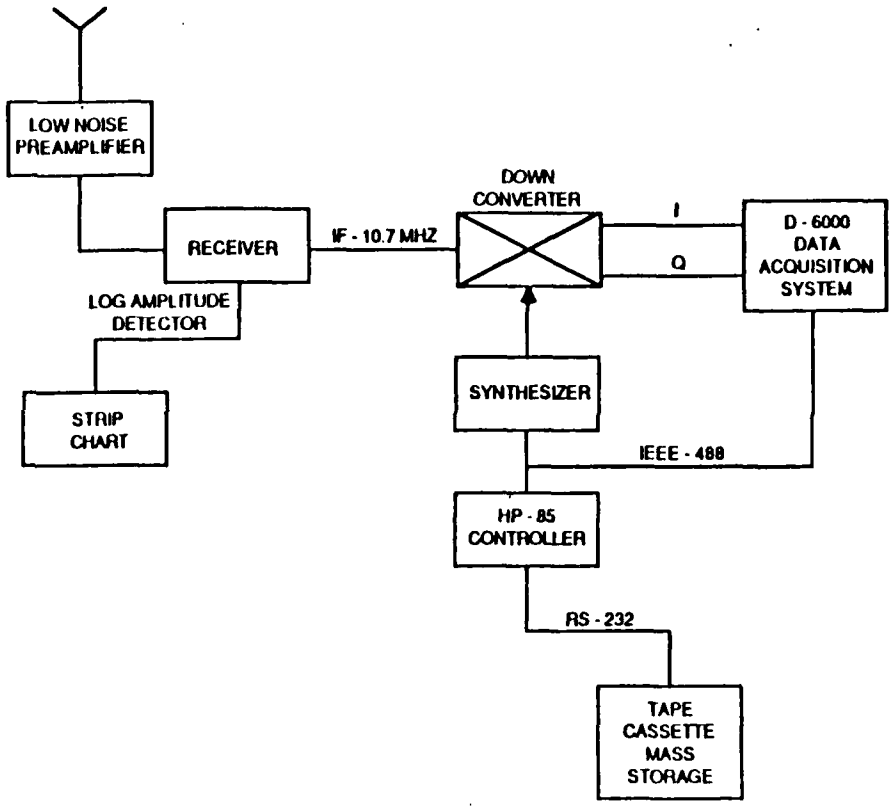

Figure 4-1b Receive Equipment Configuration for Greenland Multipath Experiment.

to optimize the processing gain and the maximum multipath spread that can be resolved while minimizing the degradation in processing gain due to frequency offsets between transmitter and receiver and Doppler shifts when noncoherent detection is used. Equation (4.1) relates the processing gain to the net frequency offset, sequence length and chip rate.

$$\text{Processing Gain} = L\left(\frac{\sin \pi \nu L T_c}{\pi \nu L T_c}\right)^2 \cdot \frac{1}{1 + \frac{2N_0}{LE_c}\left(\frac{\pi \nu L T_c}{\sin(\pi \nu L T_c)}\right)^2} \qquad (4.1)$$

where

L = Sequence length

ν = Frequency offset between transmitter and receiver including Doppler shifts and offsets

T_c = Chip period

E_c = Chip energy

N_0 = Noise density

Table 4-1 lists the characteristics of the probing waveform selected for the experiment. Assuming calibrated frequency synthesizers at receiver and transmitter so that the worst case transmitter - receiver frequency offset was 50 Hz, and assuming at most 100 Hz Doppler shift on meteor trails and sporadic-E, the worst case processing gain degradation, assuming high signal to noise ratio, is calculated from Equation (4.1) as

Gain degradation = -0.318 dB

Table 4-1 Waveform Characteristics for Greenland Experiment

Sequence Length (L)	127 Bits
Maximum Frequency Offset Between R_x and T_x	±50 Hz
Maximum Doppler Shift Expected	±100 Hz
Chip Rate	128 kb/s
Chip Period (T_c) and Multipath Resolution	7.8125 μs
Sequence Period or Maximum Multipath Resolution	992.29 μs
Processing Gain (Ideal)	21 dB
Worst Case Processing Gain Degradation (high SNR)	-0.318 dB
Number of Samples per Sequence Chip	8
Sampling Rate	1.024×10^6 samples/s
Bits/Sample	9

The receive equipment located at Thule Air Base, Greenland (see Figure 4-1b) consisted of custom designed low noise receiver with 10.7 MHz IF, quadrature IF to baseband downconverter, data acquisition system, data cassette mass storage device and HP-85 controller. The receiver had two outputs, an IF output which was non-coherently quadrature downconverted to baseband, and a log-amplitude detector calibrated to measure received signal power in the IF bandwidth of 330 kHz. A strip chart recorder was connected to the log-amplitude detector to record long term events and to aid in the determination of the multipath mechanism. RF and digital portions of the receive equipment were isolated in separate rooms to minimize interference. The data acquisition system consisted of a Data Precision D-6000 digital oscilloscope/signal analyzer with an 18 MHz dual channel A/D converter.

Data was acquired whenever the output of the log-amplitude detector, used as a trigger, exceeded a given threshold. Quadrature data was 9 bit quantized at a rate of 8 samples per PR sequence chip (1.024 Msamples/sec) and stored in D-6000 memory. In order to observe possible changes in the multipath profile during the lifetime of a meteor trail, each time the analyzer was triggered, a second trigger was forced about 850 ms later. After acquisition of two quadrature data records, post-processing was performed. Processing involved quadrature correlation of the data samples with a stored version of the transmitted PR sequence followed by computation of the square of the I and Q correlation components. The two processed waveforms and the quadrature correlations were then stored on tape for future analysis. During post-processing which required about four minutes for the two complex waveforms, data acquisition was disabled. Real-time matched filter correlation would have been a more efficient technique allowing for triggering on smaller meteors (the 20 dB processing gain is not achieved until the post trigger processing) and reducing the time required for processing; however, the cost of the equipment would have been prohibitive.

4.2 RESULTS FROM THE GREENLAND MULTIPATH EXPERIMENT

Data was collected for approximately 10 days during March 1985, after which interference with sensitive air traffic control equipment at Sondrestrom AB by harmonics of the wideband transmitted signal forced early termination of the experiment. Data from the experiment was preprocessed according to the procedure described earlier and stored on tape cassette. The final step in the data analysis which occurred after the experiment was concluded involved measuring and determining statistics of the multipath. See auroral scatter experiment for details of the process. Figure 4-2 shows an example of the correlations in which one discrete meteoric scatterer was observed. Figure 4-3 shows an example in which two discrete correlation peaks were observed. Using the strip chart recording as a guide, it was determined that the mechanism causing the multipath is most likely two meteor trails. The hundred microsecond delay between components eliminated trail warping as a possible mechanism and the strip chart showed no sign of background ionospheric or sporadic-E scatter. Figure 4-4 shows two very closely spaced components (less than 8 μs apart) which are most likely two closely spaced meteors but could possibly be due to warping of a single trail. Figure 4-5 shows the single discrete echo observed during a sporadic-E event. Figure 4-6a shows the probable occurrence of a meteor trail and sporadic-E. In Figure 4-6b, taken 850 ms later, the trail has decayed away.

Due to the long time required to process the two 1016 (127 chip sequence x 8 samples per chip) point complex correlation waveforms, sequences of snapshots showing the time history of sporadic-E events were not possible. This defficiency was corrected in the Alaska experiment. Due to early termination of the experiment, inadequate data were obtained for detailed statistical analysis; however, several qualitative conclusions from the limited data could be drawn.

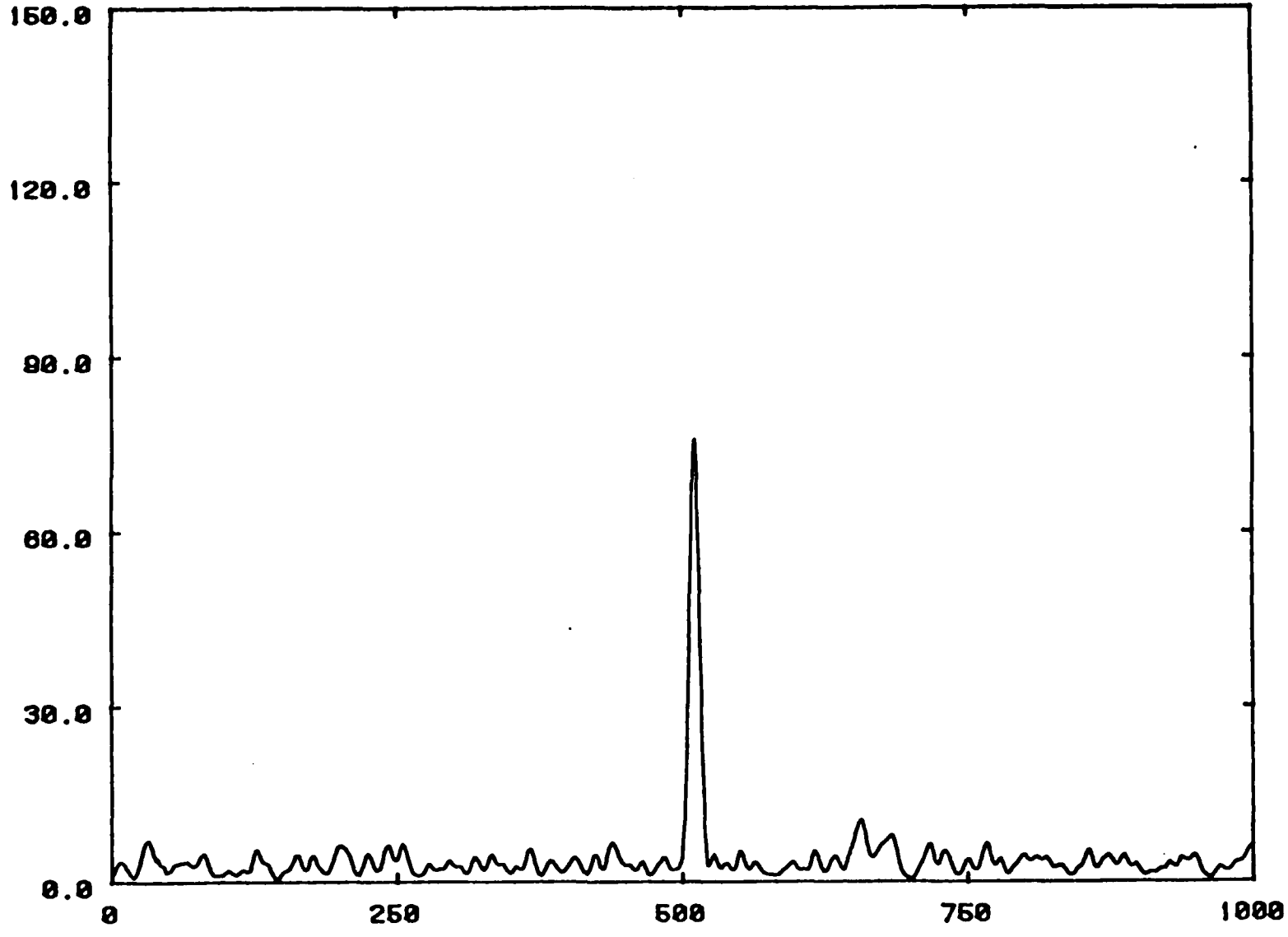

Figure 4-2 Multipath Snapshot Showing One Discrete Meteoric Component.

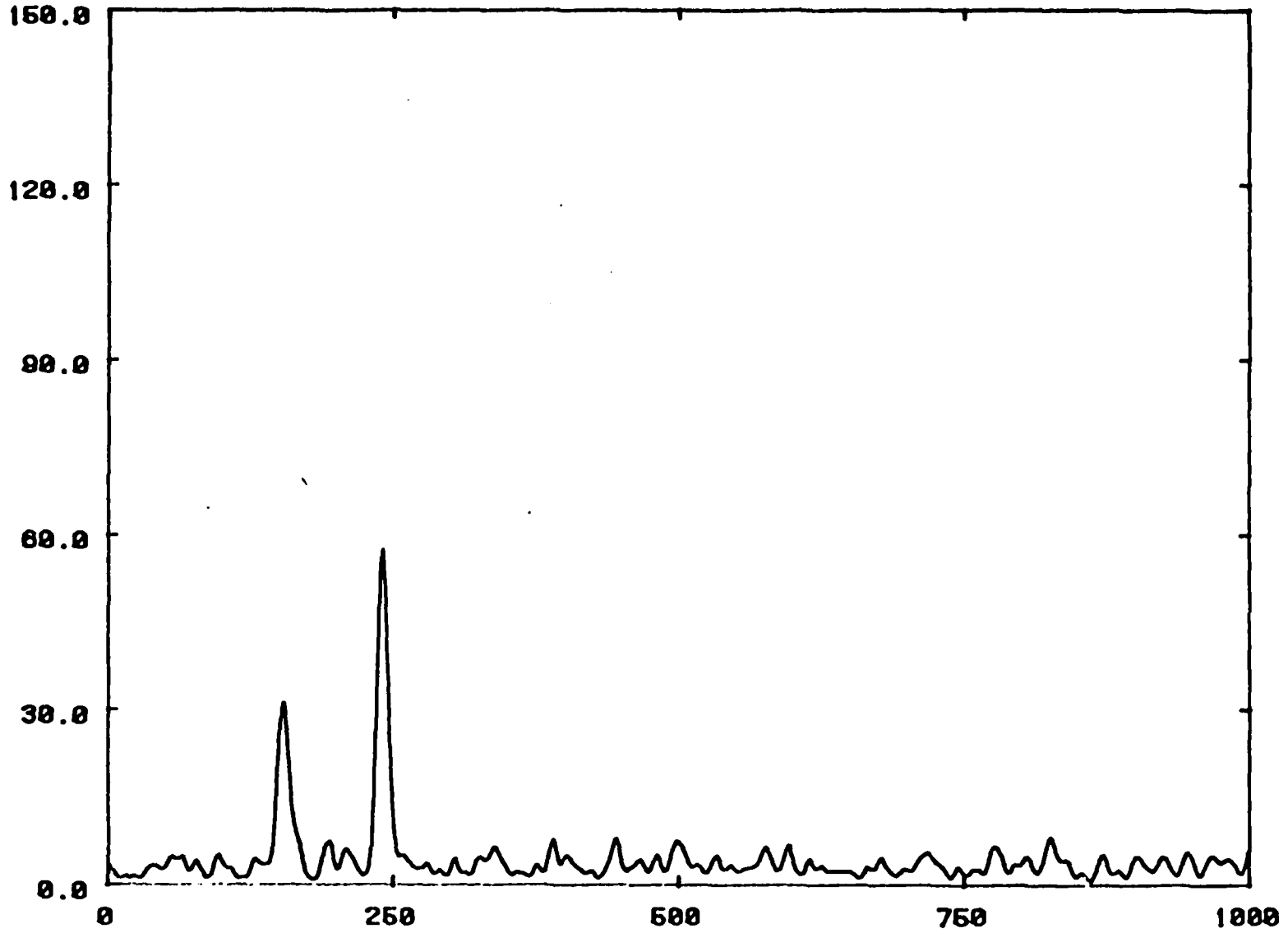

Figure 4-3 Multipath Correlation Showing Two Discrete Components Most Likely Due to Two Separate Meteor Trails.

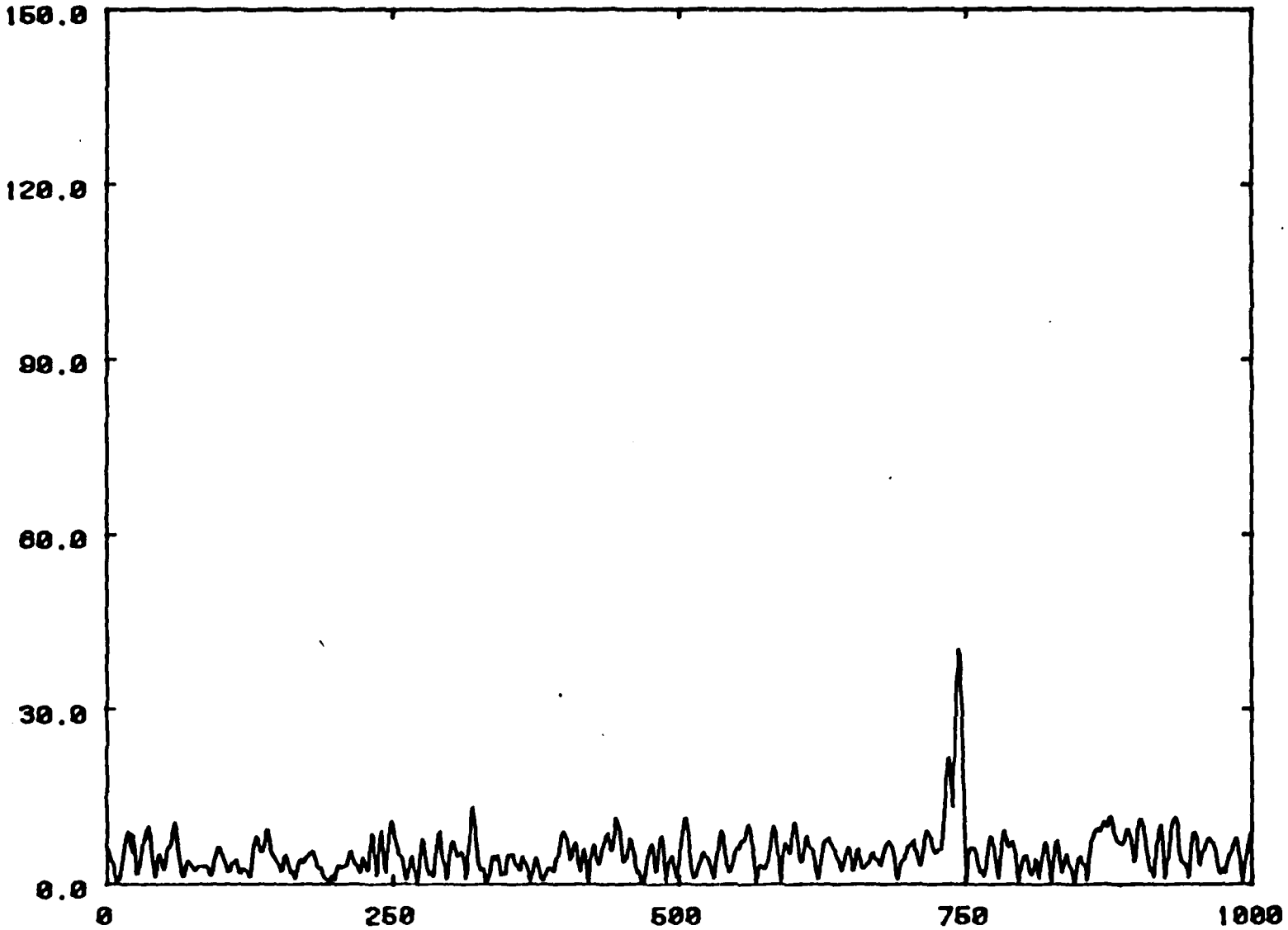

Figure 4-4 Two Closely Spaced Components Most Likely Caused By Two Meteors But Possibly Due to Warping of a Single Trail. Spacing of the peaks is less than 8 μsec.

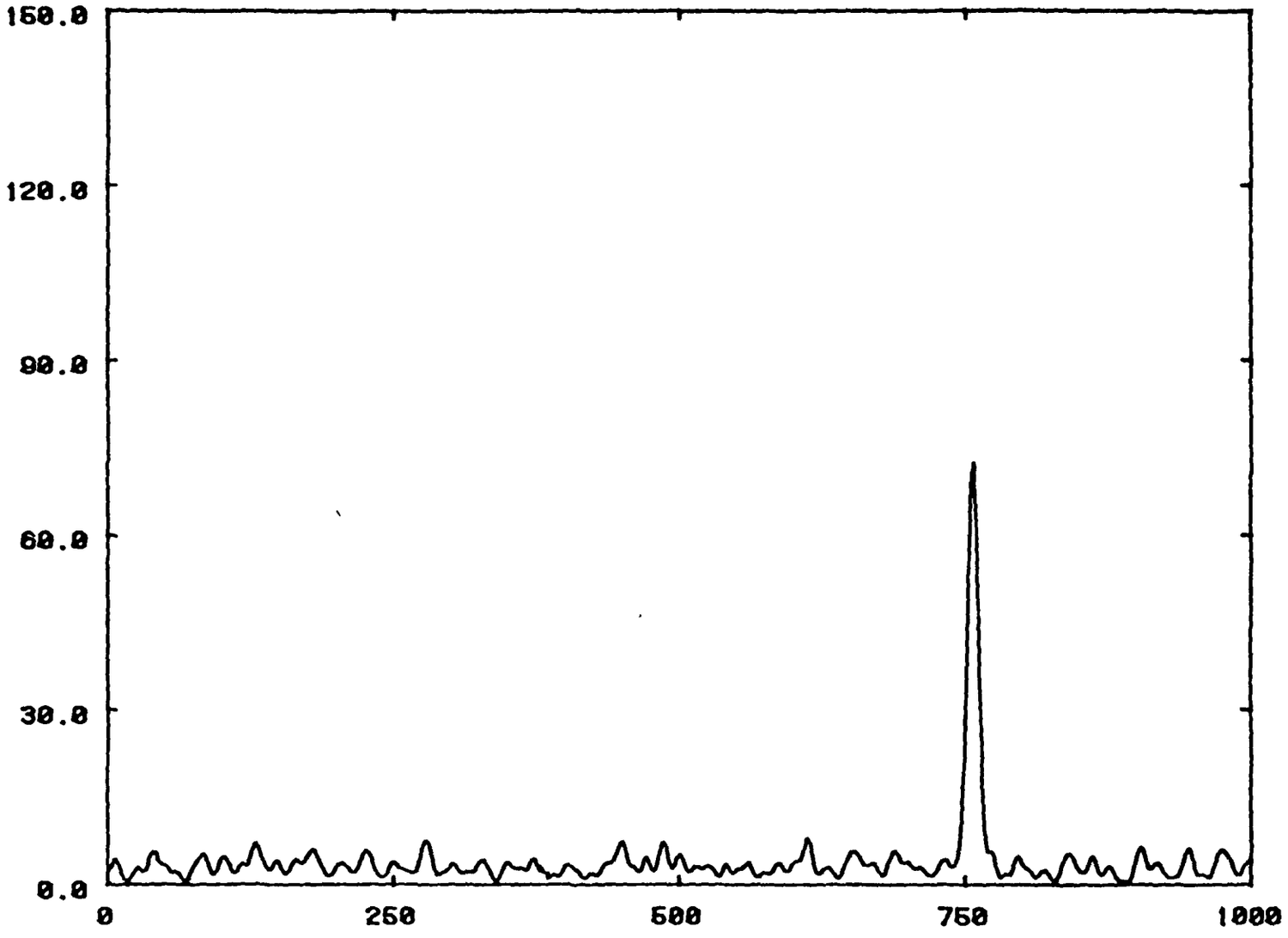

Figure 4-5 Single Discrete Scattering Component Observed During a Sporadic-E Event.

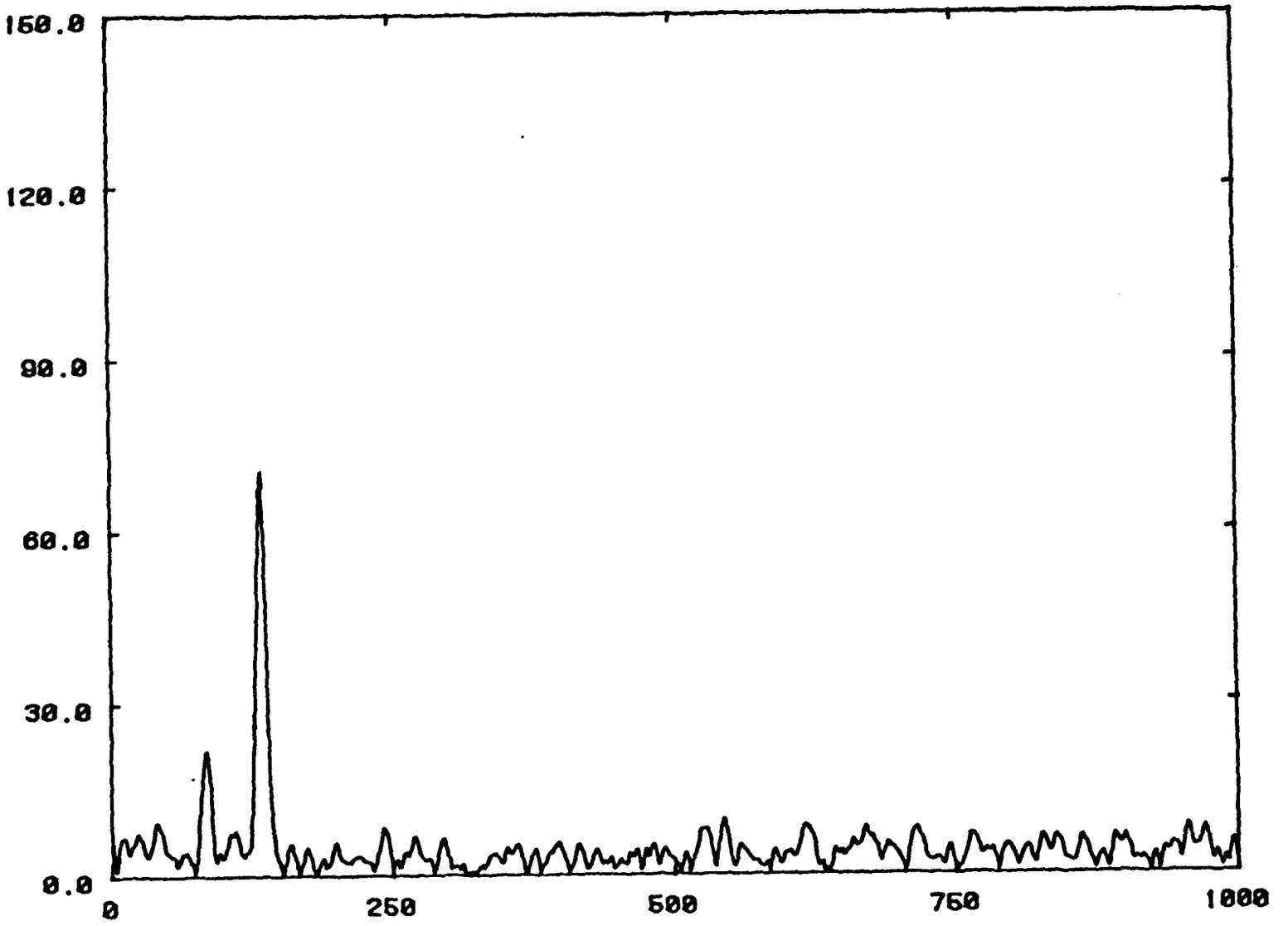

Figure 4-6a Two Discrete Echoes Most Likely Due to Combination of Sporadic-E and a Meteor Trail.

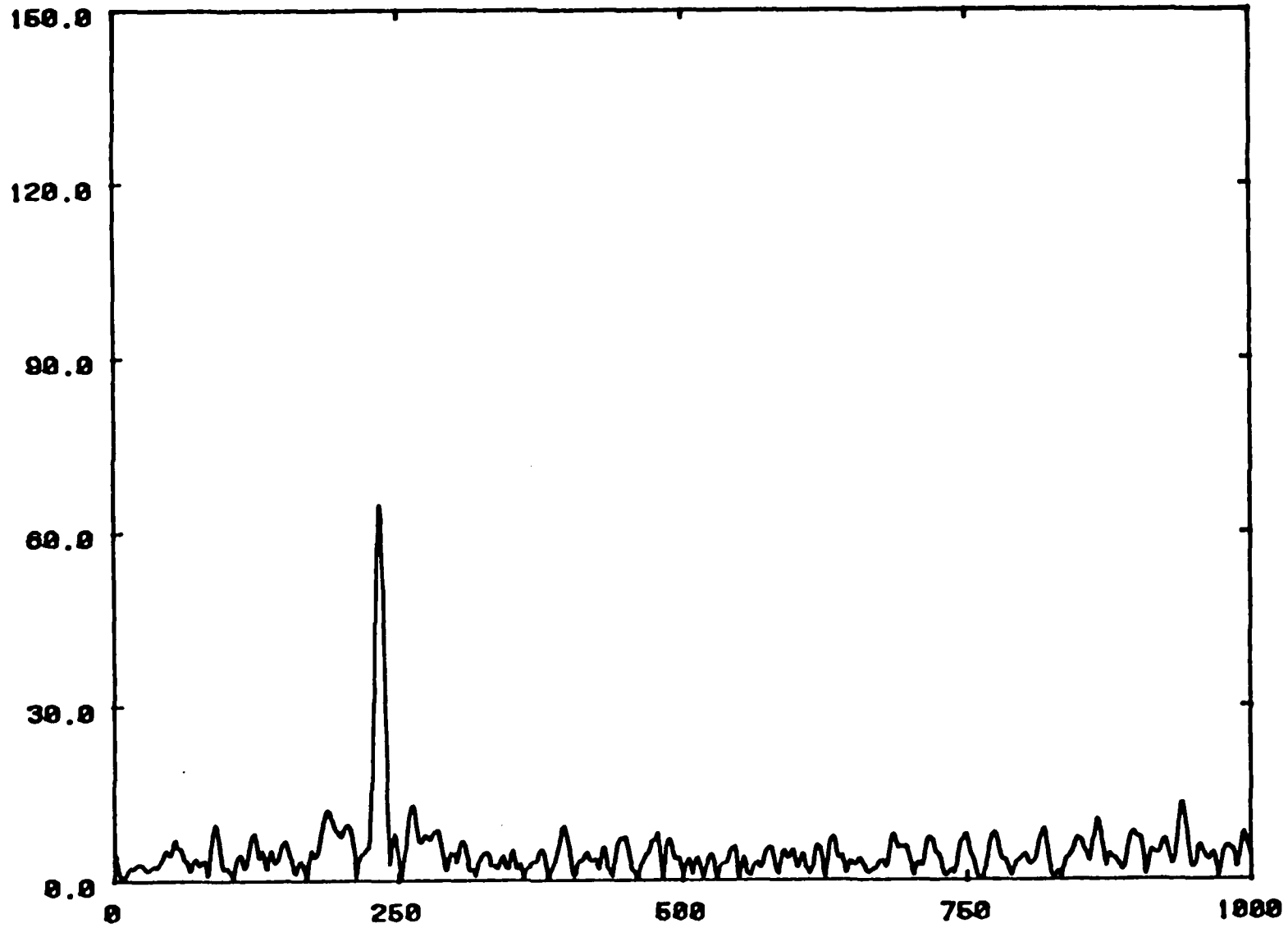

Figure 4-6b Multipath Snapshot 850 ms After Figure 4-6a, Showing Meteor Trail Having Decayed Away.

About 1500 pairs of waveforms (trigger followed by second trigger 850 ms later) were obtained during the 10 day period. About 550 of the pairs were discarded for various reasons, including false triggers and times during which the transmitter was not operational.

Of the remaining 926 records, 885 were due to meteors and the remaining 41 triggers occurred during sporadic-E events. Of the 885 meteor records, approximately 2 percent showed discrete multipath due to multiple meteors or trail warping within the 8 to 992 μs resolution of the experiment. The average spacing between discrete components was 226 μs. Sporadic-E was observed on several occasions and meteors combined with sporadic-E were observed. Table 4-2 summarizes the Greenland experiments.

While the data from this experiment was somewhat inconclusive due to the early termination of the experiment, the many lessons learned during the experiment were applied to the Alaska experiment and contributed to its success. These lessons were:

1. Collect data during events, process later rather than on the fly. This will capture data during infrequent events.

2. Add a CW probe period to perform FFT measurements to observe fading statistics.

3. Use less samples per chip to reduce processing time.

4. Collect more data records during a shorter period of time to provide time history of events. Use snapshots every few seconds rather than triggering on signals.

5. Compute histograms of received signal level.

6. Eliminate the second trigger 850 ms after first. It was of very little use and would have been of use only if we had greater resolution (less than 1 μs) to observe trail warping.

Table 4-2 Summary Greenland Multipath Experiment

Total Pairs Acquired	1482
Pairs Discarded	556
Valid Data Pairs	926
Number of Meteor Records	885
Number of Meteor Records Showing Multipath (meteors)	17 (1.92 %)
Average Spacing between Discrepancy Components	226 μs
Number of Sporadic-E Records	41
Number of Sporadic-E Records Showing Multipath	4 (9.7%)

SECTION 5
ALASKA MULTIPATH EXPERIMENT

The primary experiment was conducted in Alaska near the auroral region with the objective to observe multipath effects due to the combination of meteors, sporadic-E and scatter from the aurora. The maximum frequency allocation that could be obtained in Alaska was 15 kHz, using an existing meteor burst common carrier company. A high power transmitter (10 kW) with 16 dBi transmitter antenna was used to increase the probability of observing faint background ionospheric and auroral scatter. A ten minute period during each hour was leased from the common carrier service during which a probing waveform was transmitted. The probing sequence consisted of four minutes of CW for Doppler measurements and RSL histograms, five minutes during which a cyclic redundant 31 bit PR sequence was transmitted at 8 kbps for multipath measurements, and a one minute silent period for noise measurements. The transmitter located near Anchorage operated on an assigned carrier frequency of 42.4 MHz in a 15 kHz allocation.

5.1 EQUIPMENT FOR ALASKA EXPERIMENT

A receive site was required in which both auroral scatter and sporadic-E, in addition to meteors, were observable using the existing common carrier meteor burst transmission facility in Anchorage. Based on several prediction models [Málaga, 1986] in which the received signal level due to auroral scatter was estimated, Cape Romanzoff on the coast of Alaska was selected. Environmental conditions at the primary site were deemed to be unsuitable for the equipment and a secondary location in Bethel in southwest Alaska was selected. Figure 3-1b shows the location of the Alaska link.

Influenced by the lessons of the preliminary Greenland experiment, several changes to the basic receive equipment located in Bethel were made (See Figure 5-1). A slower speed 50 kHz/channel A/D converter was used in the D-6000 data acquisition system due to the reduced sampling requirements. Data was sampled at a rate of 5 samples per chip, 40 ksamples/sec. Instead of processing data immediately after acquisition as in Greenland, raw data was stored on flexible disc during the 10 minute transmission interval and processed during the remaining 50 minutes. The new system included an external clock with battery backup which received signals from WWV to allow for automatic restart after power failures. The experiment was designed to run for six months with only bi-weekly servicing to replace data tapes. The equipment in Greenland was designed for manual restart and required daily service.

The low bit rate and potentially high Doppler shifts due to scatter from the rapidly moving aurora limited the length of the probing sequence to 31 bits (see Equation 4.1 and Table 5-1) although a longer sequence would have been desirable to obtain improved processing gain.

Post acquisition processing on the data which was acquired during the 10 minute probing interval was performed during the remaining 50 minutes of each hour. During the first four minutes 1024 sample data records of the CW signal were acquired every five seconds and 1024 point complex FFTs were performed on every fifth record. The magnitude squared of the FFT record was computed and transferred to the controller, time tagged, and stored on tape. Due to tape storage limitations, phase information was not transferred. Cumulative histograms of the received CW signal level were performed on every CW record. During the next five minutes of the 10 minute probing period the PR sequence was repeated continuously by the transmitter. A data window corresponding to two full PR sequence periods was collected every six

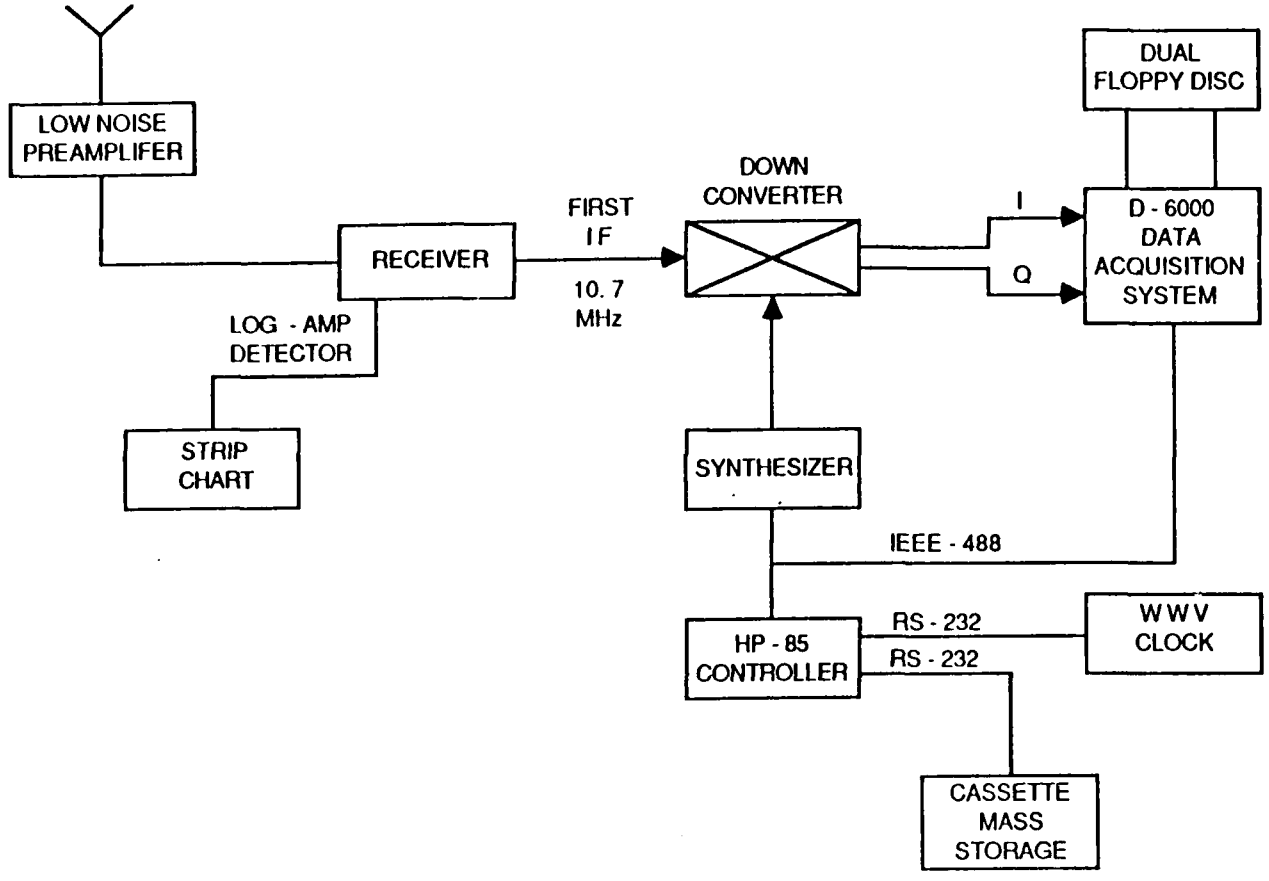

Figure 5-1 Receive Equipment for Alaska Multipath Measurement Program Located at Bethel, Alaska

Table 5-1 Probing Waveform Characteristics for Alaska Experiment

PR SEQUENCE CHARACTERISTICS	
Sequence Length (L)	31 bits
Maximum Frequency Offset Between R_x and T_x	±50 Hz
Maximum Doppler Shift Expected	±100 Hz
Chip Rate	8 kb/s
Chip Period (T_c) (Multipath Resolution)	125 μs
Sequence Repetition Rate Maximum Resolution	3.875 ms
Processing Gain (Idealized)	14.9 dB
Worst Case Expected Processing Gain Degradation	-2.6 dB
Number of Samples Per Sequence Chip	5
Sampling Rate	40×10^3 samples/sec
Snapshot Rate	1 every 6 seconds
FFT CHARACTERISTICS	
Repetition Rate	1 every 25 seconds (every 5th CW record)
Number of Points	1024 complex
FFT Duration	400 ms
Frequency Resolution	2.5 Hz
FFT Sampling Rate	390 μs/sample
HISTOGRAM CHARACTERISTICS	
Number of points	1024
Repetition Rate	5 seconds--every CW record
Sampling Rate	390 μs/sample

seconds during the five minute interval. Since there was no timing reference to align the data acquisition window with the beginning of the PR sequence, two full PR periods were acquired to insure that one full contiguous sequence resided within the acquisition window. This technique greatly simplified the receive equipment. The received complex data window was correlated with a stored version of the PR sequence. The magnitude squared of the correlation was computed, transferred to the controller, time tagged and stored on tape. The design and mix of the post-processing routines during the 50 minute idle period were driven by the processing capacity of the Data Precision 6000 and the HP-85 controller and the requirement that data tapes be changed no more than bi-weekly. It would have been desirable to acquire more FFT records and to save both magnitude and phase information; however the limited tape capacity precluded this.

During the construction and calibration phase of the experiment, synthesizers at receiver and transmitter were measured and determined to be within 50 Hz of each other. Received signal level calibration and initial noise measurements were performed at the receive site. The noise measurements showed that the receiver at Bethel was limited by man-made noise about 3 dB above Galactic noise. Some interference due to images from the several thousand Watt VOR transmitter at the nearby airfield were observed about 200 KHz from the operating frequency. They were, for the most part, removed by the 30 KHz IF filter; however, this interference represented the non-diurnal noise floor.

5.2 RESULTS FROM ALASKA EXPERIMENT

Data was collected over a seven month period from July 1985 to March 1986 with several interruptions due to transmitter or receiver equipment failures. Due to the remoteness of the receiver location, equipment failures often required four weeks to correct.

The first step in the data analysis procedure involved transferring data from tape cartridge to a mainframe computer and removing the effect of tape errors which often caused large spikes in the data records. Next, data records acquired during periods when the transmitter was not operational were eliminated.

Each FFT record was processed to determine the mean and mean squared energy of the data record, the Doppler shift (mean), Doppler spread (second central moment), and the skew of the Doppler spectrum (third central moment). Cumulative records were formed by averaging the 10 to 12 FFT records collected during each four minute acquisition period. The various moments were computed from the cumulative FFT record.

Correlation processing was more complicated. The simplification in the acquisition process which eliminated the need for aligning the acquisition window with the start of the PR sequence had two drawbacks that had to be considered in the processing. First absolute path delay could not be computed since no reference exists. Second, a potential ambiguity in the magnitude of the delay spread had to be removed (see Appendix A). Since no time reference exists, cumulative averages of the multipath profile could not be produced and only statistics of the average and variance of the spread measured on the 50 to 60 records each five minutes were computed.

It was hoped to maintain the antennas along the great circle path from Anchorage to Bethel to observe auroral effects and to maximize observation of sporadic-E and meteors. Due to low solar activity during the period of the experiments, the aurora remained further north than expected and several changes to the experiment plan were required. We divided the experiment into two phases.

In the first phase, performed from mid-July through October, the antennas were aligned along the great circle path from

Anchorage to Bethel illuminating the midpoint of the great circle path. Although we anticipated the observation of some auroral scatter activity, the primary mechanism that it was hoped to observe was meteors and daytime sporadic-E. In the second phase of the experiment, from early through mid-July and from late October 1985 through March 1986, the antennas were rotated off the great circle path to observe the aurora located to the North. The antenna in Anchorage was rotated 90 degrees so that it pointed in the direction of Fairbanks and the antenna at Bethel was rotated 45 degrees north, so that it also pointed towards Fairbanks (see Figure 3-1b). Rotating the transmitter antennas required collapsing the antenna structure to allow manual rotation of the antennas. Automatic rotation of the antennas to track the aurora was therefore not possible.

In order to accurately associate multipath conditions with the propagation mechanisms causing them, ionospheric data from the University of Alaska Ionosonde at College (near Fairbanks) and various geomagnetic indicies were obtained.

In the analysis procedure we considered the characteristics of propagation mechanisms which were similar from a communication viewpoint rather from an ionospheric physics viewpoint. For example, we grouped together all forms of sporadic-E although on a given link several different types may be observed. Also, we separated propagation mechanisms observed on and off the great circle path from transmitter to receiver.

5.2.1 Sporadic-E Propagation

E-layer propagation including enhanced ionospheric scatter and sporadic-E propagation were observed--though not as frequently as on some of the longer links in Alaska. For the purpose of communication analysis we group together all forms of sporadic-E and enhanced E-layer ionospheric scatter under the general heading sporadic-E.

The sporadic-E channel was characterized by signal strengths in excess of 8 dB above the noise floor in the 30 KHz bandwidth, slow fading (2σ fading bandwidth usually less than 20 Hz) and little, if any, multipath spreading within the 125 μs minimum resolution of the experiment. The primary multipath mechanism observed was the occasional occurrence of meteors in addition to the sporadic-E signal.

Figure 5-2 shows a series of multipath snapshots of a typical sporadic-E event acquired every six seconds for five minutes on 1 July 1985 at 0300 UT. The sporadic-E layer initial frequency, f_0E_s, measured at College Alaska was 5.14 MHz. The frames (snapshots) have been aligned so that all the peaks occur at the same relative delay. In snapshots 21, 33, 38, 44, and 49 the secondary discrete components are due most likely to meteor trails to the side of the mid-point of the great circle plane. The delays correspond to path differences of 30, 112, 75, 37, and 75 Km respectively. Figure 5-3 shows the FFT of the CW received probing signal averaged over the 4 minutes preceding the multipath snapshots. The measured 2σ Doppler spread is 11.8 Hz.

Since the time between multipath snapshots (6 seconds) is much greater than the inverse of the fading bandwidth in Figure 5-3, it is expected that the squares of the correlation peaks minus the noise floor (signal intensity I) represent the energy in the signal envelope and should be uncorrelated from sample to sample. If the fading of the correlation peaks were due to multiple, closely spaced sporadic-E echoes, then one would expect the received signal to have complex Gaussian statistics and an exponential distribution of signal energies. Figure 5-4 shows the histogram of the square of the peaks minus the noise floor. The broken line shows a MMSE exponential curve fit to the data. We observe a relatively close fit.

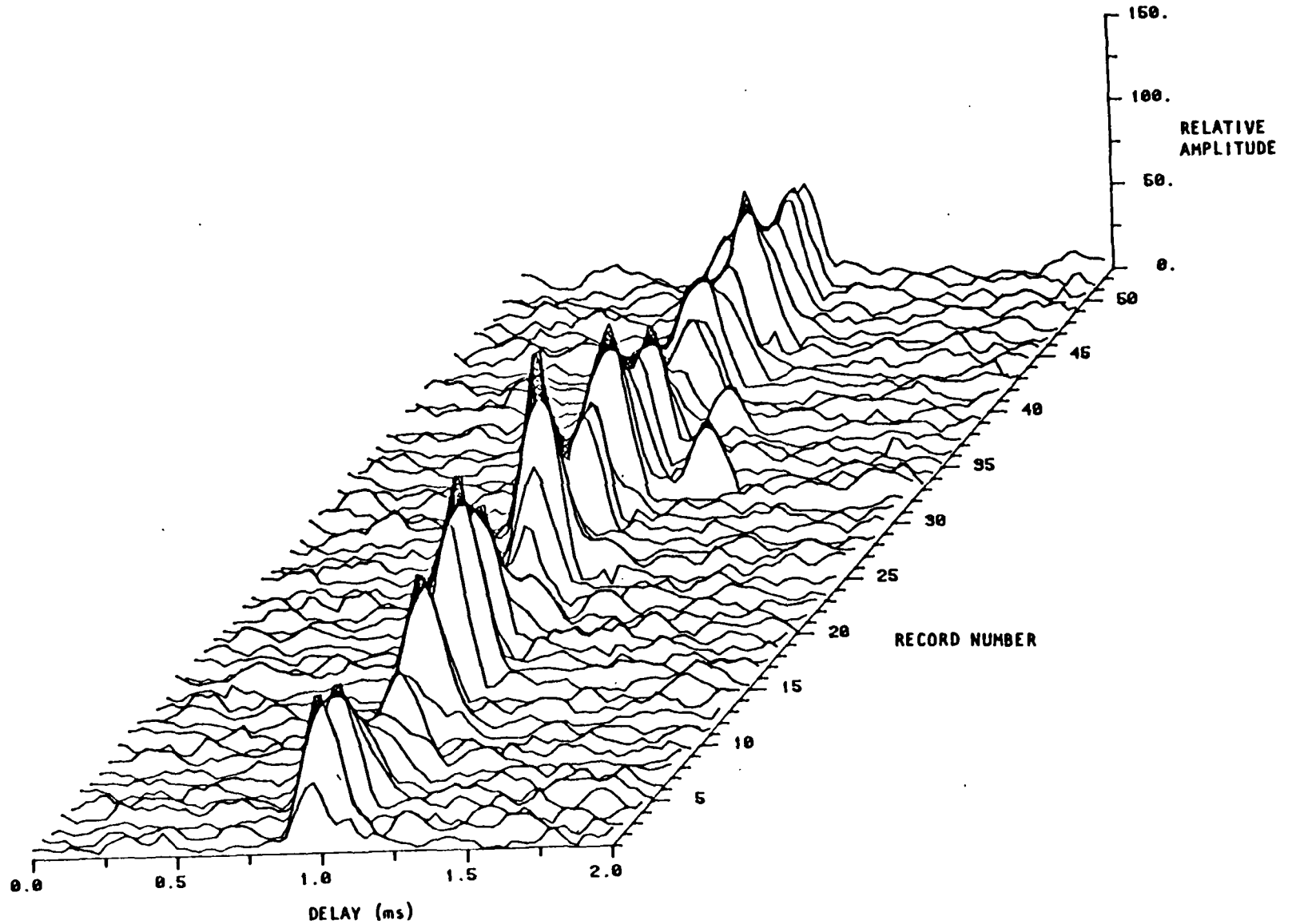

Figure 5-2 Series of Multipath Snapshots Showing Sporadic-E Event on 1 July 1985 at 0300 UT. Snapshots Were Acquired Every Six Seconds. Multipath Due to Meteors is Clearly Visible in Snapshots 21, 33, 38, 44 and 49.

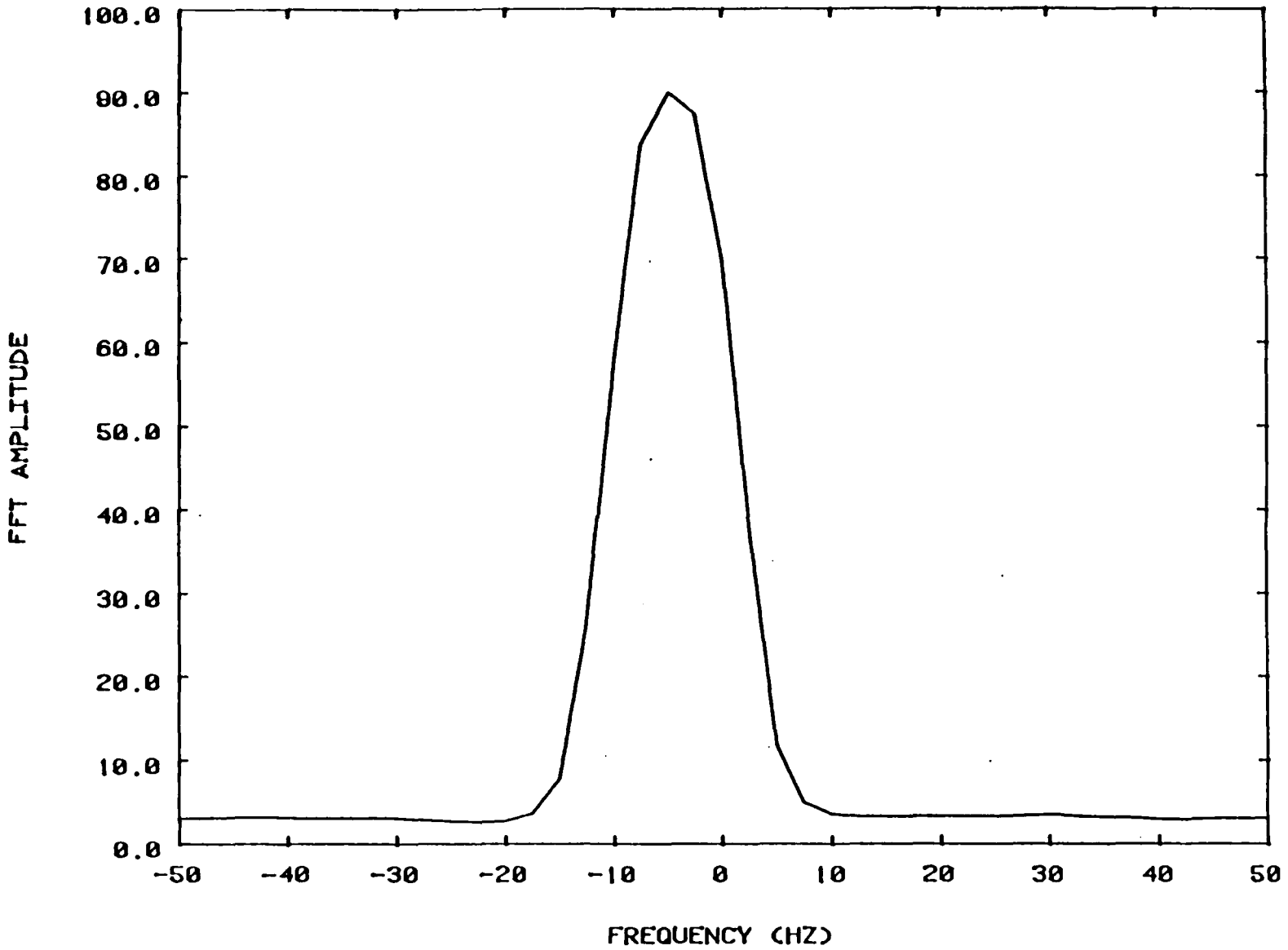

Figure 5-3 Composite FFT Formed by Averaging 10 FFT Records Acquired Every 25 Seconds for 4 Minutes Preceding the Snapshots in Figure 5-2. The 2σ Doppler Spread is 11.8 Hz.

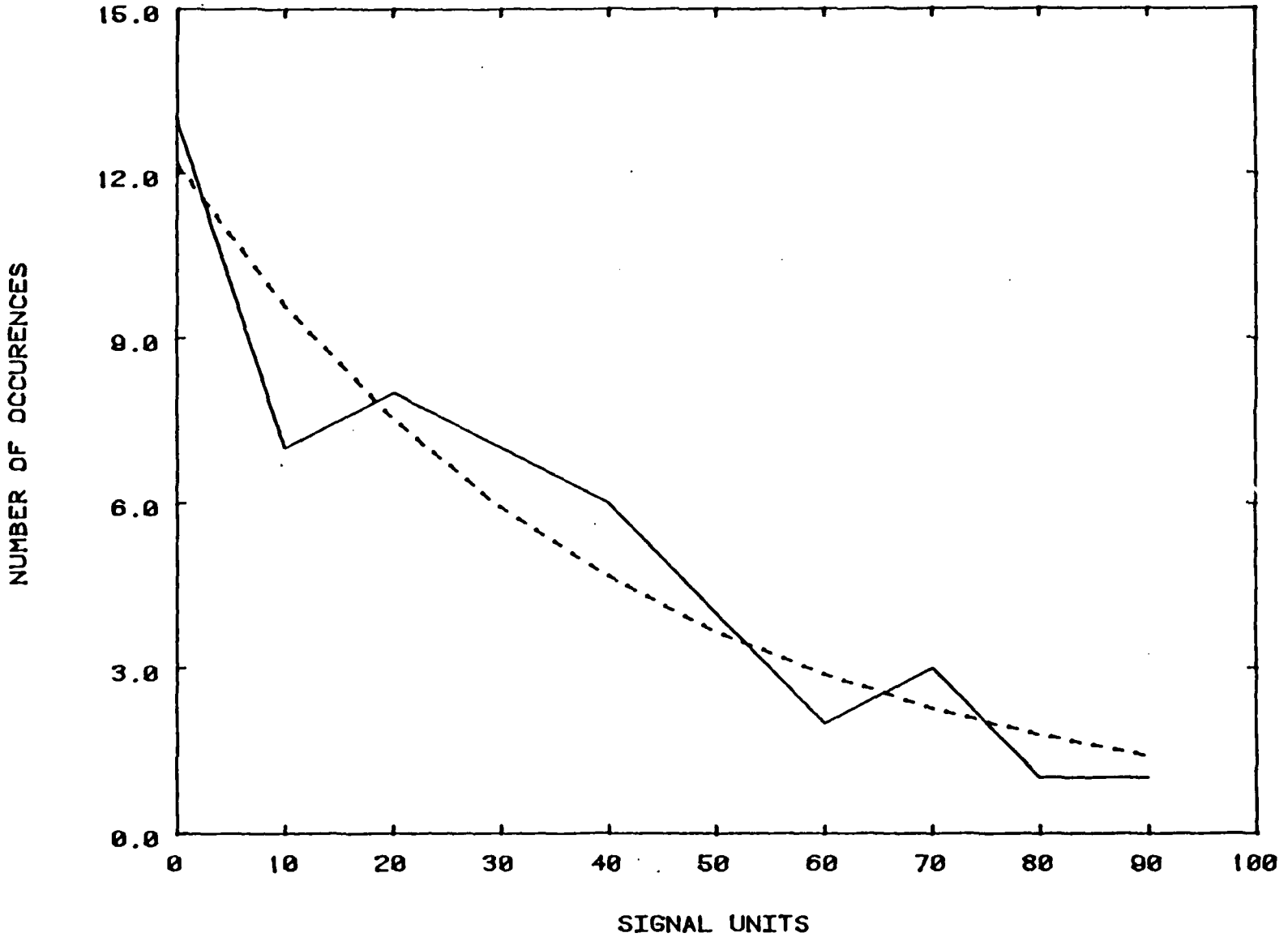

Figure 5-4 Solid Line Represents Histogram of the Squares of Correlation Peaks With Noise Floor Removed for Data Sequence in Figure 5-2. Broken Line is MMSE Exponential Curve Fit to Data.

Another statistical parameter that was computed was the Scintillation Index, S_I, defined as

$$S_I = \left(E \frac{(I-(\bar{I}))^2}{(\bar{I})^2} \right)^{1/2} \qquad (5.1)$$

where I is the signal intensity (square of the envelope with the noise floor removed.) For the data of Figure 5-2, with histogram shown in Figure 5-4, the Scintillation Index computed from Equation (5.2) was 0.89. The average Scintillation Index for all sporadic-E events was 1.21 with a standard deviation of 0.4. Scintillation Index equal to zero corresponds to a constant non-fading signal, one to a fading signal with complex Gaussian statistics, and indices larger than one correspond to data sets in which the number of multipath components is small with one component larger than the others.

Figure 5-5 shows a histogram of the 2σ Doppler spreads of Sporadic-E propagation data obtained with the antennas on the great circle path. The average Doppler spread over all Sporadic-E events was 10.958 Hz with a 3.25 Hz standard deviation. The 10,50, and 90 percentile Doppler spreads were 7 Hz, 10 Hz, and 17 Hz, respectively.

Figure 5-6 shows the percentage of time sporadic-E was observed vs time of day. Sporadic-E propagation, as shown in Figure 5-6, was observed most frequently around local noon (2100 UT) with the antennas pointed along the great circle path. Sporadic-E propagation was not observed with the antennas pointing towards Fairbanks since the region in the vicinity of the mid-point of the great circle path was not illuminated by the main lobe of the antenna patterns. Table 5-2 summarizes the characteristics of the sporadic-E channel.

We now examine briefly the relationship between observed sporadic-E conditions and ionosonde parameters. The primary

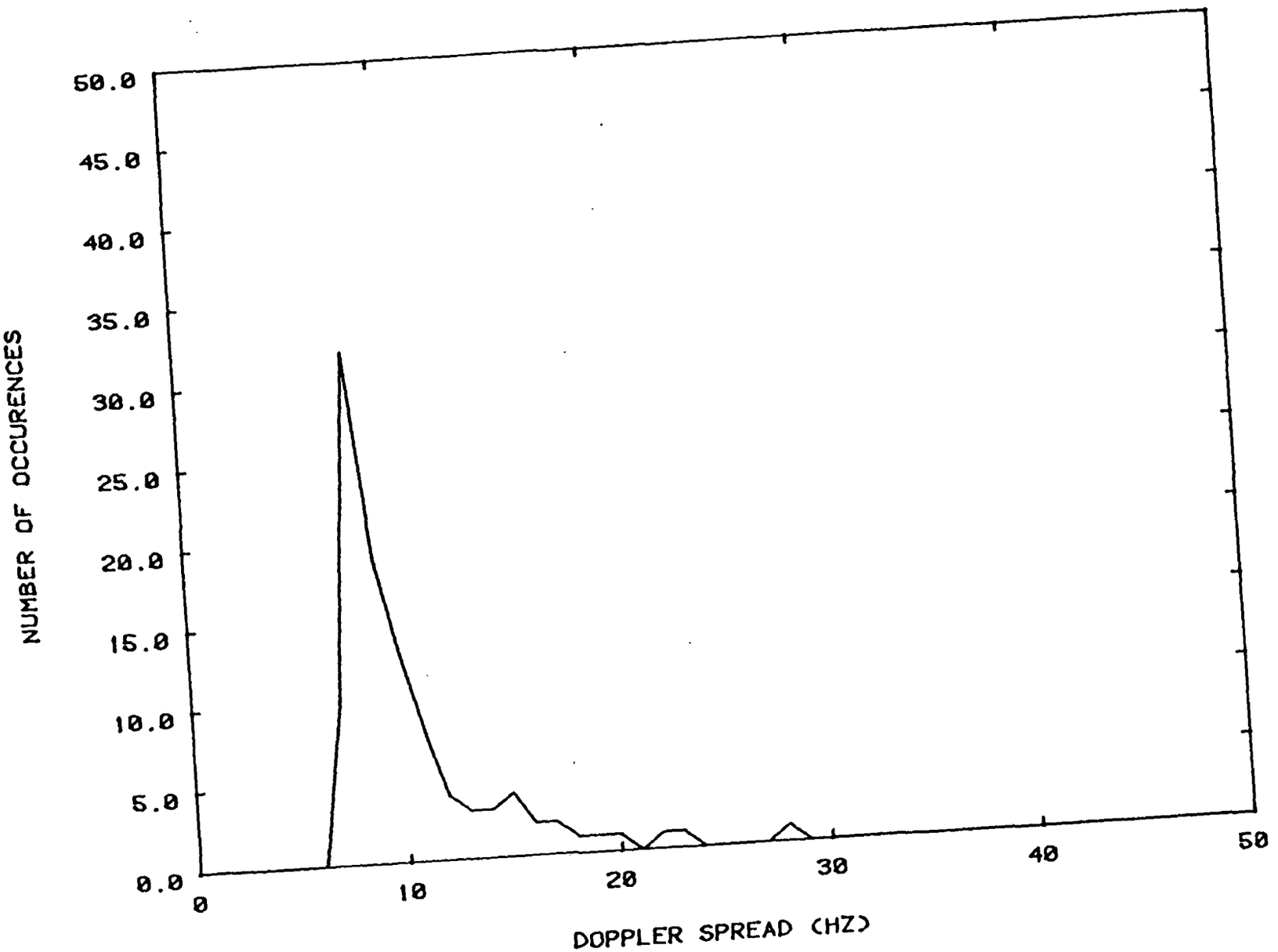

Figure 5-5 Histogram of 2σ Doppler Spreads for Events Classified as Sporadic-E.

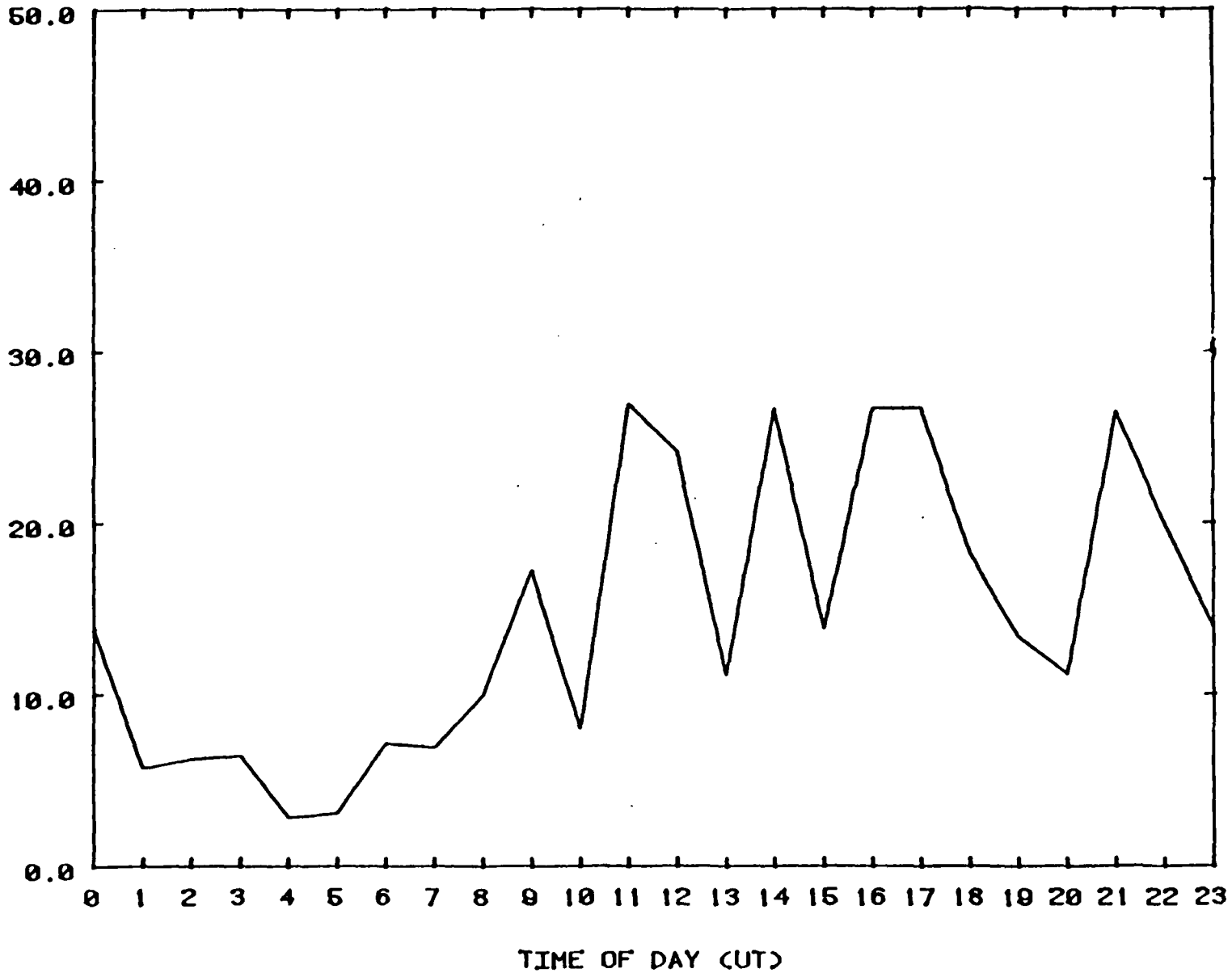

Figure 5-6 Percentage of Days on Which Sporadic-E Effects Were Observed Versus Time of Day.

Table 5-2 Characteristics of Sporadic-E Channel

Number of Observation Hours	738
Number of Observation Days	45
Number of Sporadic-E Hours	106 (14.3%)
Number of Sporadic-E Days	20 (44.44%)
Average 2σ Doppler Spread	10.95 Hz
Standard Deviation	3.25 Hz
10 Percentile Doppler Spread	7 Hz
50 Percentile Doppler Spread	10 Hz
90 Percentile Doppler Spread	17 Hz
Multipath on Sporadic-E Channel	Not Measurable
Average Scintillation Index	1.21
Standard Deviation of Scintillation Index	0.4
Average SNR (Sporadic-E) 30 KHz BW	8.9 dB

measure available was the E-layer and sporadic-E critical frequencies f_0E and f_0E_s determined by verticle swept sounding at College, Alaska. Figure 5-7 shows the correspondence between the maximum of f_0E and f_0E_s and the total received signal power. The broken line represents maximum (f_0E and f_0E_s) at College, Alaska at zero minutes past each hour. The solid line represents the total received signal power minus the noise floor in uncalibrated power units determined by integrating the energy in the composite FFT. The days shown are 30 June through 2 July 1985 with the antennas on the great circle path.

Note that with the exception of one measurement in which a very high f_0E_s was recorded at College and little sporadic-E propagation was observed, the occurrence of sporadic-E propagation on the Anchorage-Bethel link closely tracks the f_0E and f_0E_s at College.

5.2.1.1 Communicating Via Sporadic-E

From a communications point of view, sporadic-E propagation results in a continuous channel with high signal strength, slow fading and low multipath spread, providing enhanced throughput capacity *for meteor burst systems.* Ironically, the occasional occurrence of meteors represents the primary source of multipath interference *when the sporadic-E channel is present.* Sporadic-E propagation can support coherent modulation techniques with coherence bandwidths often on the order of Megahertz. Link protocols such as ARQ (automatic request) or Acknowledge/Non-acknowledge are adequate for communications although they are not optimal for the slow fading channel. Diversity reception may be necessary to fully exploit the bandwidth available. Advanced techniques which can adapt the data rates to the slowly changing capacity of the channel could be used to fully exploit the channel resource [Weitzen, 1983].

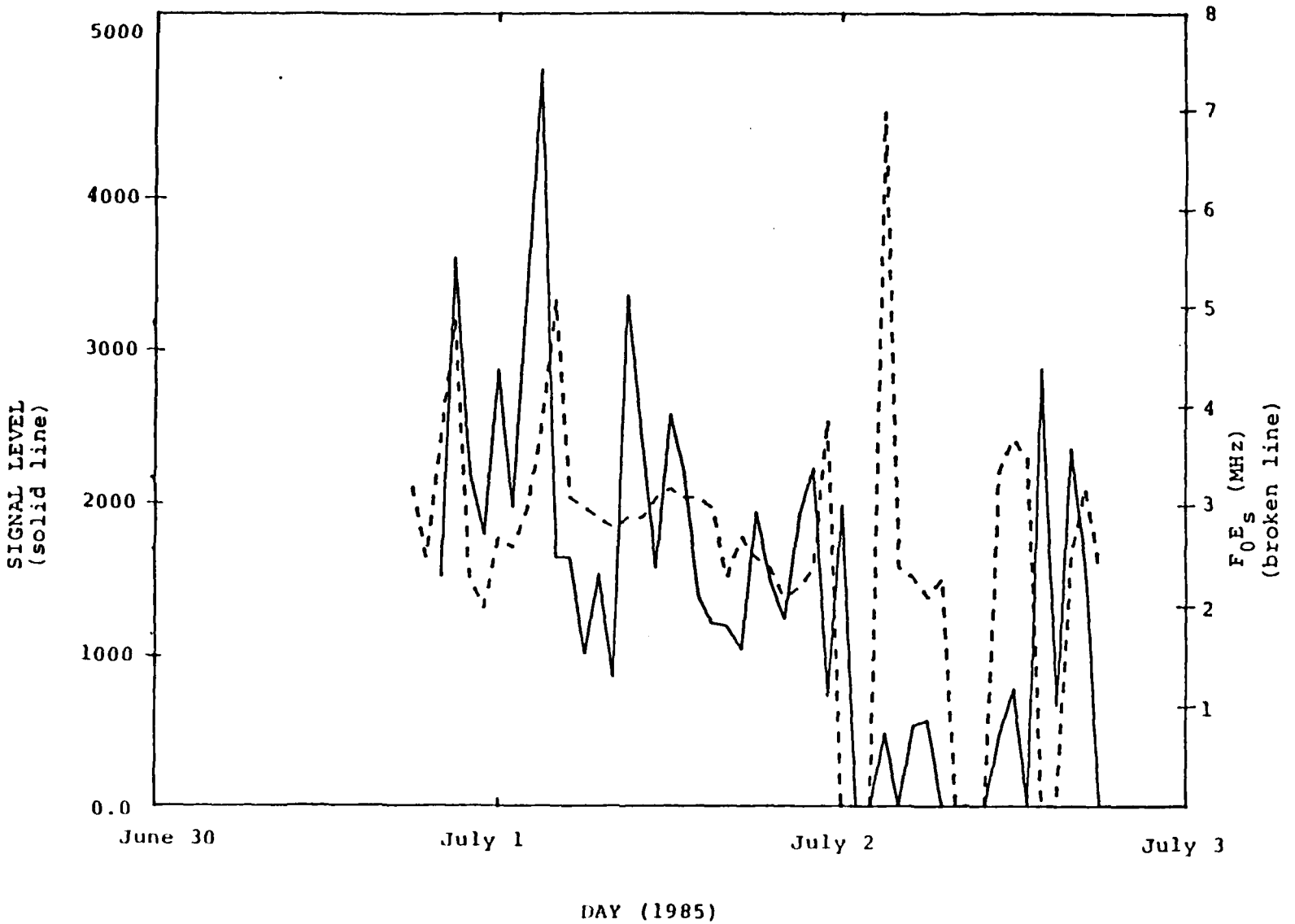

Figure 5-7 Solid Line Represents the Received Signal Energy in Uncalibrated Units Computed by Integrating the Energy in the Composite FFT for Several Days in July 1985. The Broken Line Represents the Sporadic-E Critical Frequency f_0E_s in MHz.

At the network level, protocols must be capable of full and normal operation in the high contention environment created by sporadic-E propagation in which continuous connectivity to many nodes in a network may exist for extended periods of time. Pure meteor scatter network protocols operate on the principle that the duty cycle on any given link is so low that collisions between network transmissions are negligible. A pure meteor scatter link could become collision bound in a frequent sporadic-E environment.

The primary drawback with the sporadic-E channel is that it is not as predictable or reliable as meteors. It is much more subject to ionospheric conditions than meteors. Therefore from a reliablity stand, it should be treated as a "bonus" channel rather than as the primary channel when it is used as a survivable backup communication technique. Because the sporadic-E channel has a much larger scattering area than meteors, it has much less resistance to intentional or unintentional interference than do meteors.

5.2.2 Multipath Due To Multiple Meteors

While not specifically designed for the observation of meteor trails (due to the fact that the receiver processor triggers at fixed time intervals rather than on intermittent signals such as meteors), a number of meteors were observed on the link. Meteors were observed with the antennas on the great circle path and pointing north, although as expected, many more meteors were observed with the antennas on the great circle path.

On occasion, multipath effects due to the simultaneous occurrence of more than one meteor trail were observed. Using data sets with the antennas on the great circle path with sporadic-E effects removed, a six percent duty cycle for meteor trails was observed with the 10,000 watt transmitter. Of the six

percent of all records which had meteor trails, 1.5 percent (of the six percent) showed secondary components due to multiple meteor trails. This compares favorably to the one to three percent multipath predicted by Sugar [1960].

5.2.3 Auroral Scatter

In regions in the vicinity of the aurora, scatter from the aurora represents a serious potential impairment to meteor communication at high latitudes. Scatter from the aurora can transform the relatively benign, though intermittent, meteor channel with little multipath interference into a continuous fading channel with 2σ delay spreads in excess of 1000 μs and 2σ Doppler bandwidths in excess of 200 Hz.

Auroral measurements were conducted with the antennas pointing north from early to mid-July 1985 and from late October through March 1986.

Auroral effects were observed most frequently but not exclusively during the late night and early morning hours, 11 P.M. to 6 A.M. local time (0800 to 1500 UT) and the observation of auroral effects could be correlated to increases in the standard geomagnetic planetary index Kp. Figure 5-8 shows a sequence of multipath snapshots collected every six seconds beginning at 1205 UT on 1 November 1985. Figure 5-9 shows the composite Doppler profile formed by averaging 10 individual FFT profiles acquired every 25 seconds. Figures 5-10 and 5-11 show multipath sequences and the Doppler profile respectively for a period two hours later. Figures 5-12 and 5-13 show the multipath and Doppler profiles for the spectacular event on the evening of 30 November 1985. Figure 5-14 and 5-15 show the multipath Doppler profiles for a typical auroral event on July 4, 1985.

In Figures 5-8, 5-10, 5-12, and 5-14, the noise floor has been removed for clarity and the multipath profiles have been

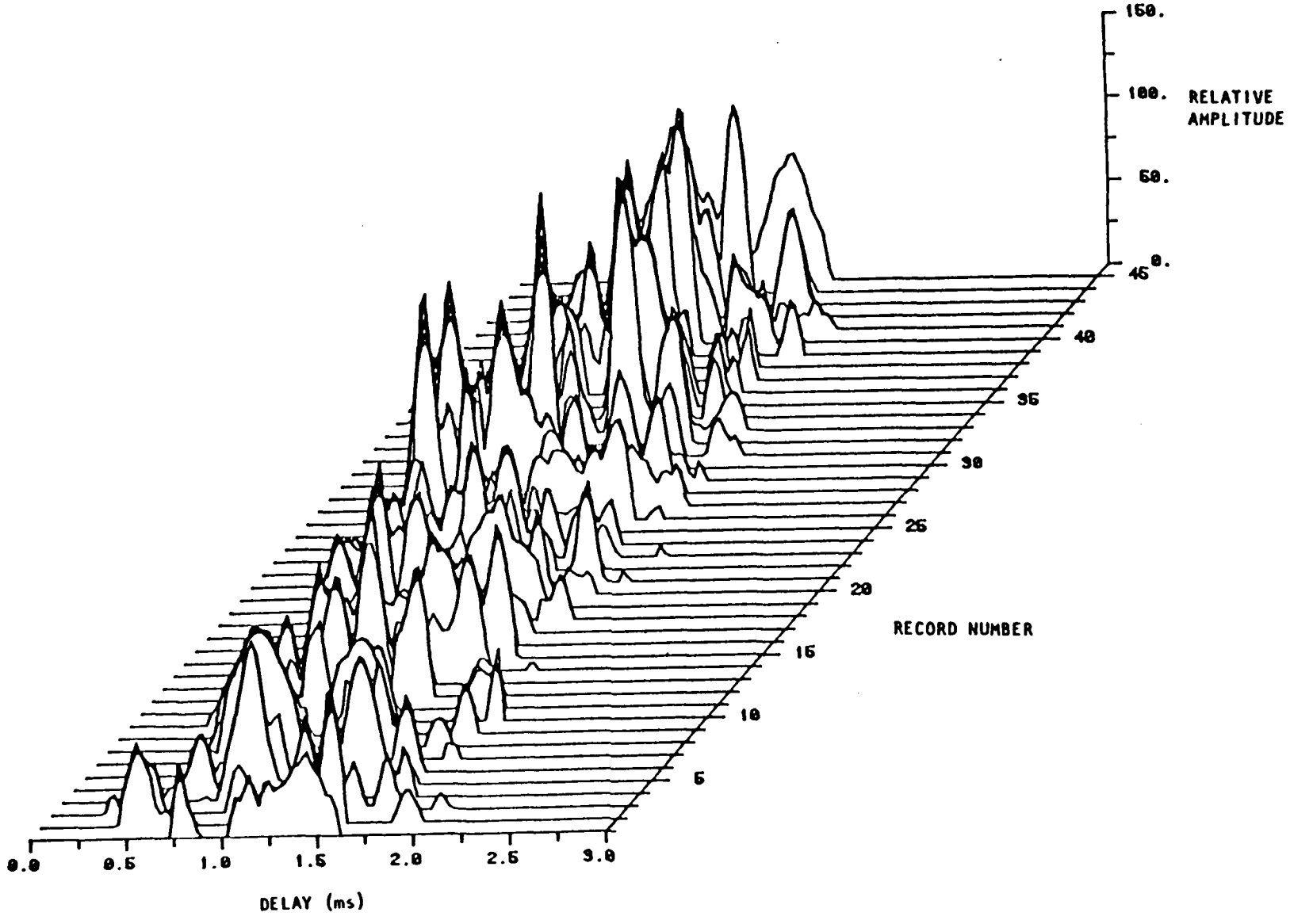

Figure 5-8 Sequence of Multipath Snapshots Showing Auroral Event on 1 November 1985 at 1200 UT. The 2σ Multipath Spread is 589 μs.

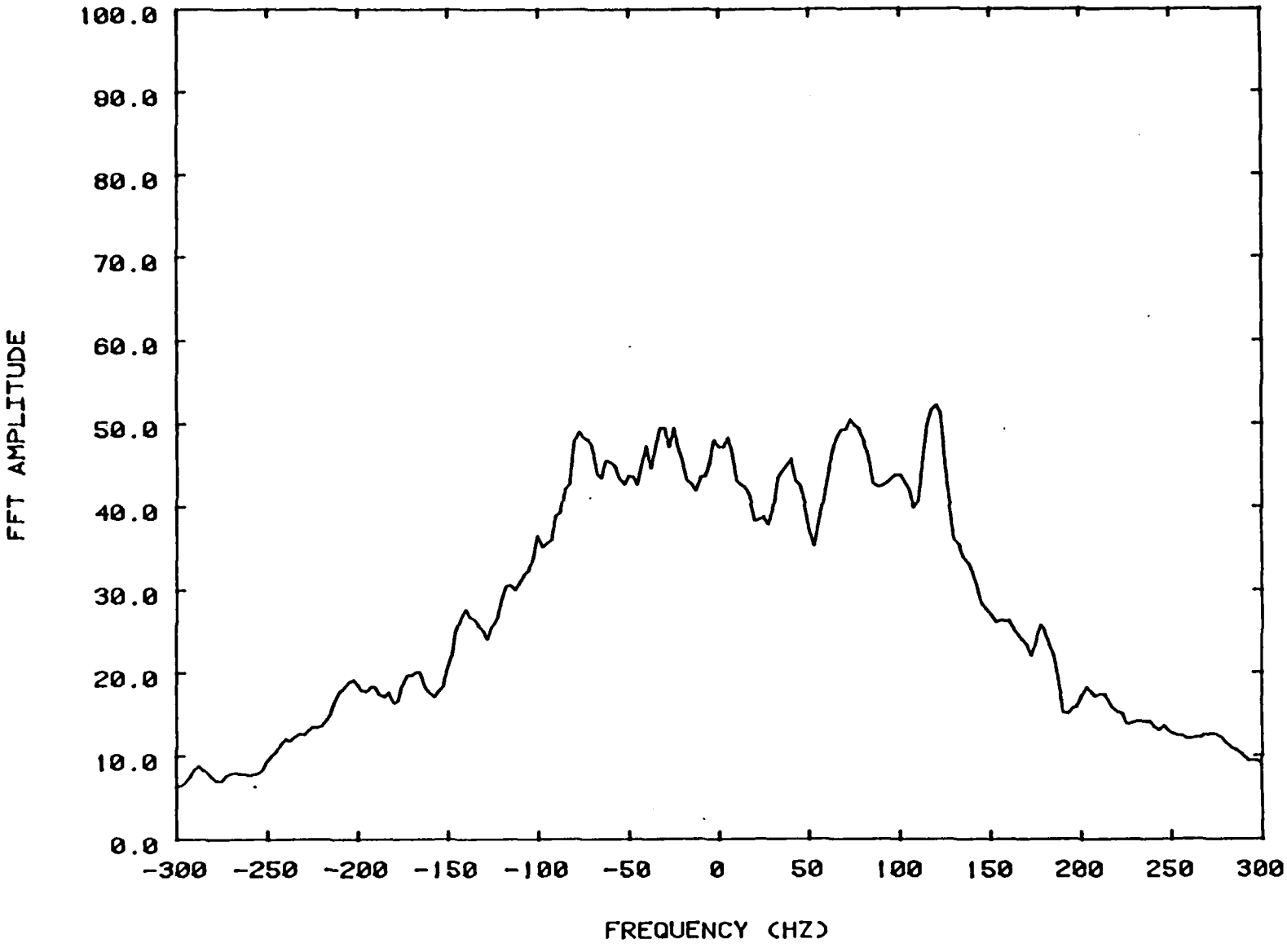

Figure 5-9 *Composite FT Frame for Same Time as Figure 5-8. The 2σ Doppler Spread is 210 μs.*

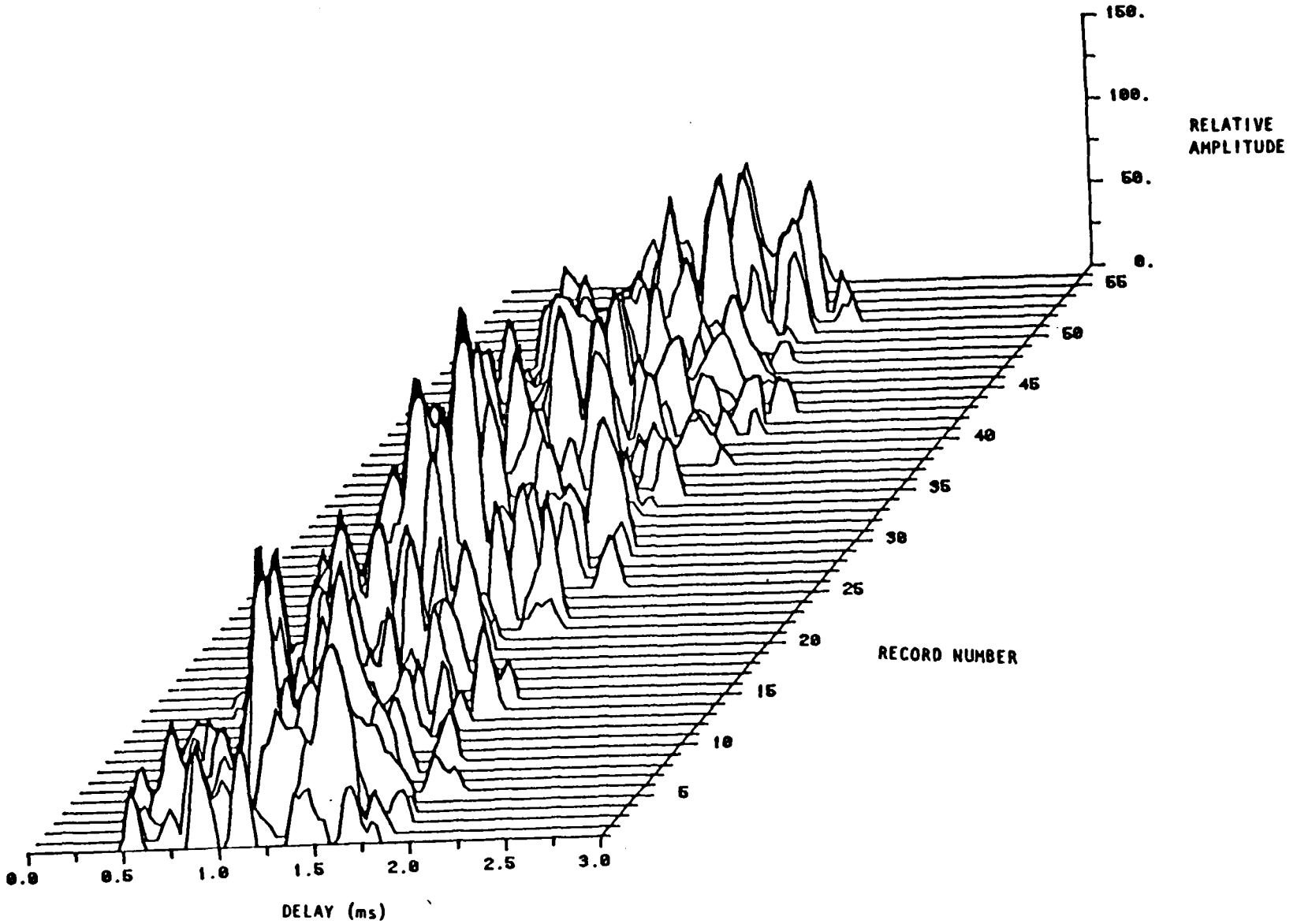

Figure 5-10 Sequence of Multipath Snapshots Showing Auroral Event at 1400 UT on 1 November 1985. The 2σ Multipath Spread is 624 μs.

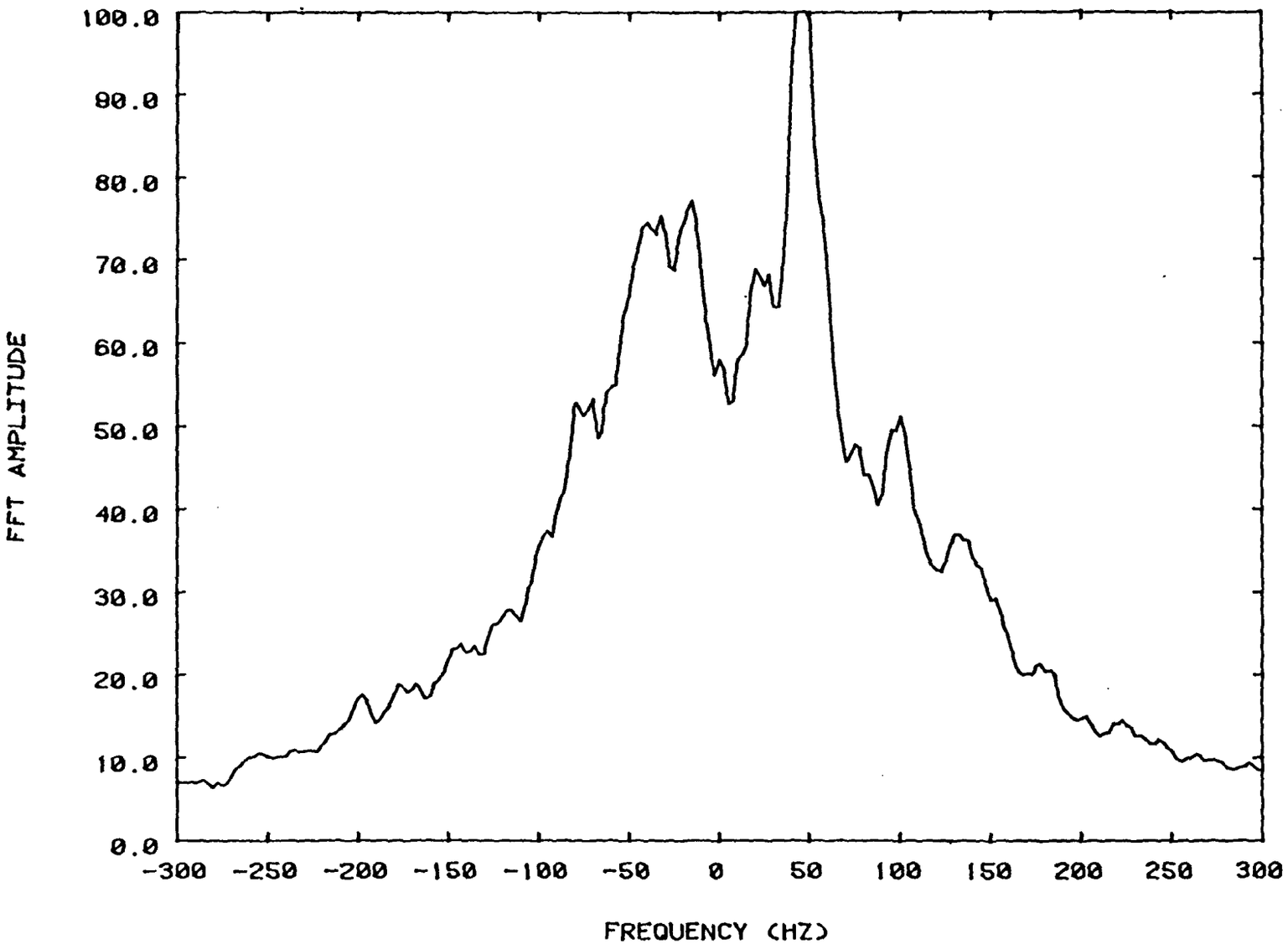

Figure 5-11 Composite FFT Frame for Same Time as Figure 5-10. The 2σ Doppler Spread is 190 Hz.

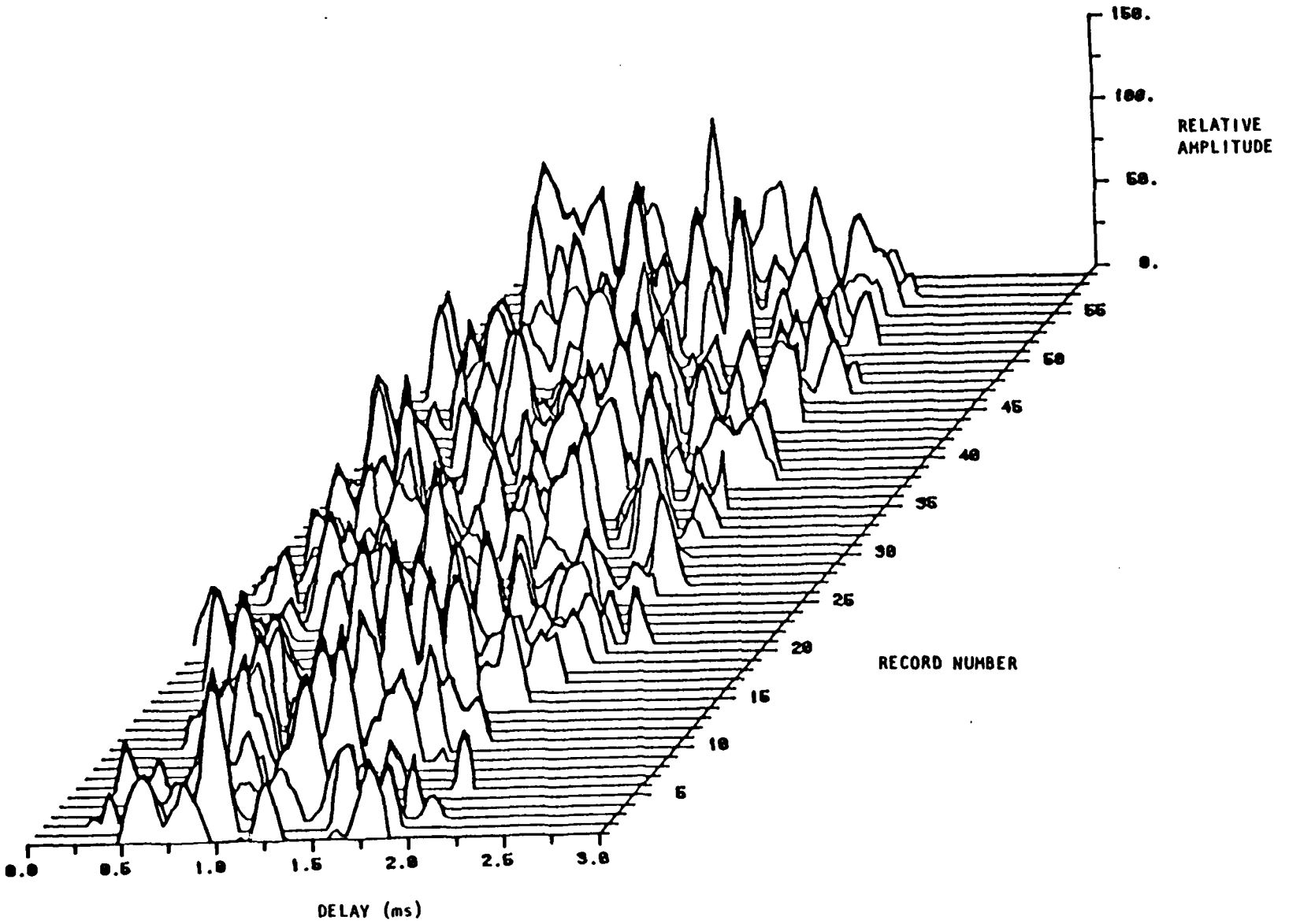

Figure 5-12 Sequence of Multipath Snapshots for Spectacular Auroral Event on 30 November 1985 at 0200 UT. The 2σ Multipath is 1005 μs.

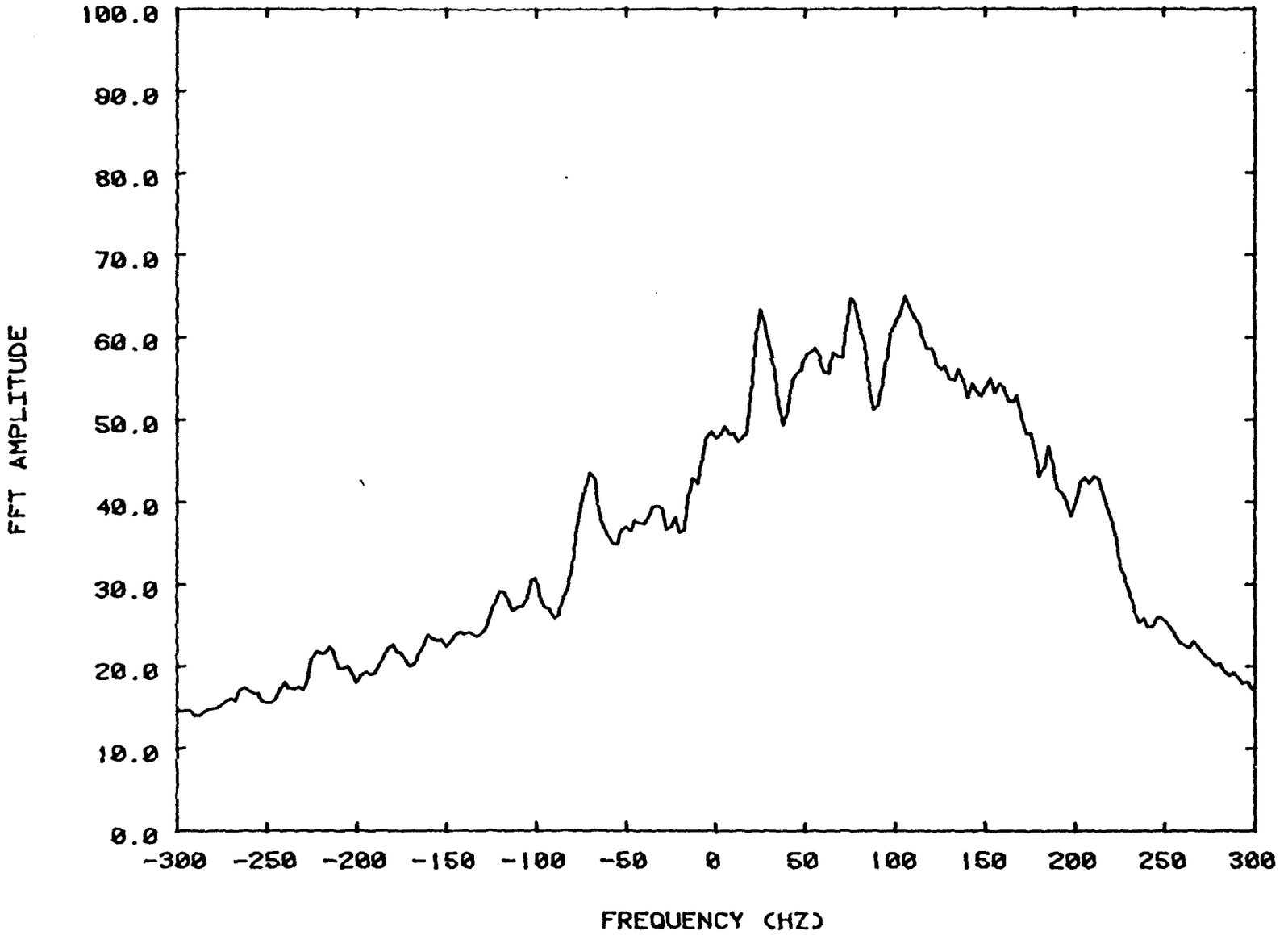

Figure 5-13 Composite FFT Frame for Same Time as Figure 5-12. The 2σ Doppler Spread is 246 Hz.

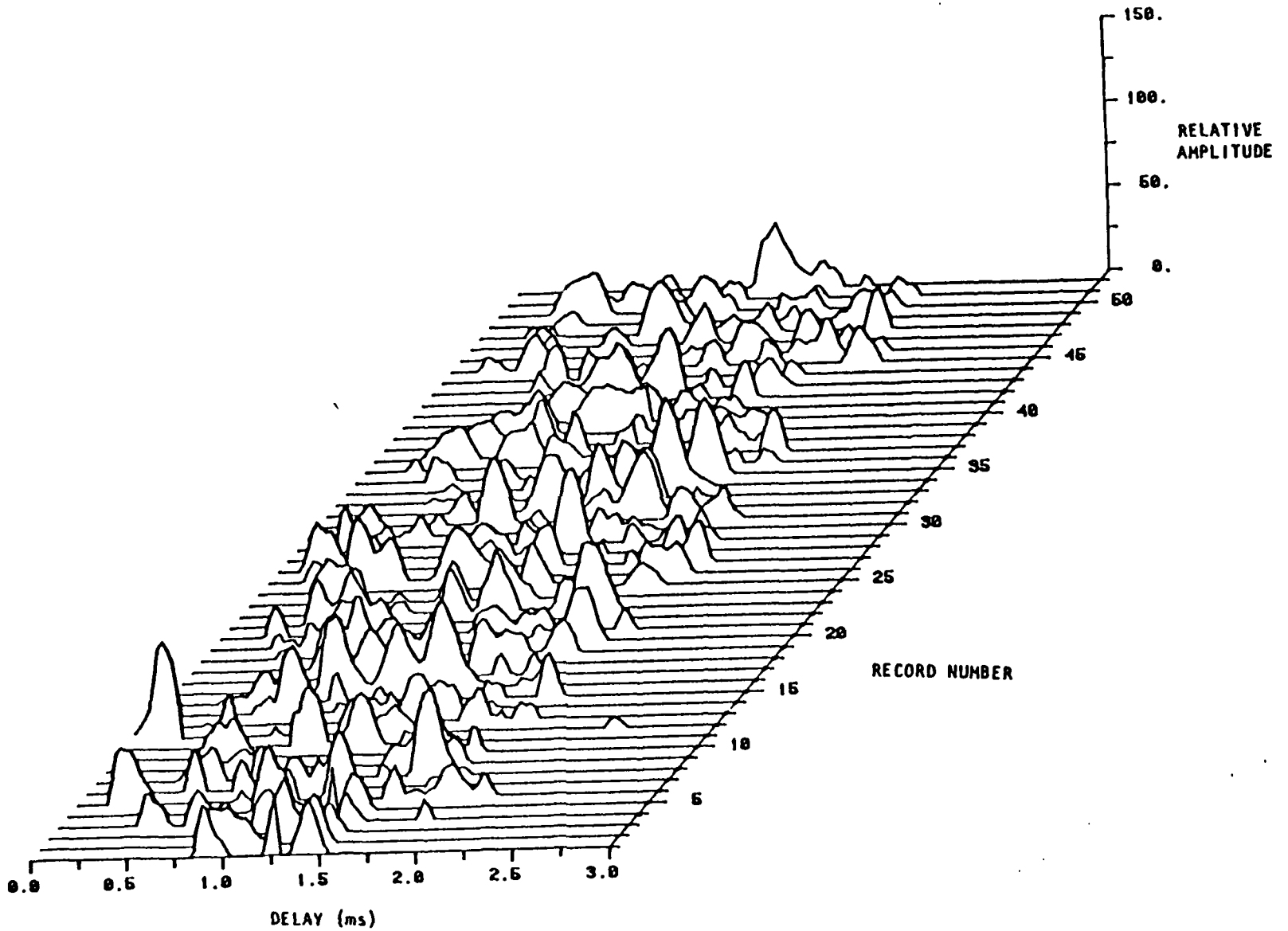

Figure 5-14 Sequence of Multipath Snapshots for Auroral Event on 4 July 1985. The 2σ Multipath Spread is 825 μs.

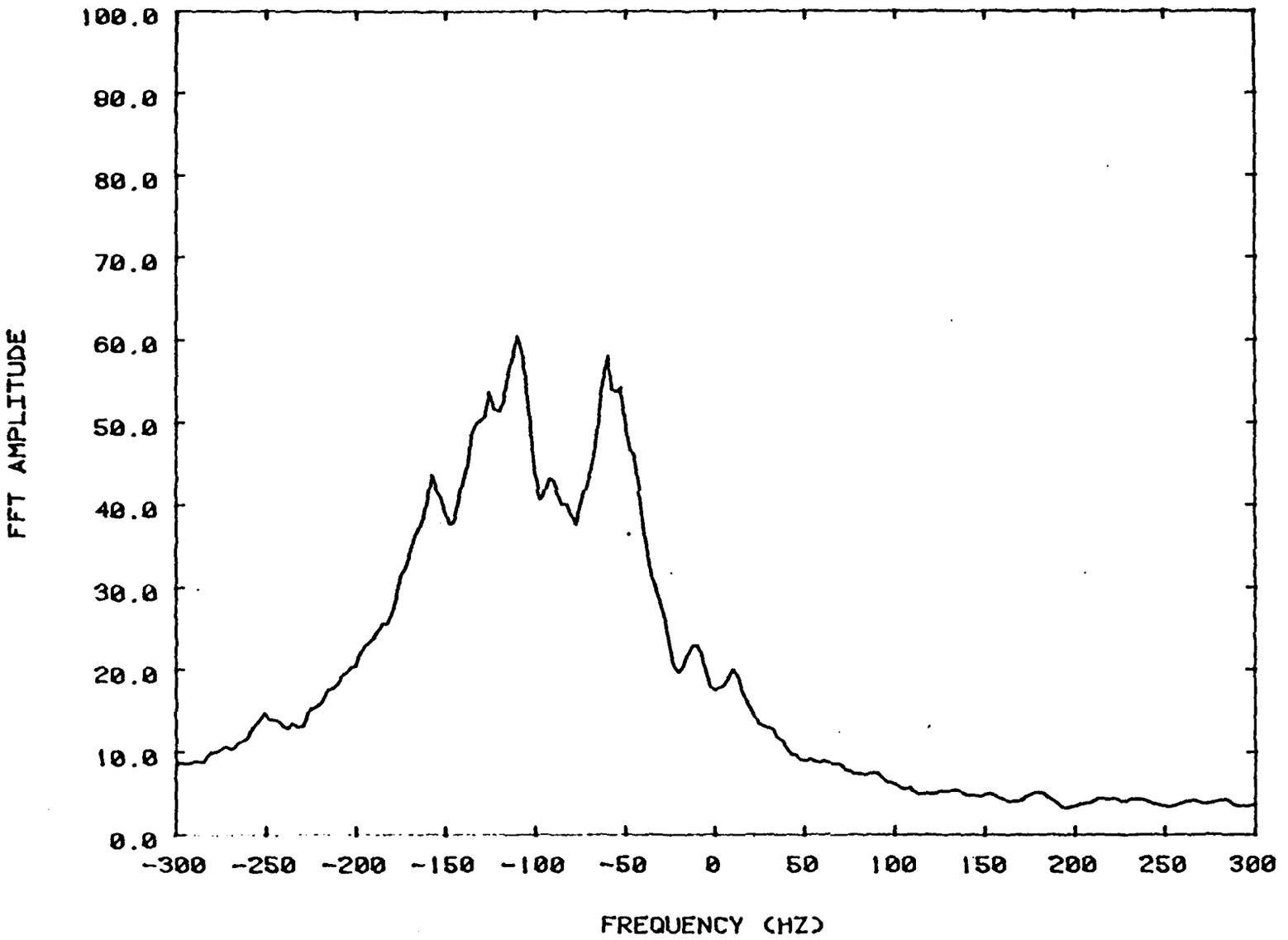

Figure 5-15 Composite Doppler Profile for Same Period as Figure 5-14. The 2σ Doppler Spread is 110 Hz.

aligned manually so that components appear in the same time bins (recall that there is no absolute time reference). Observe in the multipath sequences how components appear, fade and then disappear independently, implying an uncorrelated scatter fading channel.

Figures 5-8 through 5-15 show the characteristics of the purely auroral channel observed with the antennas off the great circle path. Because the antennas were pointed far off the great circle path, few meteors were observed and no sporadic-E was observed. The 2σ Doppler and multipath spreads in Figures 5-8 and 5-9 are 210 Hz and 589 μs, respectively. In Figures 5-10 and 5-11 the Doppler and multipath spreads are 190 Hz and 624 μs, respectively, and in Figures 5-14 and 5-15 the Doppler and multipath spreads are 110 Hz and 825 μs, respectively. For the spectacular display of 30 November, 1985, the Doppler and multipath spreads were 246 Hz and 1005 μs, respectively. Many auroral events were faint so that they were apparent from the FFT frames (400 ms records, effective processing gain = 30 dB) and not visible or faintly visible on the multipath records with less than 15 dB processing gain.

We now determine several comprehensive statistics for the pure auroral scatter channel. Figure 5-16 shows a histogram of 2σ Doppler spreads for all events classified as auroral scatter with the antennas off the great circle path. The average 2σ Doppler spread for all events was 100.3 Hz with a 67 Hz standard deviation. The 10,50, and 90 percentile Doppler spreads were 47 Hz, 105 Hz, and 200 Hz, respectively. Figure 5-17 shows the histogram of 2σ multipath spreads for each event identified as auroral scatter. The average multipath spread was 804 μs with a 174 μs standard deviation. The 10, 50, and 90 percentile multipath spreads were 420 μs, 800 μs, and 1000 μs, respectively. Table 5-3 summarizes the data in terms of basic communication parameters.

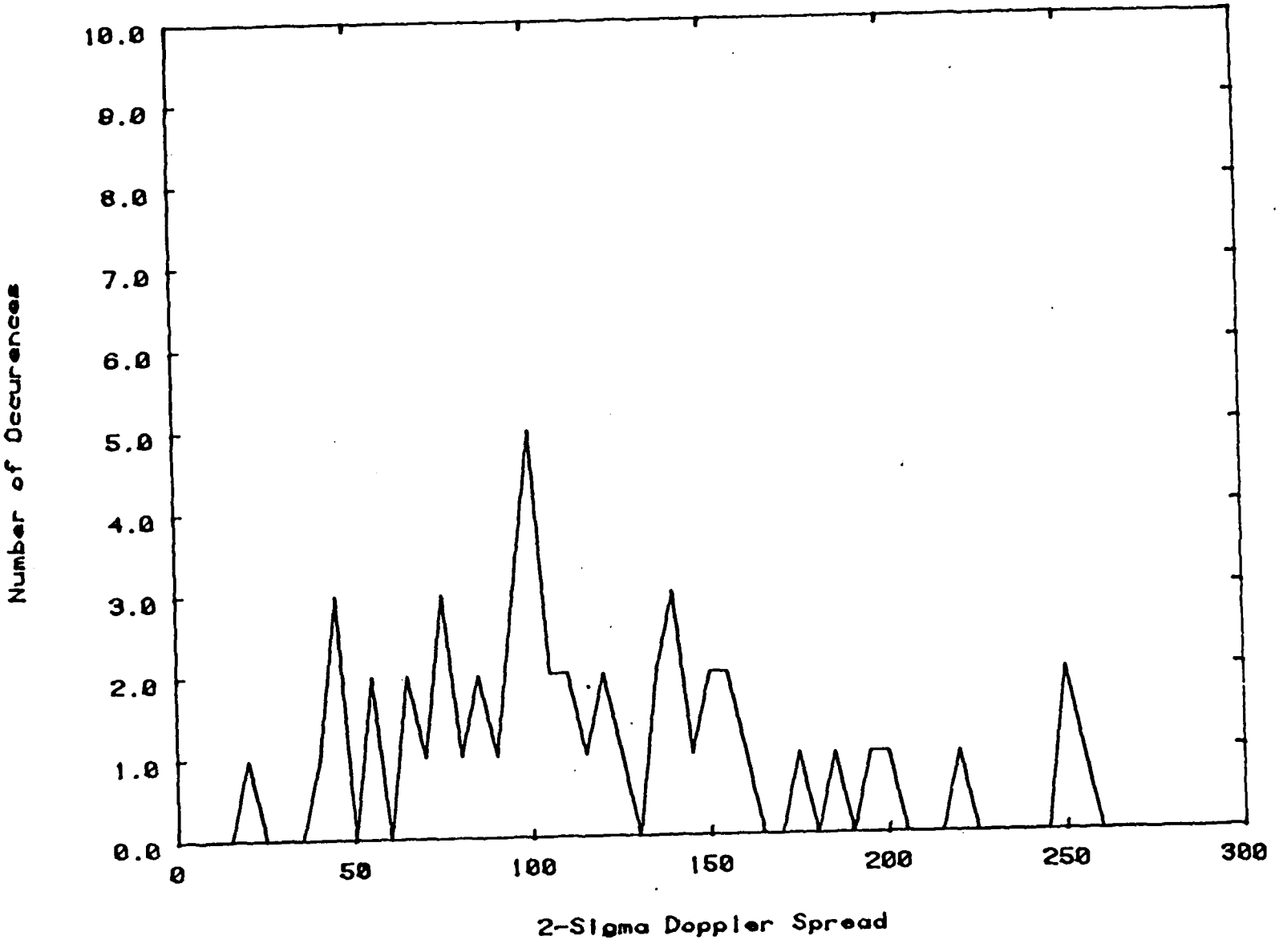

Figure 5-16 Histogram of 2σ Doppler Spreads for Events Classified as Auroral Scatter With Antennas Off the Great Circle Path.

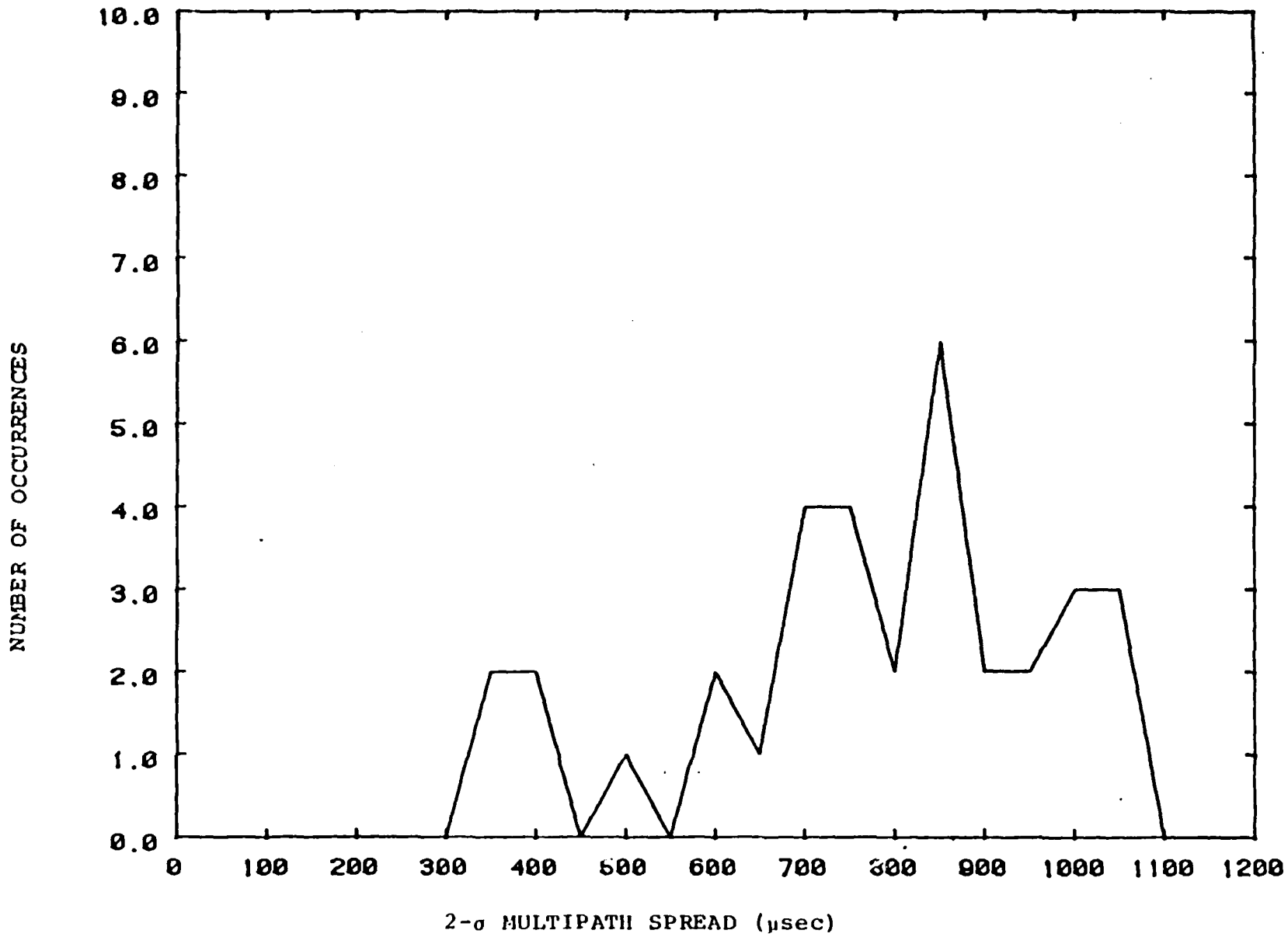

Figure 5-17 Histogram of 2σ Multipath Spreads for Events Classified as Auroral Scatter With Antennas Off the Great Circle Path.

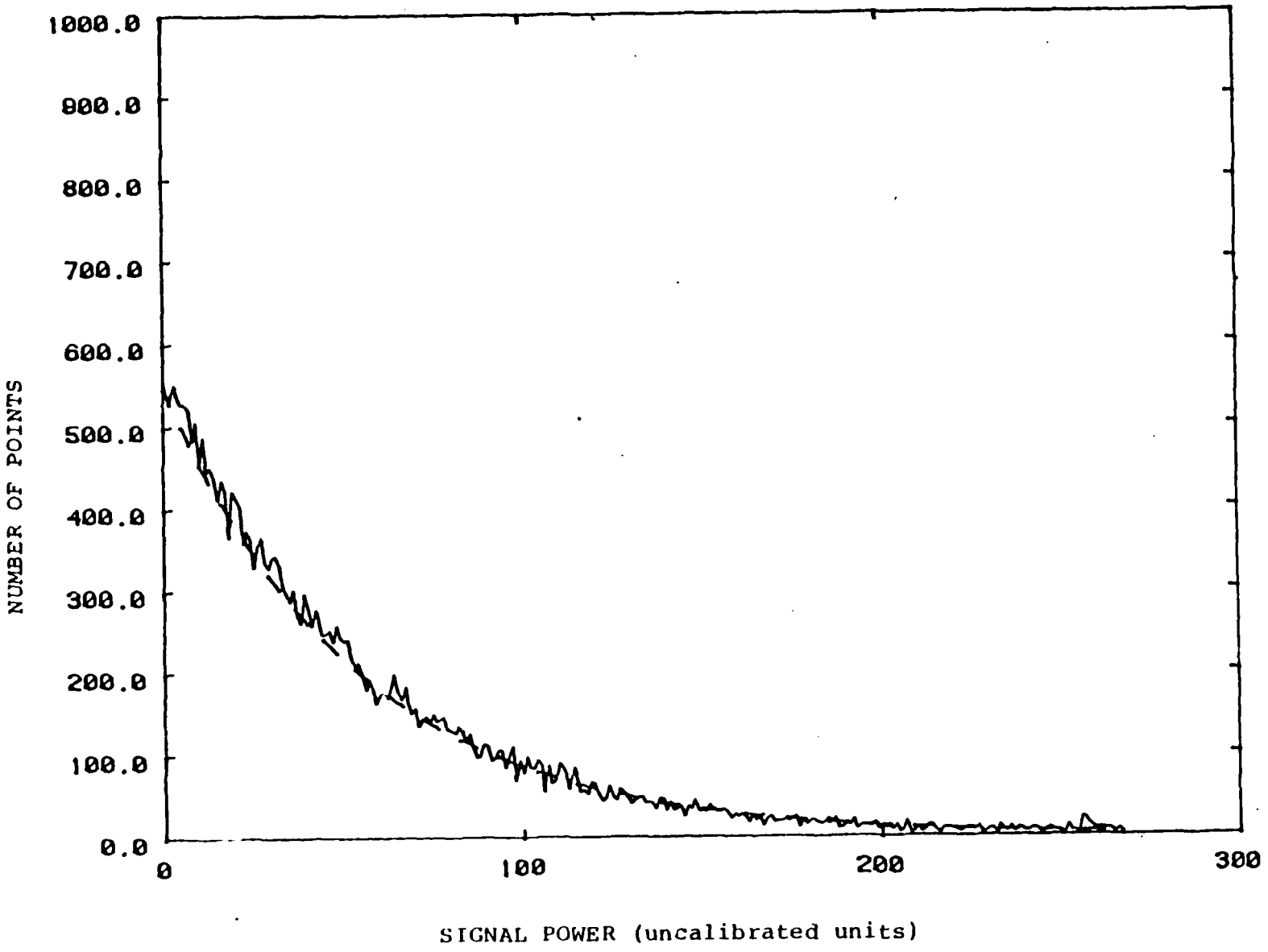

Figure 5-18 Histogram of Received Signal Power Uncalibrated Energy Units for 30 November Auroral Event at 0200 UT. Solid line represents data and the broken line represents a MMSE exponential fit to the data.

Table 5-3 Auroral Scatter Results

Number of Observation Hours	745
Number of Hours Auroral Scatter Observed	34 (4.5%)
Average 2σ Doppler Spread	100.3 Hz
STD Deviation of Doppler Spread	67 Hz
10 Percentile Doppler Spread	47 Hz
50 Percentile Doppler Spread	105 Hz
90 Percentile Doppler Spread	200 Hz
Average 2σ Multipath Spread	806 μs
STD Deviation of Multipath Spread	174.23 μs
10 Percentile Multipath Spread	420 μs
50 Percentile Multipath Spread	800 μs
90 Percentile Multipath Spread	1000 μs
Average SNR During (1 kHz BW) Auroral Events	13 dB

As observed in Figures 5-8, 5-10, 5-12, and 5-14, received auroral scatter signals generally consist of the sum of a number of independently fading components. The envelope squared of the signal should therefore be exponentially distributed. Figure 5-18 shows a histogram of the received envelope squared for the time period shown in Figures 5-14 and 5-15. The broken line represents a MMSE exponential fit to the data. We see that there appears to be a good fit to the data. Due to a calibration error, absolute signal levels are not available in Figure 5-18.

The night of September 19, 1985 provided us with an opportunity to observe aurora with the antennas on the great circle path to show what a meteor channel would look like with high level background aurora. Figure 5-19 shows the sequence of multipath snapshots for the September 19 event. Large meteors above the background aurora are observed in frames 47, 53, and 54. Figure 5-20 shows the Doppler profile in which we can see two distinct components; the zero shift component due to the meteor trails, and the more diffuse component centered at about 80 Hz represents the auroral scatter.

The observation of Auroral Effects on the Anchorage-Bethel link shows a strong correlation to increases in the geomagnetic index Kp. Figure 5-21 shows the received signal energy due to scatter from the aurora (solid line) in uncalibrated signal units and the three hour geomagnetic index Kp for 4 to 9 July 1985 (broken line) highlighted in Figures 5-14 and 5-15. Note that there appears to be several hours delay between the peak in Kp and the observation of auroral scatter effects.

Figure 5-22 shows the received signal energy due to auroral scatter and the Kp magnetic index for the period 1 November through 4 November 1985, highlighted in Figures 5-8 through 5-11. Figure 5-23 shows the received signal energy due to auroral scatter and the Kp magnetic index (broken line) for the

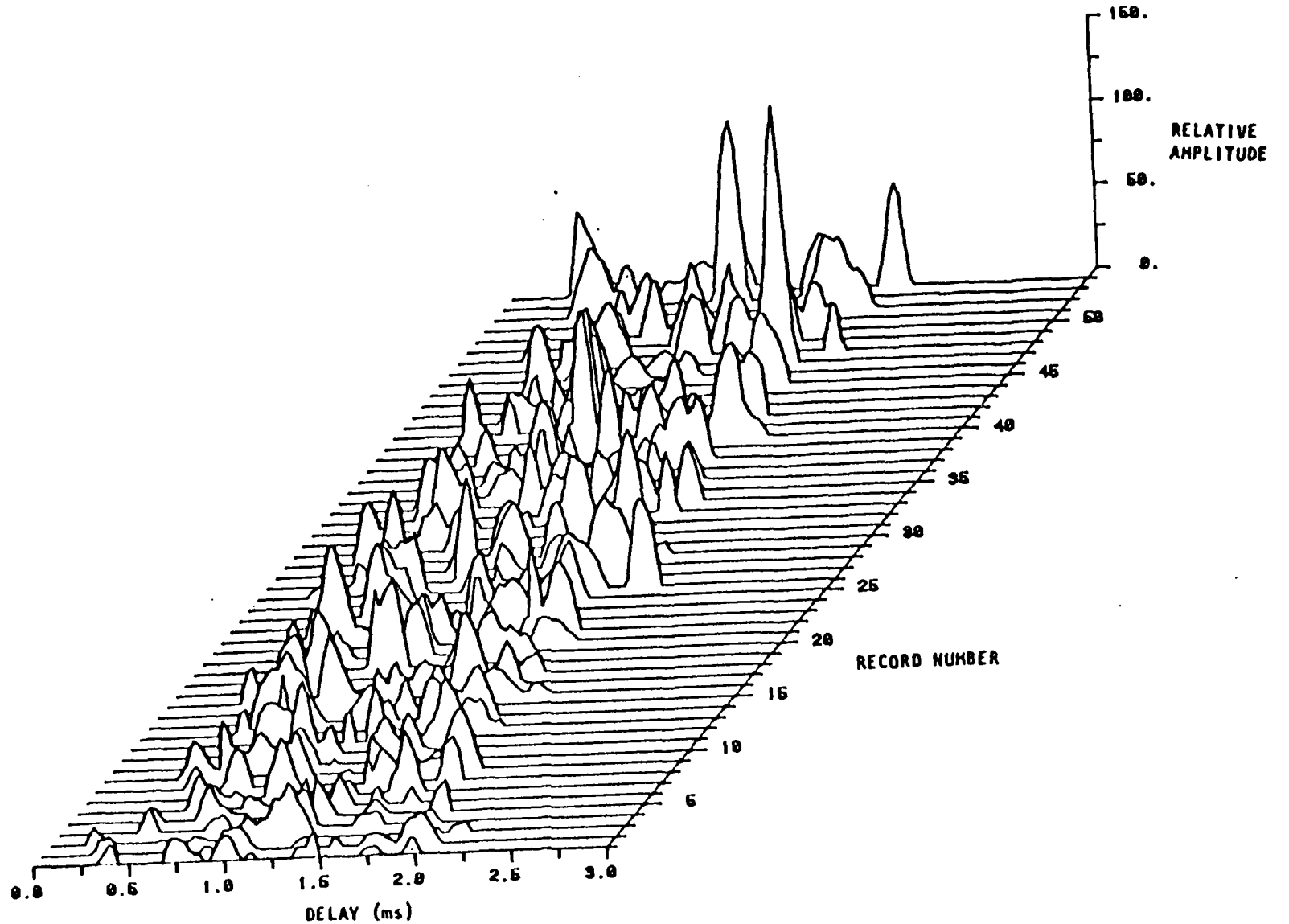

Figure 5-19 Series of multipath snapshots on 19 September 1985 with antenna's on great circle path showing combination of meteors and auroral scatter. Large meteors are evident in snapshots 46, 53 and 54.

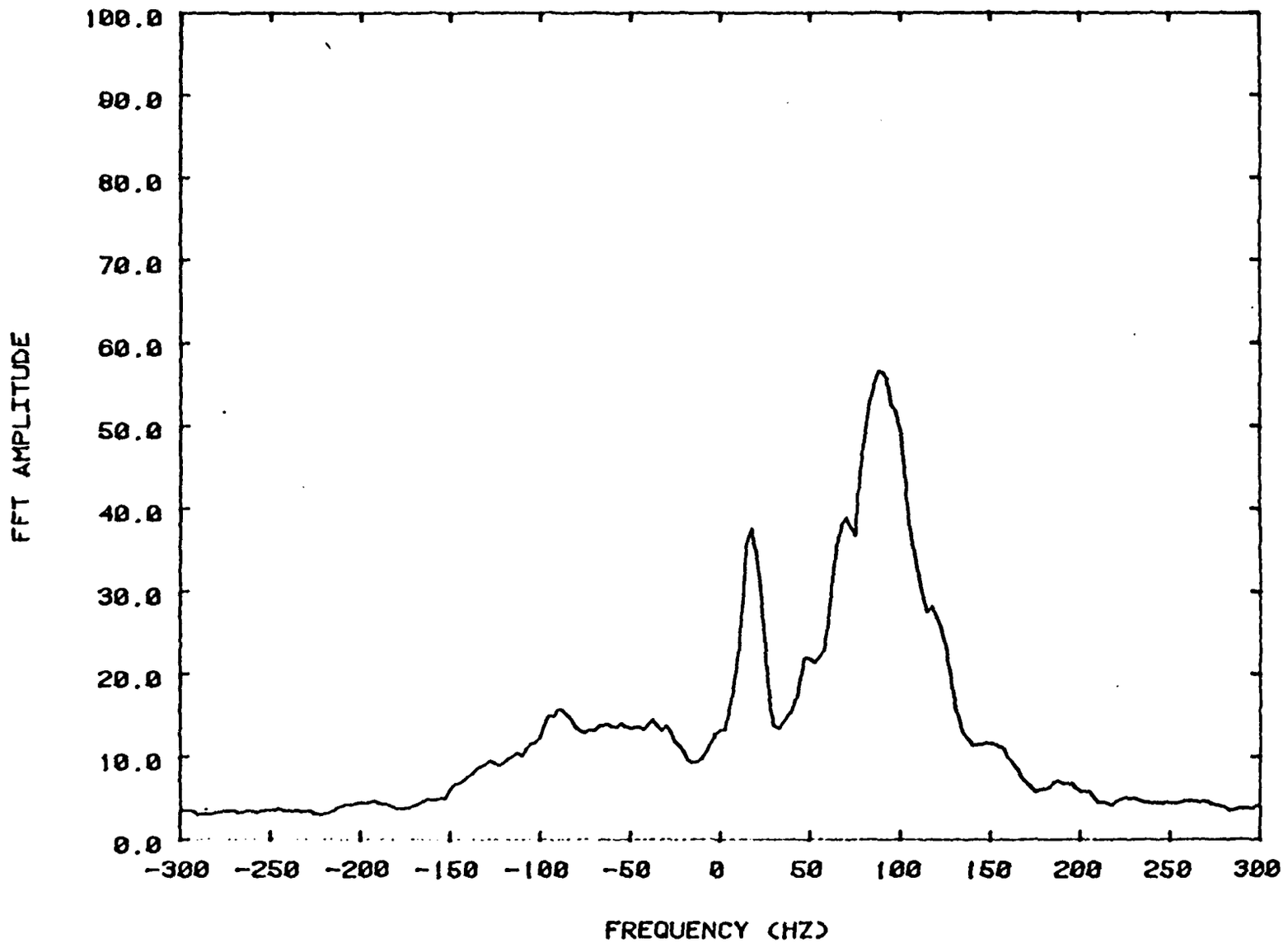

Figure 5-20 Composite Doppler Profile for Period Shown in Figure 5-19. Component Centered on Zero Shift Corresponds to Meteor Propagation and the Shifted Component is Due to the Auroral Scatter.

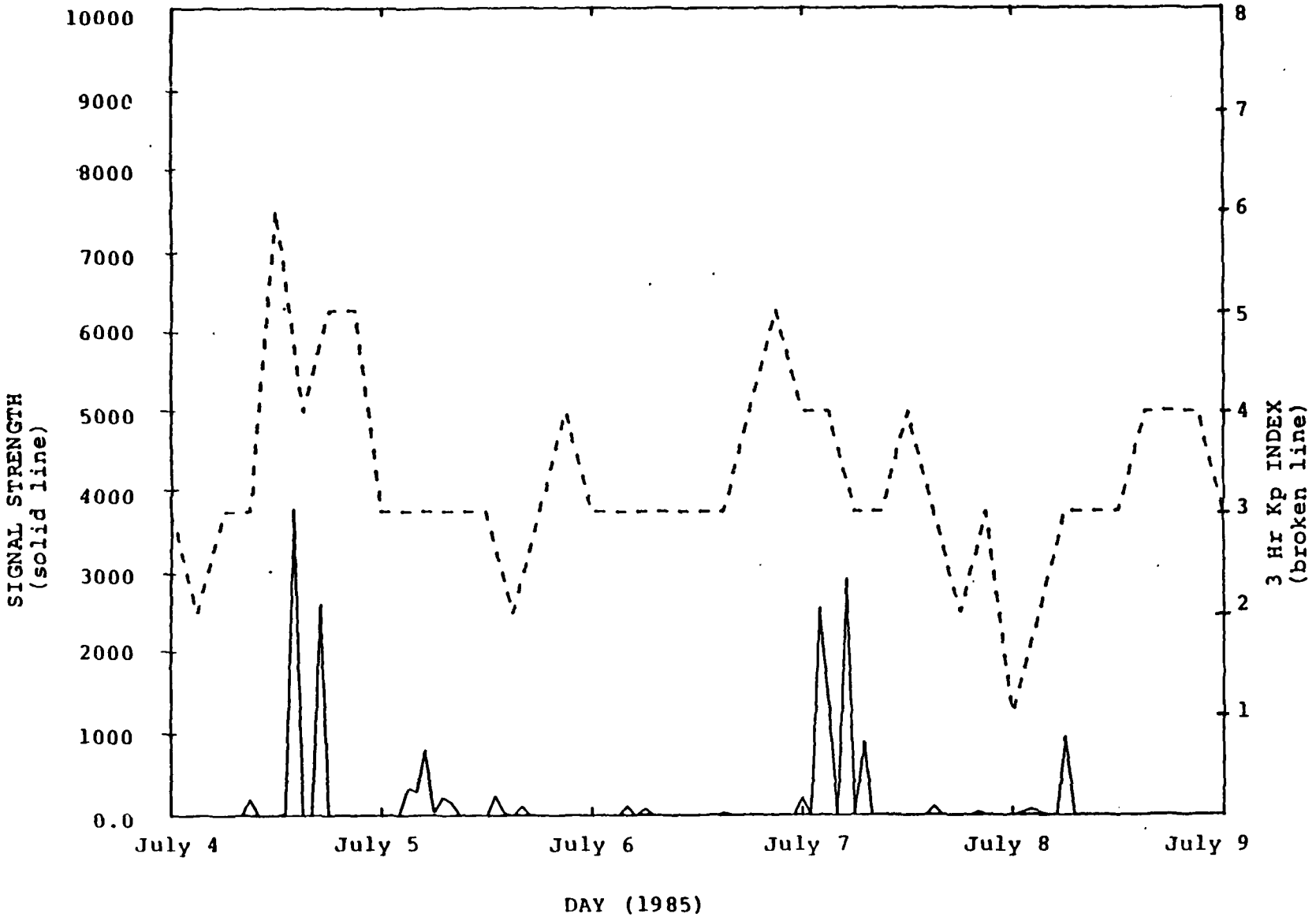

Figure 5-21 Solid line Represents Received Signal Energy in Uncalibrated Signal Units for 4 to 9 July 1985. Broken Line Represents 3 hour Kp Geomagnetic Activity Index.

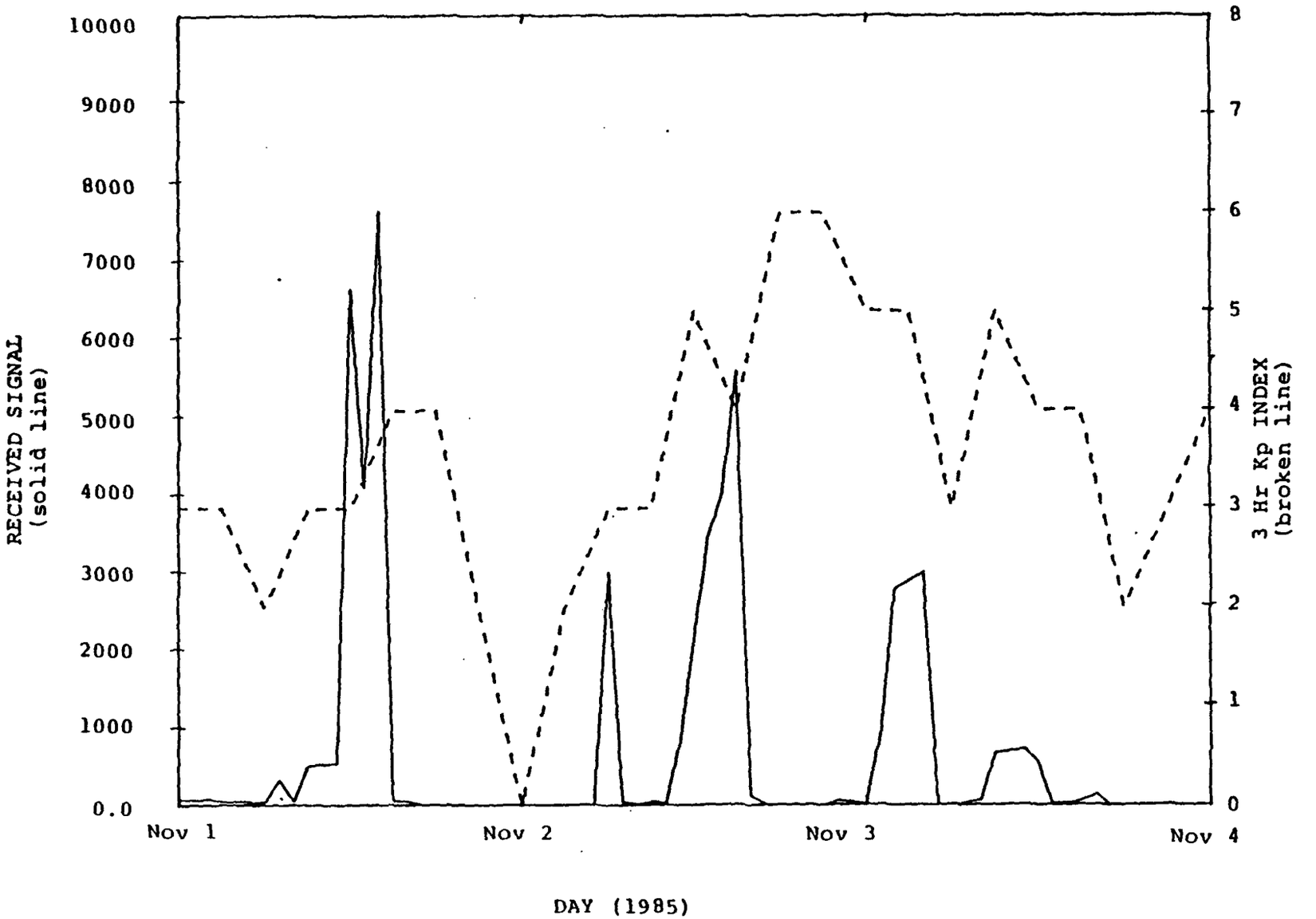

Figure 5-22 Solid Line Represents Received Signal Energy in Uncalibrated Signal Units for 1 to 3 November 1985. Broken Line Represents 3 hour Kp Geomagnetic Activity Index.

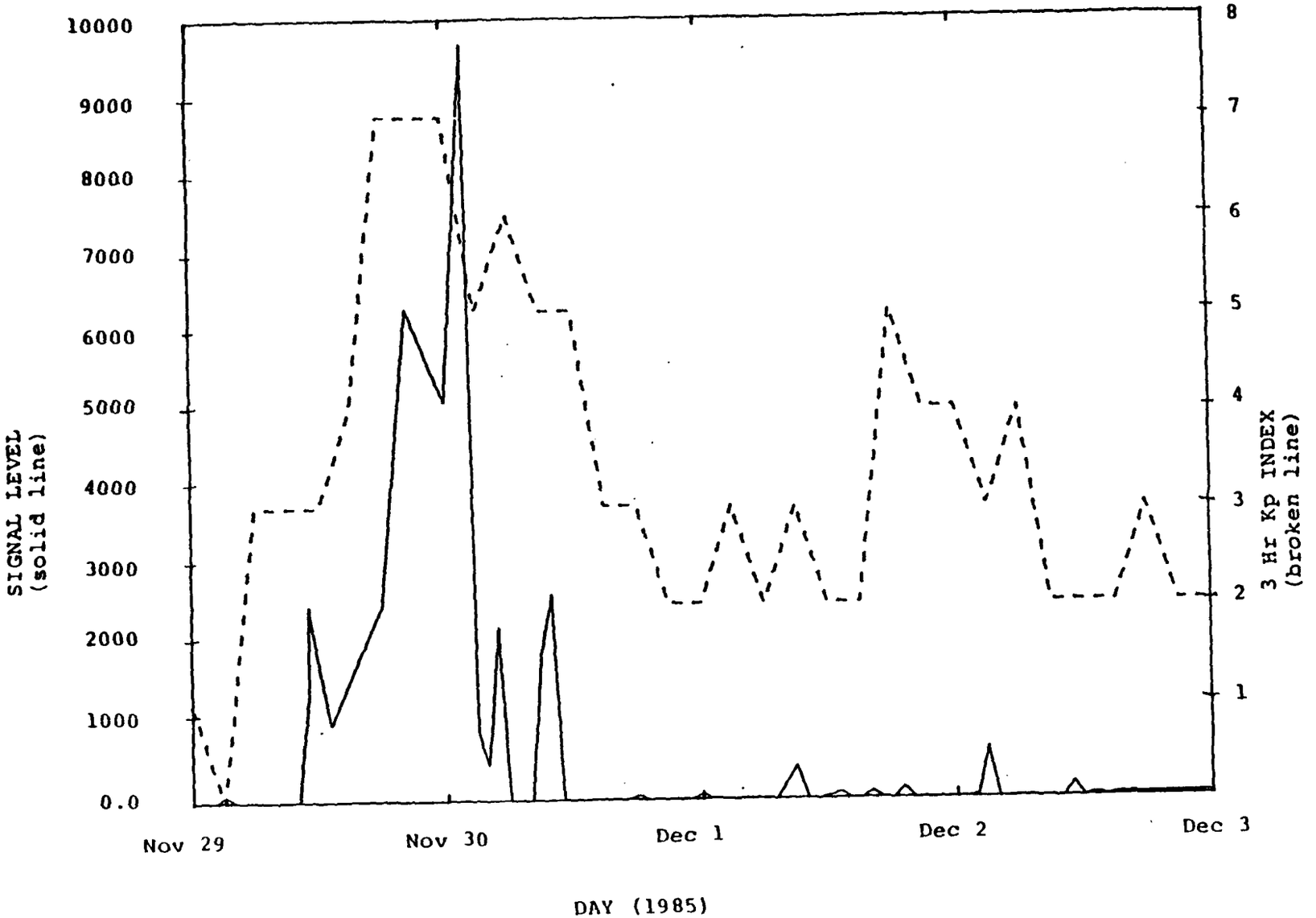

Figure 5-23 Solid Line Represents Received Signal Energy in Uncalibrated Signal Units for 29 November to 3 December. Broken Line Represents 3 hour Kp Geomagnetic Activity Index.

period 29 November through 5 December 1985, highlighted in Figure 5-12 and 5-14. Figure 5-24 shows the received signal energy to auroral scatter (solid line) and Kp magnetic index (broken line) for the period 17 September through 21 September 1985, highlighted in Figures 5-19 and 5-20.

The observation of auroral effects could also be correlated to the absence of f_0E and f_0E_s traces on the ionosonde data. This is attributable to the fact the increased ionization levels absorb the low frequency ionosonde probing signal.

Figures 5-22, 5-23, and 5-24 show the Kp index (broken line) and received signal level (solid line) for the 1 to 3 November, 29 November to 3 December 1985, and September 17 to 20 periods highlighted in Figures 5-8 through 5-13, 5-19, and 5-20. Finally, Figure 5-25 shows the percentage of days on which auroral scatter effects were observed versus time of day for the entire period of the experiment with the antennas off the great circle path. Note that the hour between 19 and 00 hours corresponding to local noon shows the lowest activity.

5.2.3.1 Comparing Theory to Data

Málaga [1986] has developed in detail the theory of VHF scatter from the aurora. The average power received due to scatter from the aurora is determined by Málaga as

$$P_r = P_T G_T G_R \left(\frac{c}{2\pi f}\right)^{m-2} \left\{\left(\frac{f_0E}{f}\right)^4 e^{-0.23K_E} C_E^2(m) I(h_E, b_E) \right. \qquad (5.2)$$

where

f_0E is the E-layer critical frequency

P_T is the transmitter power

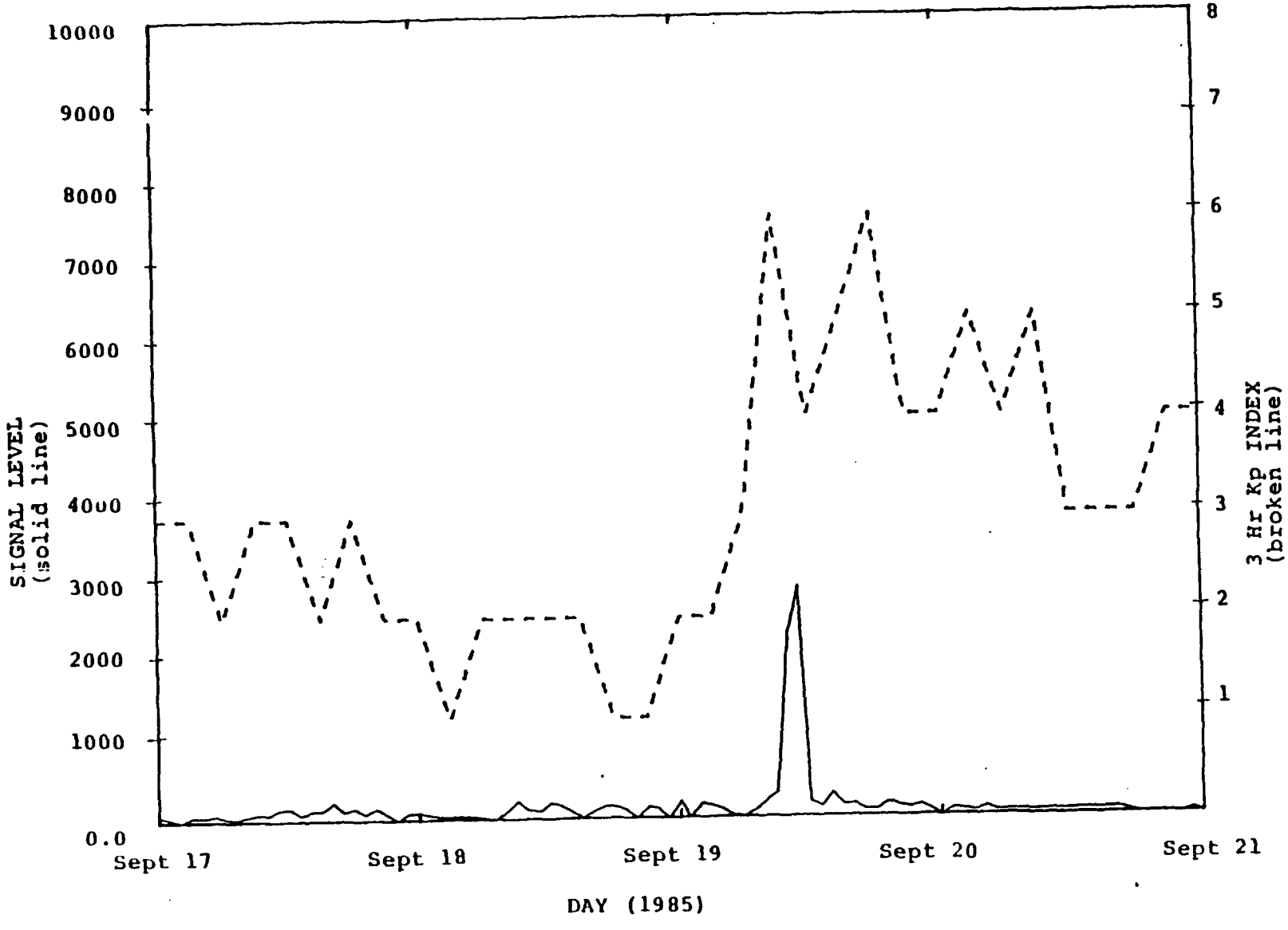

Figure 5-24 Solid Line Represents Received Signal Energy in Uncalibrated Signal Units for 17 September to 21 September. Broken Line Represents 3 hour Kp Geomagnetic Activity Index.

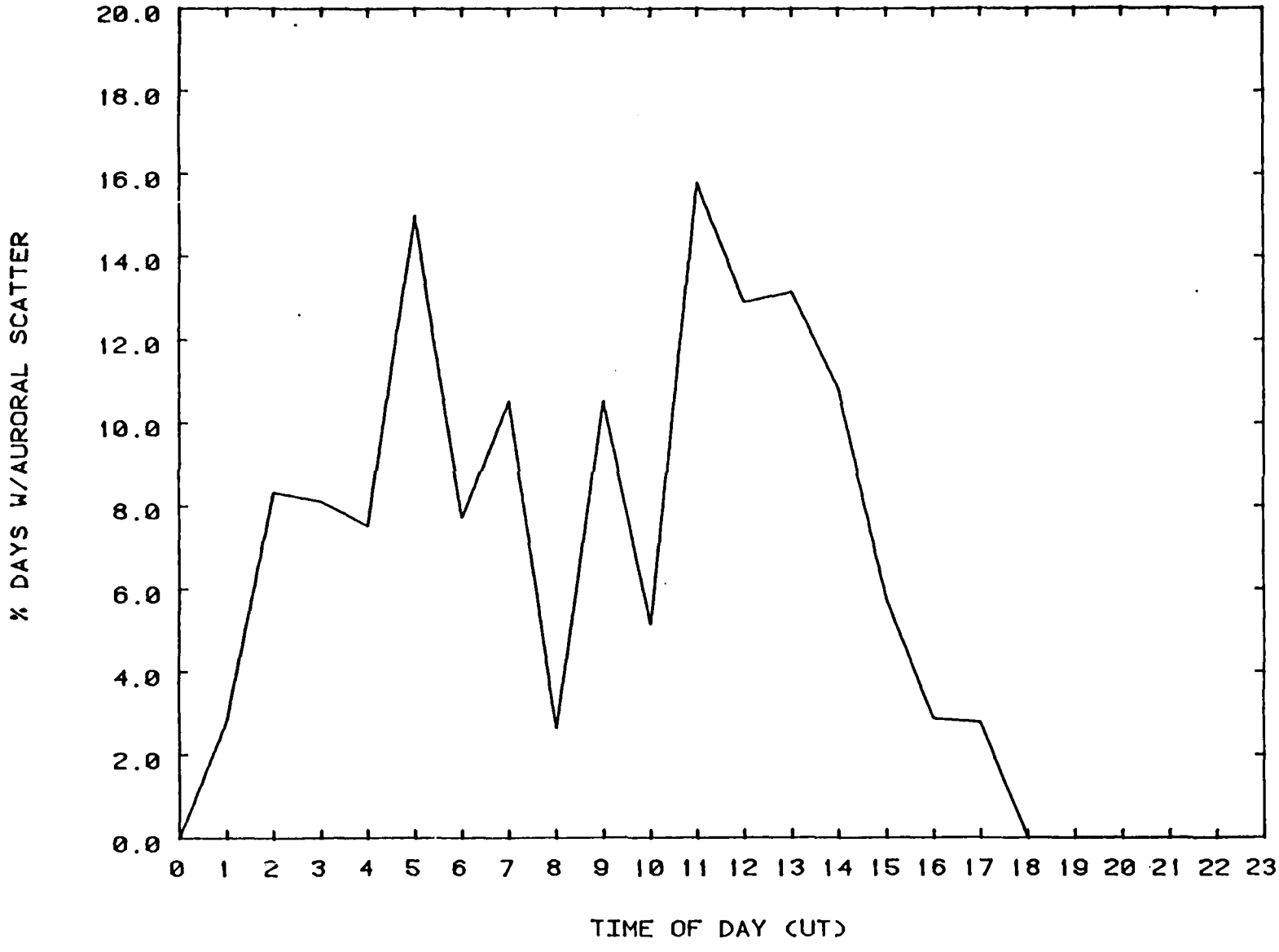

Figure 5-25 Percentage of Days on which Auroral Scatter Effects Were Observed Versus Time of Day (UT). Local Daylight Time is UT-9 Hours.

G_T is the peak transmitter antenna gain

G_R is the peak receiver antenna gain

c is the speed of light

f is the carrier frequency

K_E is the two-way absorption loss incurred as the incident and scattered waves propagate through the ionosphere.

$C_E^2(m) = (m-2)L\, L_T^{2-m} \overline{\left(\frac{\Delta N}{N}\right)_E^2}$ is the structure parameter of the irregularities

N is the mean electron density

ΔN is the perturbation in electron density due to field aligned irregularities.

L is the outer scale of the irregularities along the magnetic field lines.

L_T is the outer scale of the irregularities in the plane transverse to the magnetic field.

m is the wavenumber spectrum slope which determines the frequency dependence of the scattered field.

$$I_0(h_0,b) =$$

$$\int_{h_0-b}^{h_0+b} dh(h+a)^2\left[1-\left(\frac{h-h_0}{b}\right)^2\right]^2 \int_{\phi_1}^{\phi_2} d\phi \int_{\theta_1}^{\theta_2} \frac{d\theta g_T g_r \cos\theta \sin^2\chi\, e^{-(kLV_L)^2}}{R_T^2 R_R^2 V_T^m}$$

integrates the contribution of the scatterers over the three dimensional antenna pattern.

$g_T(h,\theta,\phi)$ is the transmitter antenna pattern

$g_r(h,\theta,\phi)$ is the receiver antenna pattern

R_T, R_R are the distances to the scatterer in the common volume from transmitter and receiver, respectively.

$\hat{u}_f$ (h,θ,ϕ) is a unit vector parallel to the direction of the magnetic field

$\hat{u}_i$ (h,θ,ϕ) is the unit vector directed from transmitter to the scatterer.

$\hat{u}_0$ (h,θ,ϕ) is the unit vector directed from the scatterer to the receiver.

$$V_L(h,\theta,\phi) = (\hat{u}_0 - \hat{u}_i) \cdot \hat{u}_f$$

$$V(h,\theta,\phi) = |\hat{u}_0 - \hat{u}_i|^2$$

$$V_T(h,\theta,\phi) = V^2 - V_L^2$$

χ is the angle between incident E vector and direction of scattering.

$$K_L = \frac{2\pi}{\lambda} V_L(h,\theta,\phi)$$

Equation (5.2) assumes that the critical frequency of the scattering layer, f_0E, and the normal electron density fluctuations are constant within the region. The triple integral

$I(h_0,b)$ depends only on the geometry and polarization of the transmit and receive antennas and can be evaluated given the geographic location of the terminals and the scattering region. Prediction of the scattered power requires modeling or measuring the critical frequency f_0E, the absorption loss K_E, and the structure parameter C_E. Due to the geometry of the scattering (see Málaga [1986]), signals observed at the earth are generally due to scatterers in the E region of the ionosphere.

The rms delay spread can be calculated from Equation (5.2) by computing various moments of the delay scaled by the power from all scatterers in the common volume as

$$\tau^n = \frac{\iiint_{\text{volume}} P\left(\frac{R_T+R_R}{C}\right)^n d^3r}{\iiint_{\text{volume}} P\, d^3r} \qquad (5.3)$$

where

n is the order of the moment

P is the received power from each scatter in the common volume as a function of location

$\frac{R_T+R_R}{C}$ is the path delay from transmitter to scatterer to receiver at each point in the common volume.

The 2σ delay spread is given by

$$2\sigma_{\text{multipath}} = 2\sqrt{\overline{\tau^2}-(\overline{\tau^1})^2} \qquad (5.5)$$

Define the total path loss L_T as

$$L_T = \frac{P_r}{P_T G_T G_R} = \frac{L_r}{C_E^2 \exp(-0.23 k_E)} . \qquad (5.5)$$

L_r is the relative path loss which accounts for all propagation effects except absorption loss, K_E, and terms incorporated in the structure parameter C_E^2.

Figure 5-26 shows contours of relative path loss versus receiver location in Alaska calculated from Equation (5.2) and (5.3) assuming a 42.4 MHz transmitter in Anchorage, $K_p = 2$, the auroral region bounds due to Gassmann [1973], and 10 km longitudinal outer scale of irregularities. Figure 5-27 shows contours of delay spread versus receiver location in Alaska with a transmitter located in Anchorage. The locations of Anchorage and Bethel are shown on the figures.

Note that computation of delay spread in Figure 5-27 does not require knowledge of the physical parameters incorporated in the structure parameter or the absorption loss. For Anchorage-Bethel we compare the 1000 μs average rms delay spread prediction to the 806 μs delay spread observed on the link. We see from Figure 5-26 that with a transmitter in Anchorage, Bethel would appear to be a good location for the equipment.

Accurate comparison of the absolute received signal predictions to data would require knowledge of the absorption K_E, the E-layer critical frequency f_0E and the structure constant C_E^2, or given the data, f_0E and K_E, we could calculate C_E^2.

In order to acquire this data, receive and transmitter equipment would require frequent and accurate calibration. In addition, accurate antenna pattern measurements would be required. Simple f_0E measurements using the College vertical swept frequency ionosonde equipment would not have been adequate due to

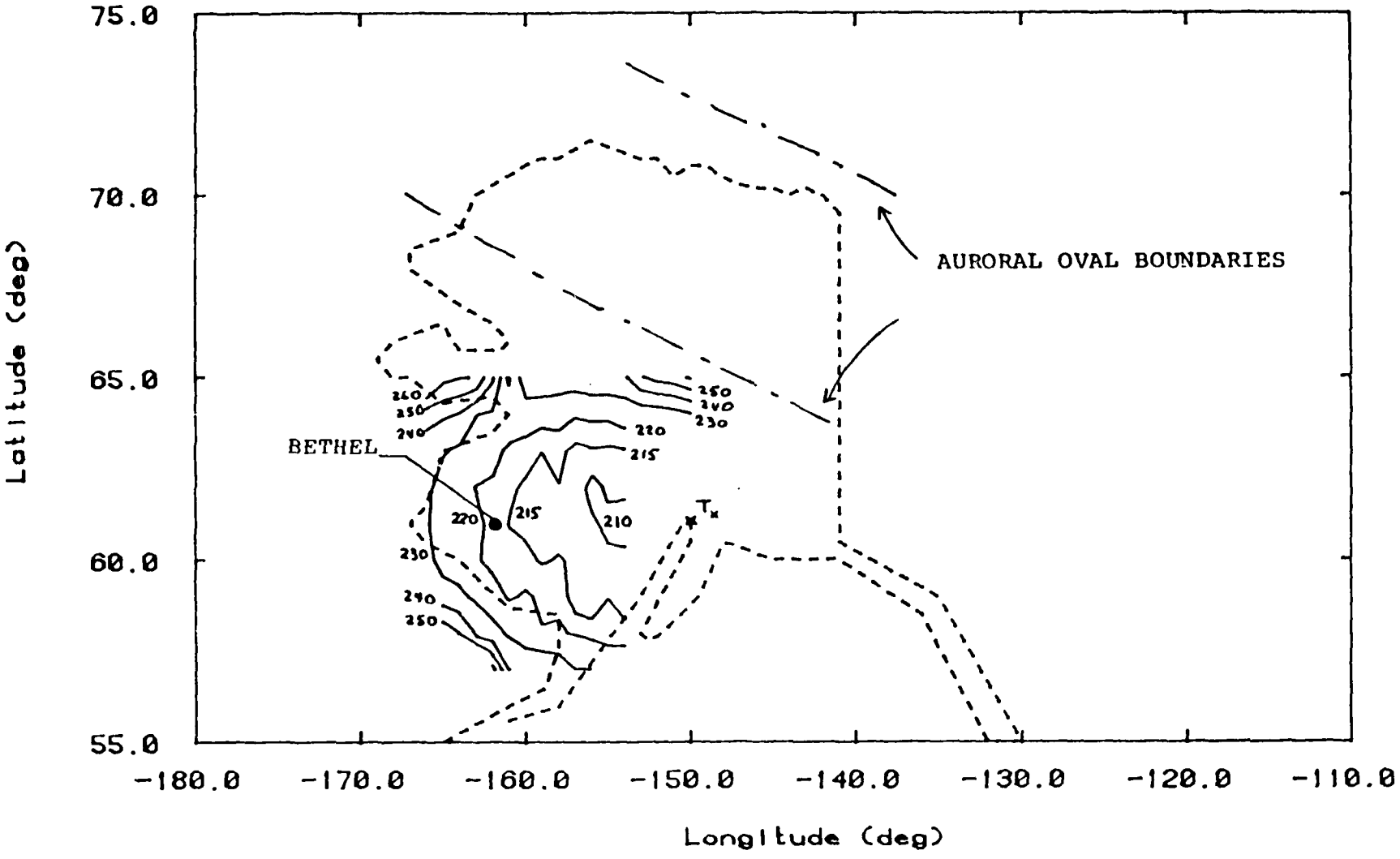

Figure 5-26 Contours of constant relative path loss in dB

AD-A174 718 THE MULTIPATH AND FADING PROFILE OF THE HIGH LATITUDE 2/2
METEOR BURST COMMUNICATION CHANNEL(U) SIGNATRON INC
LEXINGTON MA J A WEITZEN OCT 86 A447-15 RADC-TR-86-166
UNCLASSIFIED F19628-84-C-0117 F/G 17/2 1 NL

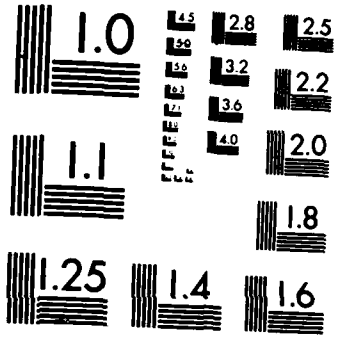

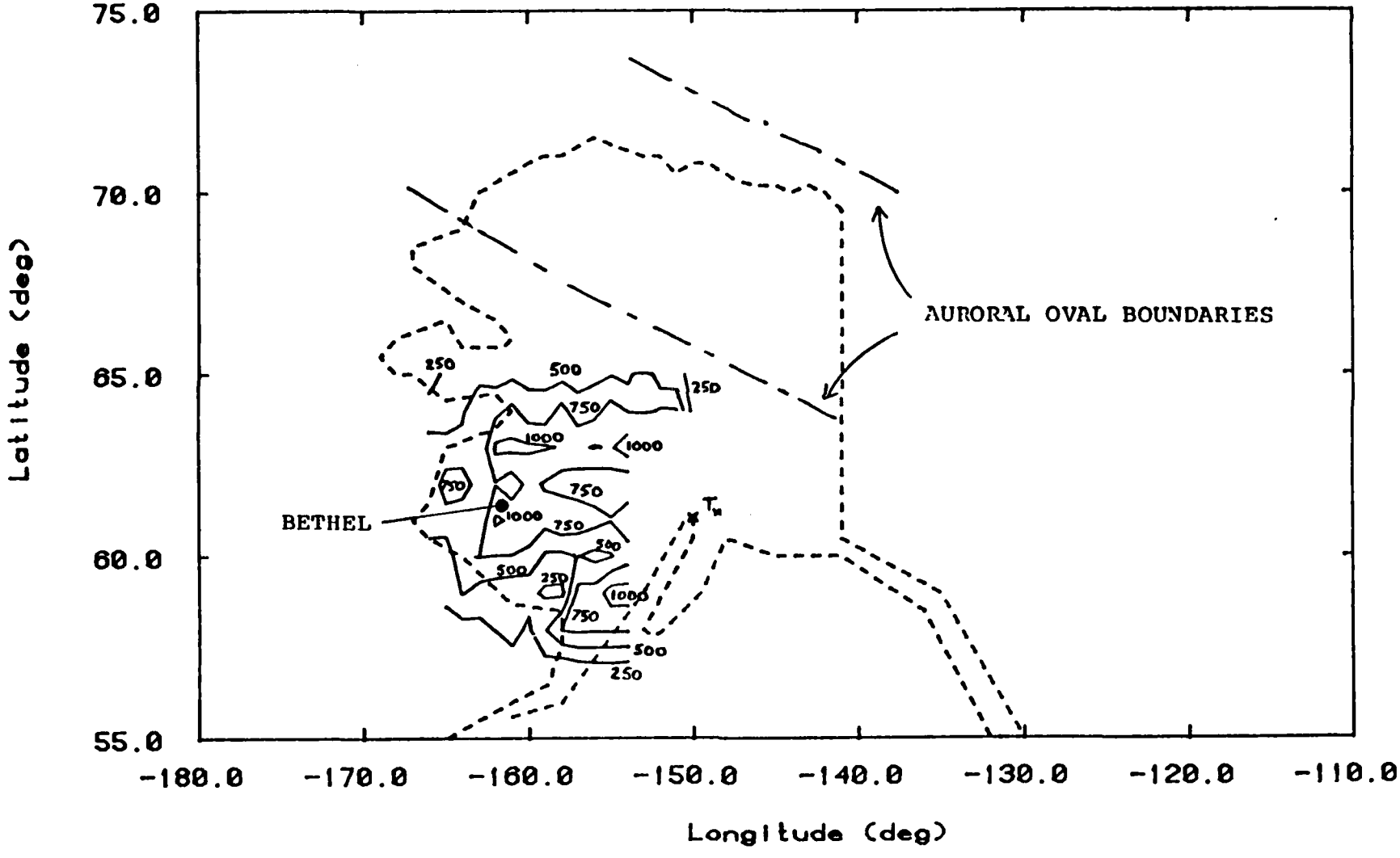

Figure 5-27 Contours of constant delay spread in microseconds

the fact that the low frequency probing waveform was often absorbed. An oblique angle prober would have been required. Due to the costs required to accurately determine these parameters, it was decided to concentrate on characterizing the multipath and Doppler spreads which could be determined without the expensive calibration and using existing ionospheric probers.

5.2.3.2 The Auroral Scatter Communication Channel

Auroral scatter at low levels represents a potential background noise source. At high signal levels, measurements described in this section show it to represent a highly disturbed channel with multipath spreads often in excess of 1000 μs and Doppler spreads of 200 Hz or more as shown in Figures 5-19 and 5-20. When, and if, the auroral channel is dominant, conventional meteor burst communication at 4-8 Kbps using coherent modulation is virtually impossible. Even non-coherent communication at these rates would be intersymbol interference limited.

At a *minimum, protocols* for a meteor burst network operating in an auroral environment must be designed so that one link operating on a continuous though unusable channel does not jam or lockout the rest of a network which may not be experiencing auroral scatter effects. A lower rate (100 to 300 bps) non-coherent operating mode might be included in a high latitude system just in case the link becomes auroral scatter limited.

Disruption of meteor communication due to scatter from the aurora is a localized condition which depends on the antenna patterns of a link and on the location and orientation of the aurora with respect to the link and the antenna patterns. Not all links in the vicinity of the aurora will be effected. The Bethel-Anchorage link was selected for the experiment because it was predicted to be one of the worst (or best depending on how we look at it) links for observing auroral maultipath effects given

a transmitter in Anchorage. Some links may experience some slight effects while other links may satisfy the requirements for scatter from the aurora and may experience the disturbed scatter conditions. Málaga [1986] describes the exact conditions required for auroral scatter and presents some predictions for scatter conditions in Alaska.

To actually communicate over the auroral channel, advanced adaptive equalization techniques are required such as those applied to troposcatter, or underwater communication systems. The alternative is to lower the data rate well below the multipath spread and operate using non-coherent modulation and coding.

SECTION 6

SUMMARY: COMMUNICATING VIA METEOR BURST AT HIGH LATITUDES

A number of propagation mechanisms in addition to meteors are observed on the high latitude meteor channel. In this report we have characterized the multipath and fading profiles of the dominant mechanisms: meteors, sporadic-E, and auroral scatter. We have observed that some of the mechanisms can, if link protocols are designed properly, be beneficial.

High latitude sporadic-E and enhanced E-layer scatter can create a continuous, slow fading, low multipath communication channel similar to a very benign single layer HF channel. In order to exploit this channel, network protocols must be carefully designed so that the network can operate in a high contention environment when all or many links have continuous connectivity to the master station. Variable rate modems capable of tracking the slow fading channel would allow optimal use of the capacity of the channel. Sporadic-E channels have been observed on many high latitude links and often confused for meteor channels. The sporadic-E channels do not have the inherent AJ/LPI of meteor channels since they have a much larger scattering area than meteors. They are also not as reliable as is the meteor channel and are much more subject to ionospheric disturbances than is the meteor channel. It therefore should be treated as a "bonus" channel rather than the backbone for survivable/reliable austere backup communication. If the meteor channel alone cannot support the throughput required for the mission, depending on the sporadic-E channel for the throughput requirements is potentially dangerous.

Scatter from the aurora can produce a low level background interference source on some links and depending on solar activity and the location of the aurora relative to a link could disrupt

meteor communication on some links. When dominant, the auroral channel is a highly disturbed channel with multipath spreads potentially in excess of 1000 μs and Doppler spreads in excess of 200 Hz. Communication using conventional 8 kbps coherent BPSK modulation on such a channel would be virtually impossible. Low rate (i.e.) 100-300 bps non-coherent modulation with frequency-hopping and coding would be better suited to the channel unless advanced equalization techniques are incorporated. With the lower data rate, a continuous channel with a throughput on the same order as the intermittent higher burst rate meteor channel could be achieved. Communication protocols must be very carefully designed so that a link with a continuous, though unusable, channel to the master station does not disrupt or lockout the entire network.

Taking into account the undesirable occasional effect of auroral scatter, meteor burst still has many advantages over HF which can be even more effected by these same phenomena. Auroral scatter degradation at meteor burst frequencies may be absorption blackout conditions at HF.

The experimental program as a whole was a success. The major goals of characterizing the multipath and Doppler profiles of the meteor, sporadic-E and auroral Channels with a short duration, relatively inexpensive, experiment were satisfied.

Interference with sensitive air traffic control equipment at Sondestrom Air Base, Greenland by the wideband probing signal forced early termination of the wideband preliminary experiment in Greenland. The results from that experiment were somewhat inconclusive due to the limited data set; however, no multipath, other than that caused by meteor trails was observed on sporadic-E channels within the 8 μs resolution of the experiment. The lessons learned during the experiment were applied to the main experiment in Alaska and contributed to its success.

The three primary propagation mechanisms observed at high latitudes, meteors, sporadic-E , and auroral scatter were observed and characterized by the Alaska experiment.

6.1 RECOMMENDATIONS FOR FUTURE STUDY

The work described in this and the companion report [Málaga, 1986] represent an important first step in scientifically evaluating the reliability of meteor burst at high latitudes. The research results must now be applied to practical communications problems. A new meteor burst communication network will become operational in 1986 to link remote long range radar (LRR) sites throughout Alaska to a central facility near Anchorage. The network will provide austere backup communication to the normal satellite communication systems. Figure 6-1 shows the location of the meteor burst sites in the network. In Figure 6-2 we superimpose a map showing the location of the radar sites upon the contour maps of relative path loss computed by Málaga. The figure shows which sites might be prime candidates for auroral degradation.

Based on these predictions from the Málaga report, the following links in the new Alaska Air Command system would be prime candidates for performance degradation due to auroral scatter.

Anchorage-Cape Romanzoff
Anchorage-Tatalina
Anchorage-Cape Newenham
Anchorage-Sparrevohn

In addition, an Anchorage-Fairbanks link would be especially susceptible. During disturbed conditions, more southerly stations might be effected.

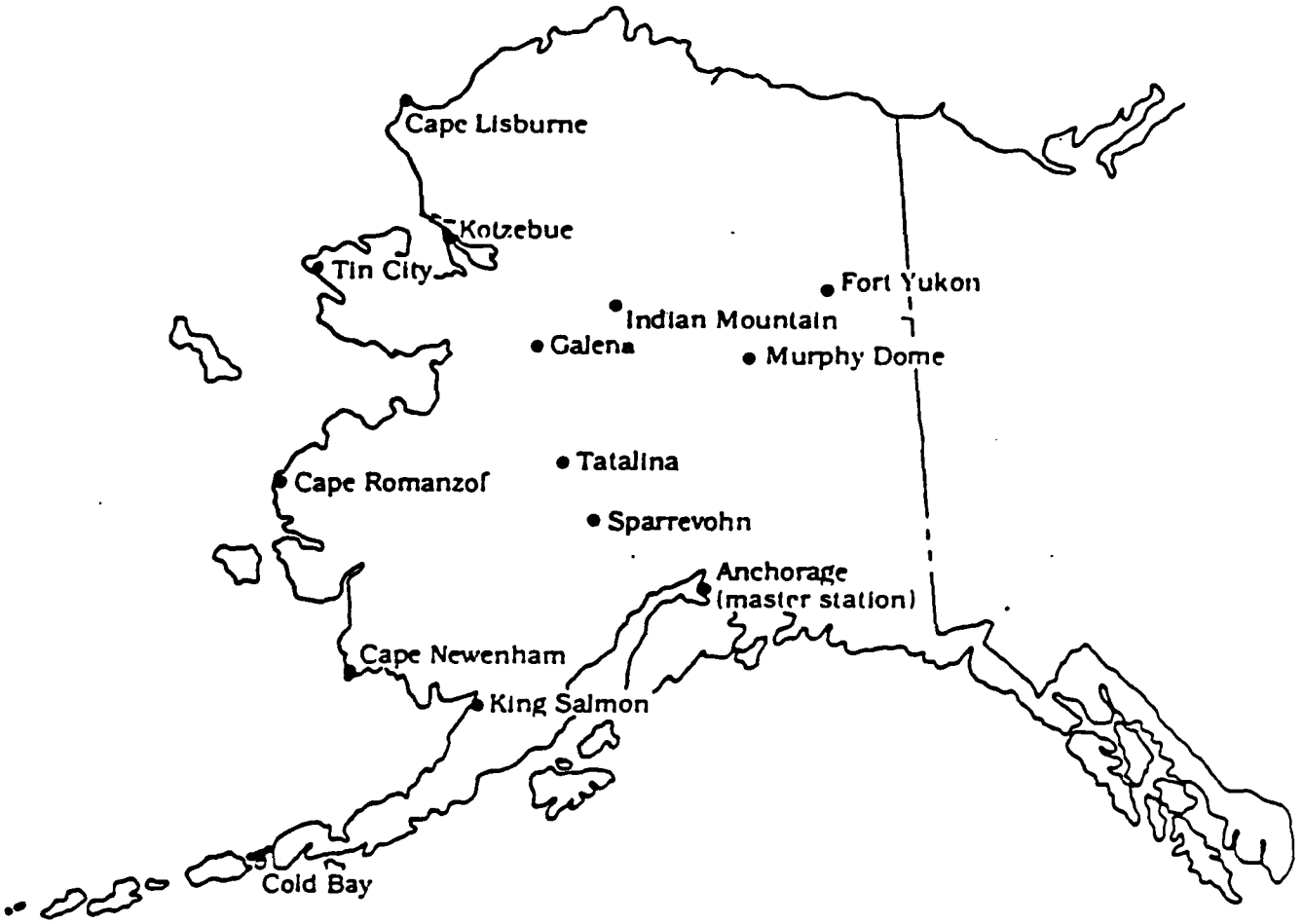

Figure 6-1 Location of Meteor Burst Stations in Alaskan Air Command Network

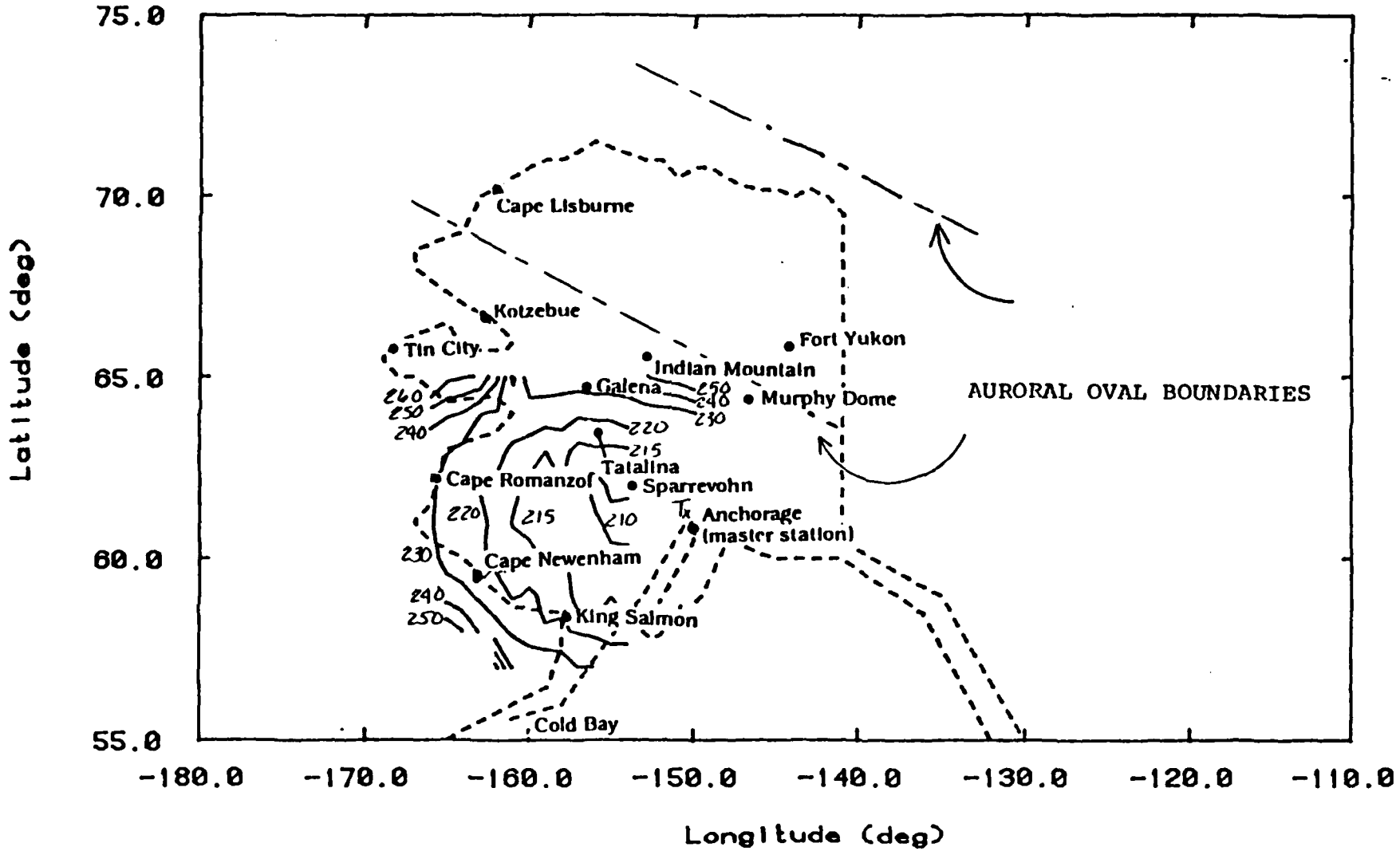

Figure 6-2 Map Showing Contours for Relative Path Loss and Location of Radar Sites

A useful and valuable follow-on to the experiment described in this report would be to collect data from the Alaskan Air Command on the performance of the various links in the network to assess which links are dominated by sporadic-E channels, which links are primarily meteor channels and which links, if any, are limited by auroral scatter effects.

On the links showing auroral scatter performance degradation, instrumentation such as used in this experiment should be set up to determine the multipath spreads on the links and to correlate measured multipath spreads with communication performance degradation. If auroral scatter proves to be a problem on the network, techniques to mitigate the effects including adaptive antenna steering, increased operating frequencies, reduced data rates, or adaptive message routing should be explored.

REFERENCES

Akram, F., N.M. Sheikh, A. Javed, and M.D. Grossi, Impulse Response of a Meteor Burst Channel Determined by Ray-Tracing Techniques, IEEE Transactions on Communications, April 1977, pp. 467-470.

Cannon, P.S., A.H. Dickenson, and M.H. Armstrong, AGARD-AR-218, 7 June 1985, Fairbanks, Alaska, ISBN:92-835-1513-7, Meteor-scatter Radio Communication at High Latitude.

Carpenter, R.S. and G.R. Ochs. High Resolution Pulse Measurements of Meteor Burst Propagation at 41 Mc/sec over a 1295 km Path, Journal of Research, National Bureau of Standards, Vol. 66D, No. 3, May 1962, pp. 249-263.

Eshlemann, V.R., Theory of Radio Reflections From Elelctron-Ion Clouds. IRE Transactions on Antennas and Propagation, January 1955, pp. 32-39.

Gassmann, G.L. Analog Model 1972 of the Arctic Ionosphere, Technical Report AFCR-TR-73-0151, Air Force Cambridge Research Labs, 1973.

Grossi, M.D. and A. Javed, Time and Frequency Spread in Meteor Burst Propagation Paths, AGARD-23rd EWPP Symposium, 3-7 October 1977.

Hines, C.O. and P.A. Forsythe, The Forward Scattering of Radio Waves From Overdense Meteor Trails, Canadian Journal of Physics, Vol. 35, September 1957, pp. 1033-1041.

Málaga A., Theory of VHF Scattering by Field Aligned Irregularities in the Ionosphere, RADC Technical Report, RADC-TR-86-118, 1986.

Manning, L.A., Air Motions and the Fading, Diversity and Aspect Sensitivity of Meteoric Echoes, Journal of Geophysical Research, Vol. 64, No. 10, October 1959, pp. 1415-1425.

Maynard, L.A., Meteor Burst Communications in the Arctic, Ionospheric Radio Communications: Proceedings of NATO Institute on Ionospheric Radio Communication in the Artic, Finae, Norway, April 13-19, 1967, New York, Plenum Press, 1968, pp. 165-173.

Ostergaard, J.C., J.E. Rasmussen, M.S. Sowa, J.M. Quinn, and P.A. Kossey, Characteristics of High Latitude Meteor Scatter Propagation Parameters Over the 45-104 MHz Band, AGARD-AR-218, 7 June 1985, Fairbanks, Alaska, ISBN:92-835-15512-7.

REFERENCES (Concluded)

Sugar, G.R., Radio Propagation From Meteor Trails, Proceedings of IEEE, February 1964, pp. 116-137.

Sugar, G.R. and G.R. Ochs, Elementary Consideration of the Effect of Multipath Propagation in Meteor Burst Communications, Journal of Research, National Bureau of Standards, Vol. 64D, No. 5, September 1960, pp. 495-500.

Weitzen, J.A., The Feasibility of High Speed Digital Communications on the Meteor Scatter Channel, Ph.D. dissertation, University of Wisconsin, Madison, Wisconsin, June 1983.

Weitzen, J.A., M.D. Grossi, and W.P. Birkemeser, High Resolution Multipath Measurements of the Meteor Scatter Channel, Radio Science, Vol. 19, Number 1, January 1984, pp. 375-381.

Weitzen, J.A., M.D. Grossi, and W.P. Birkemeier, An Estimate of the Capacity of the Meteor Burst Channel, IEEE Transactions on Communication, Vol. Com-32, No. 8, August 1984.

APPENDIX A
REMOVING THE AMBIGUITY IN THE MULTIPATH SPREAD

To show how an ambiguity in the measured delay spread can be created by the data processing algorithms and then removed, consider a multipath profile that consists of two discrete components with relative delay 0.75 P, where P is the period of the PR probing sequence. The location of the multipath profile relative to the data acquisition window is random from window to window. Consider first the case in which the first component is located at the beginning of the data acquisition window and the second component is delayed by 0.75 P. In this case, there is no ambiguity. Next consider the case in which the window is aligned so that the first component is located approximately in the middle of the data window. Because the correlation is modulo P, the second component occurs at (P/2 + 0.75P) mod P = P/4. The relative delay between components appears as P/4 instead of 3P/4. Thus, components which were delayed by 3P/4 could appear to be delayed by P/4 and the reverse could also occur. The safe approach, used in analysis of data from the experiment, is to measure the spread under all possible rotations of the data window modulo P and select the minimum delay under all rotations. This approach yields slightly conservative values for the average delay spread.

MISSION
of
Rome Air Development Center

RADC plans and executes research, development, test and selected acquisition programs in support of Command, Control, Communications and Intelligence (C^3I) activities. Technical and engineering support within areas of competence is provided to ESD Program Offices (POs) and other ESD elements to perform effective acquisition of C^3I systems. The areas of technical competence include communications, command and control, battle management, information processing, surveillance sensors, intelligence data collection and handling, solid state sciences, electromagnetics, and propagation, and electronic, maintainability, and compatibility.

END

1-87

DTIC